Understanding Landscape and Ice Sheet Evolution in the Gamburtsev Subglacial Mountains, East Antarctica, using Ice Sheet Surface Mapping

EDMUND JAMES LEA

Understanding Landscape and Ice Sheet Evolution in the Gamburtsev Subglacial Mountains, East Antarctica, using Ice Sheet Surface Mapping

Edmund J. Lea

Landscapes buried beneath the Antarctic Ice Sheet preserve information about the geologic and geomorphic evolution of the continent both before and during the wide-scale glaciation that began roughly 34 million years ago. Throughout this time, some areas of the ice sheet have remained cold-based and non-erosive, preserving ancient landscapes remarkably intact. The Gamburtsev Subglacial Mountains in central East Antarctica are one such landscape, maintaining evidence of tectonic, fluvial and glacial controls on their distinctly alpine morphology. The central Gamburtsevs have previously been surveyed using airborne ice-penetrating radar, however, many questions remain as to their evolution and their influence on the East Antarctic Ice Sheet, including where in the region to drill for a 1.5-million-year-long 'Oldest Ice' core. In this thesis, new maps of the planform geometry of the Gamburtsev Subglacial Mountains are derived from satellite remote sensing datasets of the ice sheet surface, based on the relationship between bed roughness and ice surface morphology. Automated and manual approaches to mapping were tested and validated against existing radar data and elevation models. Manual mapping was more effective than automated approaches at reproducing bed features observed in radar data, but a hybrid approach is suggested for future work. The maps produced here show detail of mountain ridges and valleys on wavelengths significantly smaller than the spacing of existing radar flightlines, and mapping has extended well beyond the confines of existing radar surveys. Morphometric analysis of the mapped landscape reveals that it constitutes a preserved (> 34 Ma) dendritic valley network, with some evidence for modification by topographically-confined glaciation prior to ice sheet inception. The planform geometry of the landscape is a significant control on locations of basal melting, subglacial hydrological flows, and the stability of the ice sheet over time, so the maps presented here may help to guide decisions about where to search for Oldest Ice.

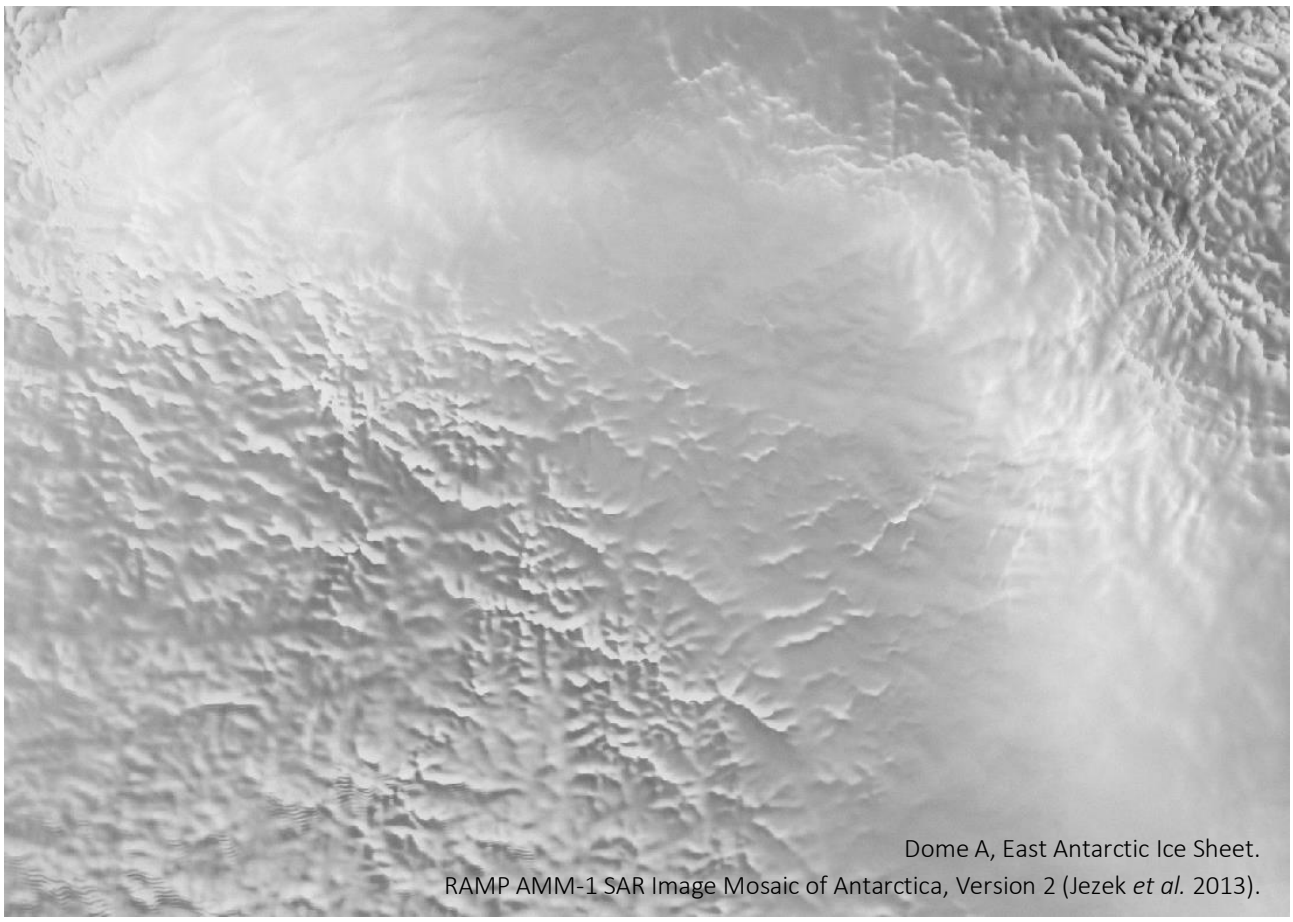

Dome A, East Antarctic Ice Sheet.
RAMP AMM-1 SAR Image Mosaic of Antarctica, Version 2 (Jezek *et al.* 2013).

Understanding Landscape and Ice Sheet Evolution in the Gamburtsev Subglacial Mountains, East Antarctica, using Ice Sheet Surface Mapping

Edmund James Lea
Master of Science by Research
2022

Department of Geography
Durham University

Table of Contents

List of Figures

Acknowledgements

I would like to thank my supervisors, Profs. Stewart Jamieson and Mike Bentley, for their invaluable guidance and encouragement throughout the formulation and undertaking of this research, and especially for their trust in me during stretches of slow and difficult progress. I am grateful for their helpful comments on this thesis, and for additional comments received on oral presentations of sections of the work from members of the Antarctic Science community. My thanks go to the whole staff and postgraduate community in the Department of Geography for making me feel welcome and valued, even as one of its youngest and least experienced members. I am especially grateful for the camaraderie of my fellow MRes students, and the many others whom I am privileged to call my friends.

This thesis is dedicated with special thanks to my Mum and Dad, and all my family, for all their love and support.

In this, as in all things, I give thanks to my God, the author of all Creation, my good and gentle Father, in whom I have life and hope and joy, and all good things in abundance.

1. Introduction

Subglacial landscapes are a unique and mysterious archive of Earth history, embracing the past climate and environments, as well as the present realities and potential futures of our changing world. Buried beneath kilometres of ice, some may have remained isolated and practically unchanged for millions of years (Sugden and John, 1976; Jamieson et al., 2014; Rose et al., 2013); on the other hand, some may have been subject to severe modification, with climate oscillation, fluctuating ice margins, and different styles of erosion responsible for the destruction, creation, and transformation of landscapes over time (Jamieson et al., 2014; Thomson et al., 2013; Paxman et al., 2020). Many landscapes are composites, altered to a lesser or greater extent by different suites of processes at different times (e.g. Young et al., 2011; Rose et al., 2014; Paxman et al., 2018). In the case of Antarctic landscapes, a long history of almost total submersion beneath a continent-wide ice sheet appears to have exacerbated this trend, juxtaposing ancient landscapes “frozen in time” with those that have undergone major transformation beneath the ice (Sugden and John, 1976; Jamieson et al., 2014; Rose et al., 2015; Franke et al., 2021). Unfortunately, this same ice history leaves us with very few ways to investigate these hidden worlds.

If we could see these landscapes that are buried under the ice, what would they tell us? Landscapes are records of the processes that shape them, informing us about past climate and environmental conditions – Antarctic landscapes are unusual in that they may have been preserved beneath ice for up to 34 million years (Zachos et al., 2001; Jamieson et al., 2010, 2014), letting us peer much deeper into the past than might otherwise be possible. Where landscapes have been modified by glaciation, they are indicators of the past behaviour of the Antarctic ice sheet, telling the story of changing ice and climate in complex patterns of erosion and preservation (e.g. Young et al., 2011; Rose et al., 2014; Paxman et al., 2018). Additionally, the shape of the subglacial topography is itself a control on ice flow (Sugden and John, 1976), necessary to understanding and modelling ice sheet behaviour (Jamieson et al., 2008), as well as finding suitable locations for extracting climate records in the form of ice cores, because of its influence on long-term ice stability (Fischer et al., 2013; Van Liefferinge and Pattyn, 2013).

In the context of a rapidly warming climate (IPCC, 2021) and threats to the stability of the Antarctic Ice Sheet (Joughin et al., 2014; Stokes et al., 2022), and the need to model ice sheet behaviour, knowledge of subglacial landscapes has never been more important. This is recognised and evidenced by the proliferation in collection of subglacial datasets in the past few decades, including the locations of subglacial lakes (Smith et al., 2009; Siegert et

al., 2016; Livingstone et al., 2022), measurements of ice thickness from radio echo sounding (RES) surveys (e.g. Holt et al., 2006; Vaughan et al., 2006; Bo et al., 2009; Bell et al., 2011; Franke et al., 2021; Popov, 2022), and other geophysical data useful for studying the Earth's mantle and crust (Block et al., 2009; Heeszel et al., 2013; Shen et al., 2018). The quantity of data is sufficient to produce continent-scale models of bedrock topography (Fretwell et al., 2013; Morlighem et al., 2020; Frémand et al., 2022), subglacial hydrology (Siegert et al., 2009; Livingstone et al., 2013), and geothermal heat flux (Shen et al., 2018; Ferraccioli et al., 2022), among other unknowns; on local and regional levels, however, there remains in general an alarming sparsity of direct observations, with various methods of interpolation used to produce datasets that are spatially continuous, but sometimes highly uncertain or coarsely resolved (Fretwell et al., 2013).

One approach to gathering subglacial data with the potential to address some of these issues is to make use of information about the subglacial domain that is encoded on the ice sheet surface (Rémy and Minster, 1997; Le Brocq et al., 2008; Ross et al., 2014; Jamieson et al., 2016). Several observations of subglacial lakes have come from their smooth ice surface expressions (Ridley et al., 1993; Bamber et al., 2009; Jamieson et al., 2016), and other authors have shown that rough bed topography also transmits its presence to the surface through its influence on ice flow (Gudmundsson, 2003, 2008; Raymond and Gudmundsson, 2005; De Rydt et al., 2013). Combining input datasets such as ice surface elevation and flow velocity, mathematical models of ice flow may be employed in reverse to reconstruct the shapes of subglacial landforms (Ockenden et al., 2021), though this is generally effective only where ice velocities are high, such as in ice streams (Gudmundsson, 2003). It is possible in some areas of the ice sheet to make more direct inferences of bed topography from the shape, or curvature, of the ice surface (Rémy and Minster, 1997; Le Brocq et al., 2008), including the locations of major valleys or channels (Jamieson et al., 2016), or even the wider-scale two-dimensional (planform) layout of an ancient buried landscape (Ross et al., 2014; Chang et al., 2016), in finer detail than may be possible from even the densest clusters of ice thickness measurements. Moreover, observations of the ice surface can be made from space rather than from aircraft, giving these methods a major advantage in quantity of data, spatial coverage, and cost.

An enigmatic landscape at the crossroads of East Antarctica may provide an ideal testing ground for wider application of these methods: the Gamburtsev Subglacial Mountains (GSM) are a high-relief, alpine mountain range (Bo et al., 2009; Rose et al., 2013), entirely submerged beneath the central dome and highest point of the Antarctic Ice Sheet (Fig. 1.1),

bounded by the Lambert Graben to the north, the South Pole Basin to the south, and a complex system of linear faults to east and west (Ferraccioli et al., 2011). Prior to the internationally collaborative Antarctica's Gamburtsev Province (AGAP) geophysical survey during the International Polar Year of 2007-2009 (Bell et al., 2011; Ferraccioli et al., 2011), very little at all was known about their structure (Cox et al., 2010). Subsequent analysis of the RES data collected by the AGAP survey revealed a dendritic network of subglacial valleys surrounded by large mountain massifs, bearing evidence of multiple stages of glacial modification (Rose et al., 2013). The high level of detail achieved by the AGAP survey does not persist outside of the survey area – however, the few existing measurements suggest that the surrounding foothills of the GSM may be much more extensive. The survey provides a clear benchmark against which to validate interpretations made from the ice surface (c.f. Ross et al., 2014), which may then expand detail of the landscape beyond the currently known regions. The high relief and low ice velocities experienced in the GSM are suitable for producing the kind of surface expressions that can be used to infer landscape structure, making them an attractive target for this work.

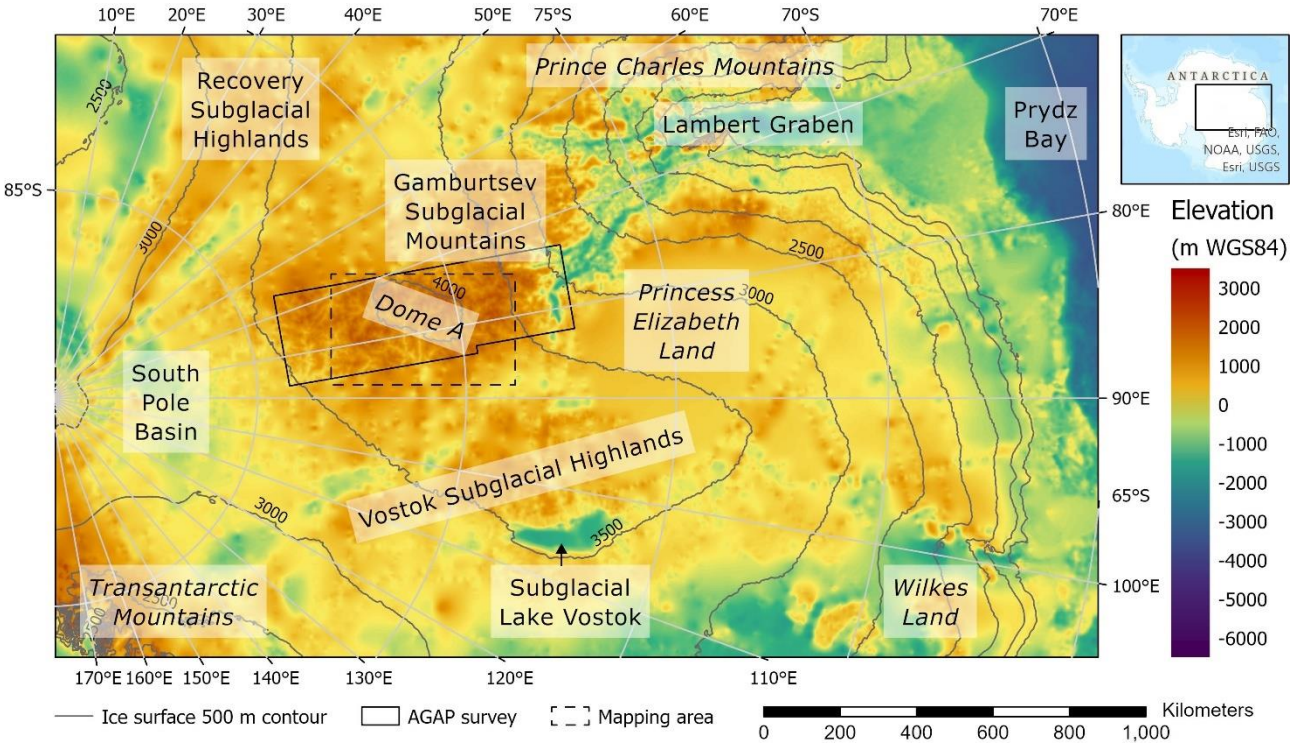

Figure 1.1 – The regional subglacial topography of central East Antarctica from Bedmap2 (Fretwell et al., 2013), including placenames mentioned in the text. Names in italics = surficial/subaerial features, names in regular typeface = bed features. The area of interest for this thesis (Fig. 2.3) is indicated by the dashed box. AGAP = Antarctica's Gamburtsev Province (Fig 2.4a).

2. Literature Review

2.1. Mapping the Antarctic Ice Sheet bed

The most commonly used method to study the bed of the Antarctic Ice Sheet is the collection of geophysical data, in particular, airborne radio echo sounding (RES) or ice-penetrating radar transects. The ice bed is identified as a highly reflective layer in the two-dimensional vertical profile of a radargram, due to the difference in electrostatic properties between the ice and the bed (Siegert, 1999). Its elevation is calculated based on the known speed and two-way travel time of the radar wave. The resulting bed elevation profile can be used to investigate the morphometry of the subglacial landscape, for instance, by measuring the width and cross-sectional shape of valleys traversed (e.g. Siegert et al., 2005; Bell et al., 2011). Elevation profiles from closely spaced flightlines may be interpolated into a grid of data points to form a digital elevation model (DEM) of the local subglacial topography, useful for morphometric analysis of the subglacial landscape in three dimensions (e.g. Bo et al., 2009; Young et al., 2011; Rose et al., 2013; Paxman et al., 2018, 2019a, b). Large quantities of elevation data have been collected in individual surveys (few 1000 km extent) and are collated to produce continent-wide maps of subglacial topography, including the widely-used Bedmap[1] products (Lythe and Vaughan, 2001; Fretwell et al., 2013), as well as the more recent BedMachine Antarctica (Morlighem et al., 2020). Where large gaps exist between survey lines (Fig. 2.1), the topography may be interpolated, or filled using coarser-resolution techniques such as satellite gravimetry (Fretwell et al., 2013). In areas where ice is fast-flowing, a computational inversion of ice surface velocity can be used, based on the principle of mass conservation along discrete flow lines (Morlighem et al., 2011). In the central EAIS, where ice flow is minimal, the applicability of such techniques is limited. The bed in areas between survey lines is therefore often poorly resolved, and areas that may well host highly variable topography appear artificially smooth in topographic reconstructions.

[1] As of submission of this thesis, the third major version of Bedmap (Bedmap3) is in the process of being published. A discussion of the methodology used to construct it is available at: https://essd.copernicus.org/preprints/essd-2022-355/ [Accessed 01/12/2022].

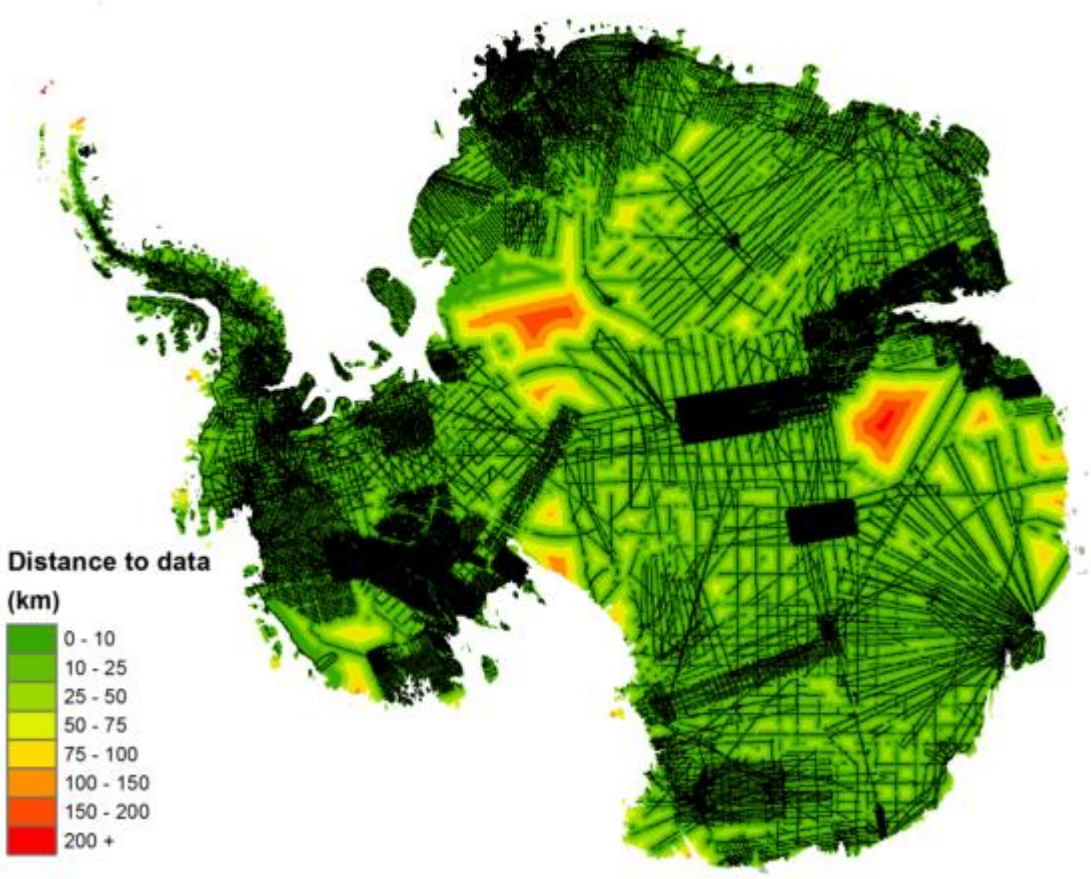

Figure 2.1 – Bedmap2 data coverage (black lines represent RES surveys), and distance to nearest data point in areas where no data are present. From Fretwell et al. (2013). Note that the upcoming Bedmap3 compilation (Frémand et al., 2022) improves coverage in several regions using data published since Bedmap2, but no new data have been gathered in the study area for this thesis.

One way to improve knowledge of the subglacial topography in these areas is by mapping the ice sheet surface (Rémy and Minster, 1997; Le Brocq et al., 2008; Ross et al., 2014). Areas where ice is thinner (i.e. over ridges) are likely to have a more rugged surface, while thicker ice dampens the impact of bed topography, and so appears smoother (Ross et al., 2014). The ice sheet surface can be observed and mapped using satellite-derived datasets, such as the Moderate-Resolution Imaging Spectroradiometer (MODIS) Mosaic of Antarctica (MOA) (Scambos et al., 2007), or the Radarsat Antarctic Mapping Project (RAMP) Image Mosaic of Antarctica (Jezek et al., 2013). Ice surface DEMs such as the recently compiled Reference Elevation Model of Antarctica (REMA; Howat et al., 2019) are also useful for observing ice sheet surface topography. Processing these data to derive surface parameters such as slope and curvature can highlight changes in slope resulting from differential ice flow over rough topography (Rémy and Minster, 1997). This allows the subglacial network

of ridges and valleys to be mapped, and in areas where there are not very closely-spaced RES surveys this can be to a greater level of detail than permitted by gridded bed products (Fig. 2.2; Ross et al., 2014; Chang et al., 2016; Jamieson et al., 2016). Mapping may be conducted by manual digitising, or can potentially be automated across larger areas, though the effectiveness of automated approaches has been found to vary regionally (Chang et al., 2016). In areas where RES transect data are also available, these have been found to verify the locations of subglacial ridges and valleys mapped from satellite datasets (Ross et al., 2014; Jamieson et al., 2016), supporting the robustness of this method for identifying these features. To date, only a few studies (Ross et al., 2014; Chang et al., 2016) have made use of surface mapping at high resolution (valley-scale) over large areas.

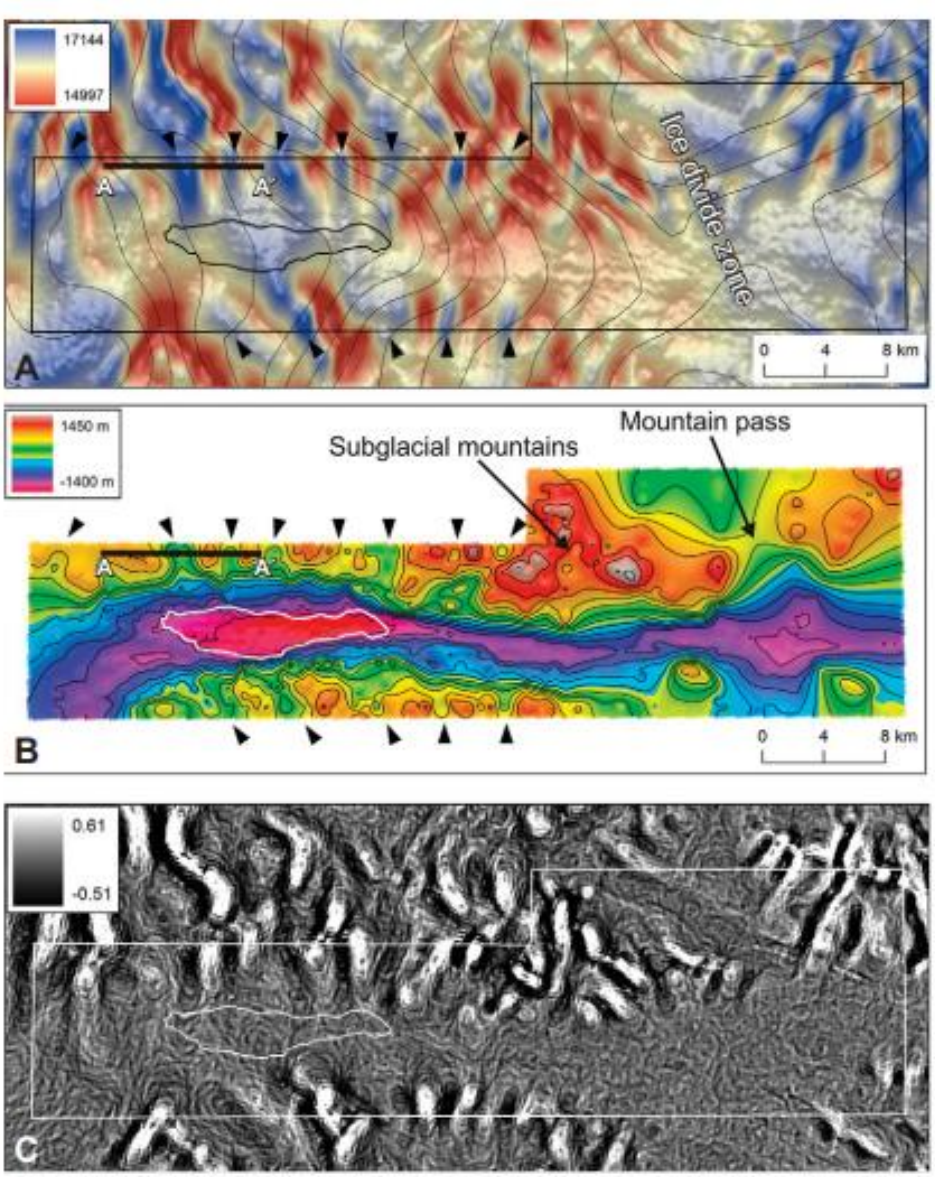

Figure 2.2 – Comparison of (a) MODIS MOA imagery (draped over hillshade), (b) DEM of subglacial topography interpolated from radar echo sounding (RES) data, and (c) profile curvature of MODIS MOA imagery, all for an area of the Ellsworth Highlands in West Antarctica. From Ross et al. (2014).

2.2. Gamburtsev Subglacial Mountains (GSM)

The Gamburtsev Subglacial Mountains (GSM) are a high mountain range in central East Antarctica, stretching from the head of the Lambert rift towards the South Pole basin (Fig. 1.1). Despite peak elevations in excess of 3 km above sea level (Rose et al., 2013), the entire range is submerged beneath the East Antarctic Ice Sheet (EAIS), which reaches its highest point at Dome A, above the central GSM (Fig. 2.3). Bed models interpolated from AGAP RES data (Bell et al., 2011; Ferraccioli et al., 2011; Rose et al., 2013) reveal that the morphological character of the GSM is distinctly alpine, with relief averaging more than 2 km, and valley cross-profiles indicative of fluvial and/or glacial incision (Bo et al., 2009; Rose et al., 2013). Modelling studies of the evolution of the Antarctic Ice Sheet are consistent in finding that the development of regional ice masses, particularly with valley glaciers in the GSM, was key to the expansion of glaciation in Antarctica (DeConto and Pollard, 2003; Jamieson et al., 2010). It is therefore important to understand how this landscape formed and evolved prior to and in tandem with the nascent ice sheet.

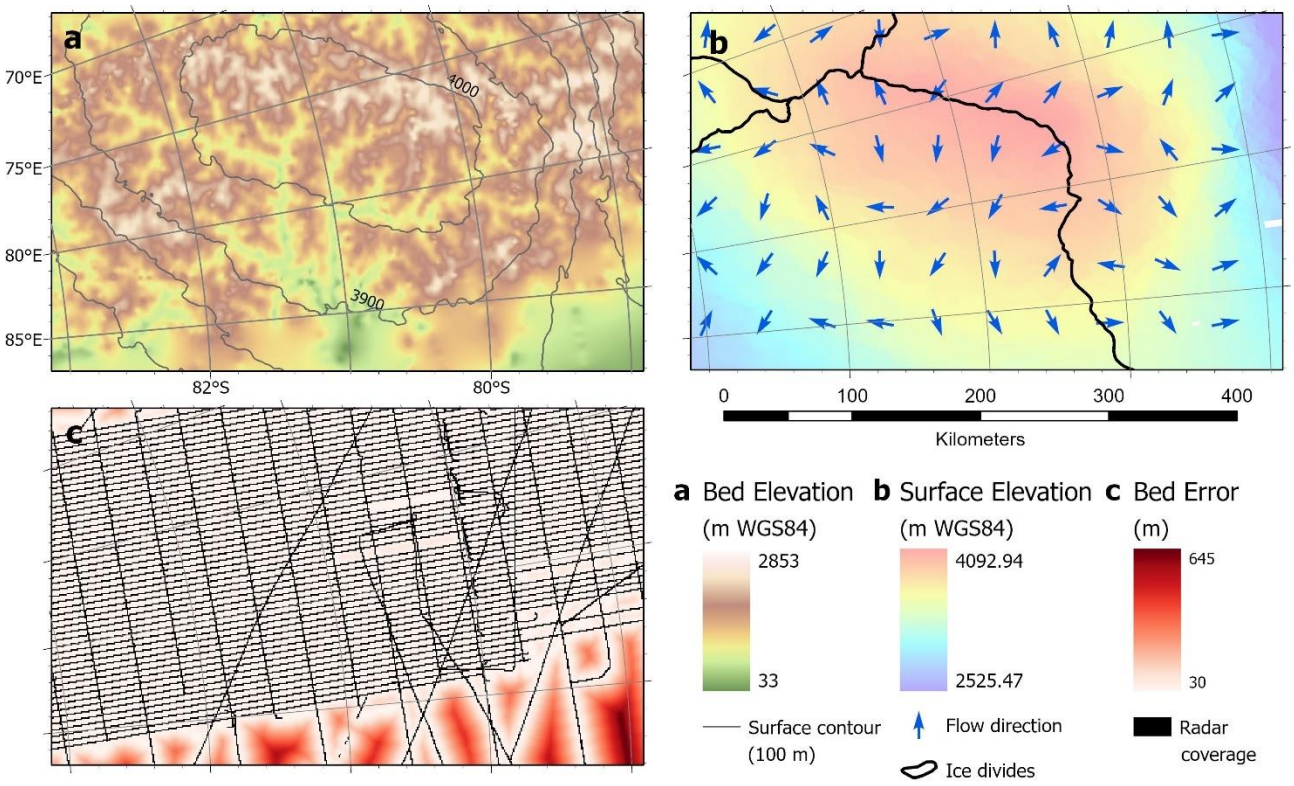

Figure 2.3 – Area of the Gamburtsev Subglacial Mountains being targeted for mapping in this thesis: a) Bed elevation and ice surface contour; b) Surface elevation, surface flow directions and ice divides; c) Bed elevation error and locations of radio echo sounding (RES) survey lines. Bed elevation and errors from BedMachine Antarctica (Morlighem et al., 2020). Surface elevation from Reference Elevation Model of Antarctica (Howat et al., 2019). Flow vectors from Mouginot et al. (2019). Ice divides from Zwally et al. (2012). RES flightlines from Bedmap2 (Fretwell et al., 2013).

2.2.1. Origin of the GSM

The origin of the GSM has become a persistent question, with debate around the cause and timing of uplift remaining largely unresolved (van de Flierdt et al., 2008; Block et al., 2009; Ferraccioli et al., 2011; Heeszel et al., 2013; Paxman et al., 2016). Several hypotheses have been proposed, including geologically recent thermal uplift associated with mantle hot spot activity (Sleep, 2006), ancient orogeny in a continental collision zone (Fitzsimmons, 2000, 2003; Block et al., 2009), crustal shortening in response to long-distance stress transmission (Veevers, 1994), and uplift associated with rifting during continental breakup (Ferraccioli et al., 2011). A key difficulty in resolving the issue is the inaccessibility of the GSM for direct sampling and dating of bedrock, although attempts have been made to date their formation using detrital materials likely of ancestral Gamburtsev provenance from coastal and offshore sediment deposits in the Prince Charles Mountains and Prydz Bay (Veevers and Saeed, 2008; Veevers et al., 2008; van de Flierdt et al., 2008; Gupta et al., 2022). The ages derived support the hypothesis of an ancient origin for the GSM, and suggest uplift associated with the formation of the supercontinents Rodinia (~1200-800 Ma) and Gondwana (~620-460 Ma) (Veevers and Saeed, 2008; van de Flierdt et al., 2008), with another potential period of activity ca. 700 Ma (Gupta et al., 2022). Supporting evidence is provided by geophysical data, including seismic (Heeszel et al., 2013; An et al., 2015; Shen et al., 2018; Kumar et al., 2021) and gravitational measurements (Block et al., 2009; Ferraccioli et al., 2011; Swain and Kirby, 2021) of the East Antarctic lithosphere. Crust beneath the GSM is thicker than the continental average (Block et al., 2009), indicating that a recent thermal origin is unlikely, though estimates range widely, from 42-43 km (Block et al., 2009), to greater than 55 km (Heeszel et al., 2013), or greater than 70 km (Ferraccioli et al., 2011).

2.2.2. Pre-glacial landscape evolution

Fluvial influences on the landscape of the GSM have been identified in the form of dendritic valley networks organised into discrete drainage basins (Fig. 2.4a), concave long-profiles, and the prevalence of V-shaped valley forms (Bo et al., 2009; Rose et al., 2013). If rifting during Gondwanaland breakup was indeed a source of uplift in the GSM (Ferraccioli et al., 2011), analogy to other Southern Hemisphere rifting margins suggests that rivers may have played a significant role in maintaining high elevations through a process of selective denudation driving further uplift (Sugden and Jamieson, 2018), which leads to the significant relief observed. Modelling based on low rates of erosion (to provide an *upper* bound with respect to age) suggests that the fluvial network of the GSM developed over no more than 200 Myr, and that approximately 20% of their current elevation is accounted for by the

isostatic response to erosional unloading (Paxman et al., 2016). If erosion rates had been higher then < 200 Myr would be required for the network to have developed.

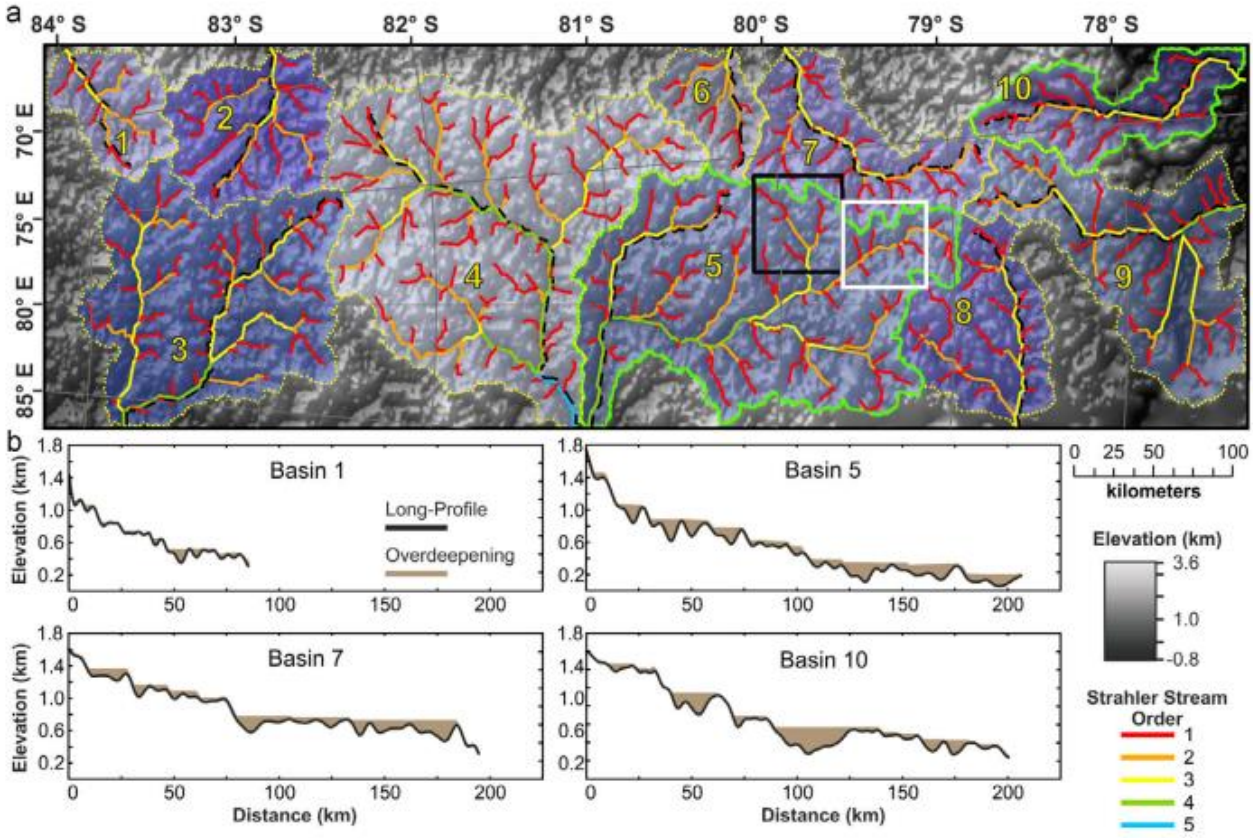

Figure 2.4 – (a) Drainage basins and dendritic fluvial networks preserved in the GSM and (b) evidence for subsequent modification of valley profiles by alpine glaciation in the form of overdeepenings along long-profiles in several catchments. For location of (a) see Fig. 1.1. From Rose et al. (2013).

2.2.3. Onset of glaciation

Evidence is also found for subsequent modification of the fluvial landscape by topographically confined, alpine-style glaciation, prior to the formation of regional or continental-scale ice caps (Bo et al., 2009; Rose et al., 2013). Glacial landforms such as U-shaped troughs and overdeepenings (Fig. 2.4b), cirques and hanging valleys, are all indicative of this style of glaciation, and incompatible with formation under modern ice sheet flow (Bo et al., 2009; Rose et al., 2013). A significant step-change in the benthic oxygen isotope ratio is used to place continental ice sheet inception at the Eocene-Oligocene transition ca. 34 Ma, due to the link between terrestrial ice volume and storage of heavy (^{18}O) isotopes (Coxall et al., 2005). It may therefore be inferred that phases of cirque and alpine-style glaciation in the GSM were likely associated with periods of climatic cooling that predate this change (Rose et al., 2013), though the exact timing of such episodes remains

uncertain. There is growing evidence for fluctuating glaciations in Antarctica during the late Eocene ca. 38-34 Ma (Van Breedam et al., 2022, and references therein), but some authors argue for the existence of terrestrial ice as far back as the late Cretaceous, ca. 130 Ma, to explain changes in sea level and ocean chemistry which occurred at that time (Stoll and Schrag, 1996; Miller et al., 2008).

2.2.4. Landscape preservation in the GSM

The basal thermal regime is key to patterns of landscape erosion and preservation beneath the Antarctic Ice Sheet (Jamieson et al., 2014), as significant glacial erosion is dependent on the occurrence of basal melting (Sugden and John, 1976). Models suggest that ice in the GSM has remained cold-based since the early Oligocene (Fig. 2.5; DeConto and Pollard, 2003; Jamieson et al., 2010), leading to minimal rates of erosion (Jamieson et al., 2010, Jaieson and Sugden, 2008). This conclusion is supported by low rates of offshore sedimentation in the catchments down-ice from the GSM (Cox et al., 2010), and the preservation of the alpine landscape observed by Bo et al. (2009) and Rose et al. (2013). Bright reflections in AGAP RES profiles indicate that meltwater is present in the bottom of some overdeepened valleys of the GSM (Bell et al., 2011; Wolovick et al., 2013; Creyts et al., 2014), but suggest that on peaks and valley sides, basal ice remains frozen to the bed.

The preservation of fluvial and/or alpine subglacial topography in the GSM and other locations in Antarctica is significant, because it records the imprint of geomorphological processes that operated prior to the formation of a continent-wide ice sheet, providing a key insight into the landscape evolution of Antarctica potentially going back tens of millions of years (e.g. Young et al., 2011; Rose et al., 2013; Ross et al., 2014; Paxman et al., 2018). It can also inform us about the stability of the ice sheet, serving to constrain any potential retreat during past warm periods such as the Pliocene (ca. 3.5 Ma) by establishing zones where cold-based ice must have been continuously present since glacial inception to prevent the subsequent erosion of small-scale topographic features by large-scale ice sheet flow (Jamieson et al., 2014). If landscape characteristics can be paired with knowledge of the climatic conditions under which they were formed, they will be useful for informing predictions of future ice sheet extent under different climate scenarios, facilitating mitigation and adaption to global climate change.

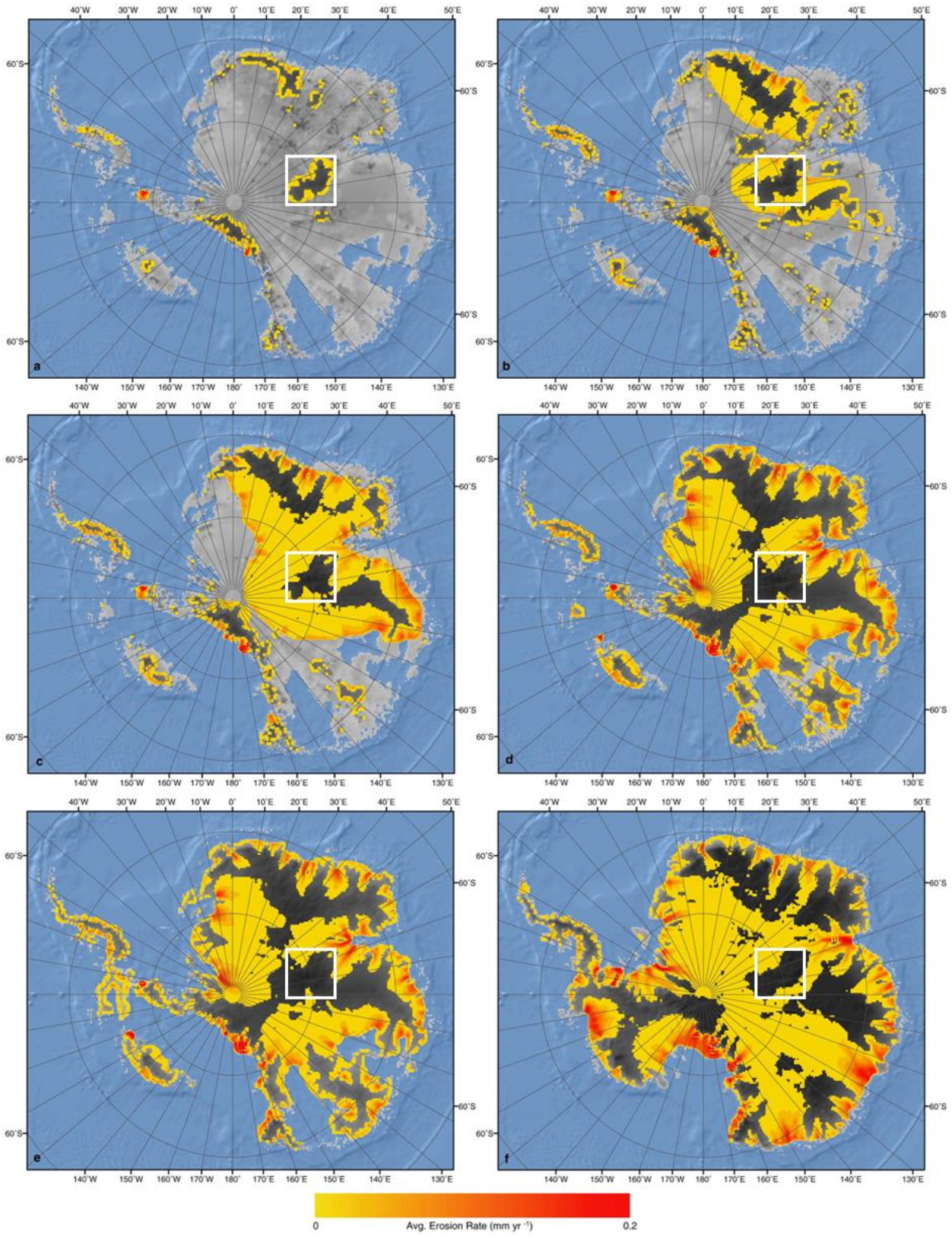

Figure 2.5 – Modelled erosion rates for six stages of Antarctic Ice Sheet growth, from Jamieson et al. (2010). Light grey shading = unglaciated land elevation, dark shading = cold-based ice. White outlines indicate the location of the Gamburtsev Subglacial Mountains (GSM). Panels A-C represent a range of possible ice sheet configurations during orbitally driven oscillations 34-14 Ma, panels D-F represent possible ice sheet extents from 14 Ma up to the present day. Note that cold-based ice is present in the GSM in all scenarios.

2.3. Preservation of basal ice

In addition to its implications for landscape preservation and subglacial hydrology, basal thermal regime is an important control on the preservation of ice itself. Only in locations where an ice sheet has remained continuously cold-based and slow-moving is old basal ice likely to be preserved as part of an undisturbed ice column rather than subject to basal melting, a fact which is of key importance when selecting drilling sites for the extraction of ice cores to provide long-term, high-resolution climate records (Fischer et al., 2013; Van Liefferinge and Pattyn, 2013). While basal thermal conditions depend significantly on geothermal heat flux, pressure-induced melting means that there is an important control exerted by ice thickness. Multiple studies suggest a critical threshold in the range of 2200-2400 m (Fujita et al., 2012; Fischer et al. 2013; Creyts et al., 2014), with basal melting likely at greater ice thicknesses. Highly variable subglacial topography further complicates matters, causing ice flow disturbance (Meyer and Creyts, 2017) or refreezing (Bell et al., 2011), with the result that ice recovered during coring may not be in stratigraphic order, or there may be gaps in the record. Consequently, gaining detailed knowledge of ice thickness and bed topography is an important part of the process for choosing an ice core location, particularly when searching for 1.5 Myr “Oldest Ice” (Fischer et al., 2013). Potential locations for Oldest Ice cores include buried high topography areas in and surrounding the GSM (Fischer et al., 2013), such as the Dome A ice divide (Wolovick et al., 2021), and the region south of Dome A, which is to be the target of an exploratory aerogeophysical survey by the American National Science Foundation (NSF) funded *C*entre for *Old*est Ice *Ex*ploration (COLDEX) during the 2022-2023 Antarctic field season (Fig. 2.6).

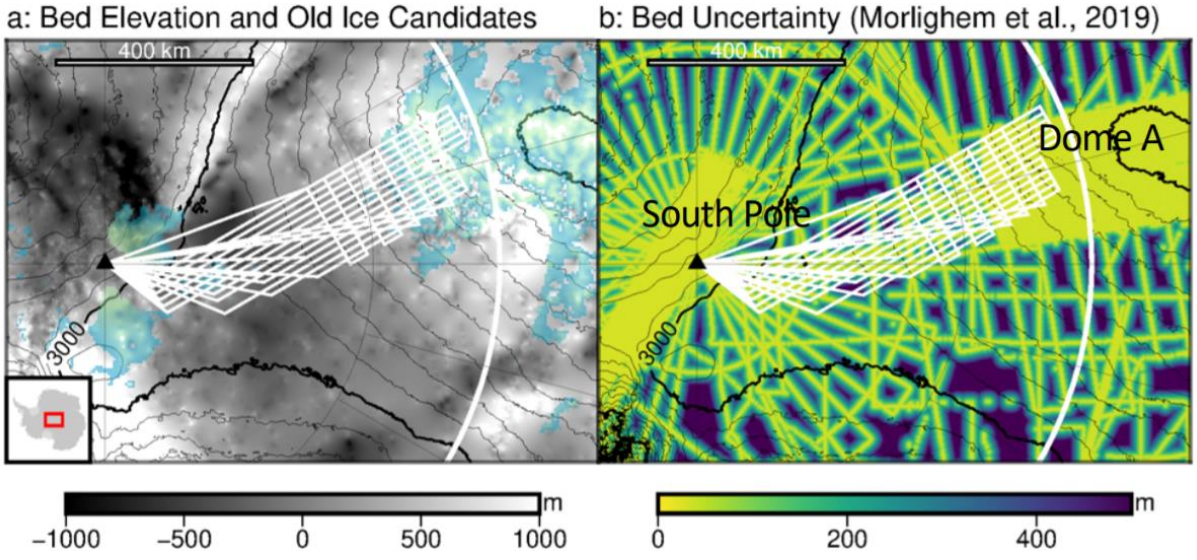

Figure 2.6 – Proposed exploratory survey for COLDEX search for oldest continuous ice core project. Black triangle = South Pole, white lines = proposed aerogeophysical flightlines. From Brook (2020).

3. Project Aim

The overall aim of this thesis is to use ice sheet surface mapping to understand the long-term landscape and ice sheet evolution in the Gamburtsev Subglacial Mountains (GSM) region of East Antarctica.

3.1. Research Themes

The research will address research questions across three key themes:

Theme 1: Developing techniques for mapping subglacial landscapes from the ice surface

1.A. Can manual and/or automated methods of processing ice surface datasets produce useful maps of subglacial landscapes?

1.B. Which methods (manual/automated) are most effective at mapping the locations of subglacial features?

Theme 2: Interpreting processes of landscape evolution in the GSM

2.A. How have glacial, fluvial, and tectonic processes shaped the subglacial landscape of the Gamburtsev Subglacial Mountains?

Theme 3: Understanding ice sheet-landscape interactions in the GSM

3.A. Where in the GSM is cold-based ice likely to have persisted for long periods of time, and thus which sites may be suitable as candidates for ca. 1.5 Ma “Oldest Ice” ice cores?

3.B. What can be inferred from the subglacial landscape about the history and behaviour of the EAIS in the GSM region?

3.2. Objectives

Objectives 1-3 will address questions in Theme 1.

1. To test and compare automated and manual methods for delineating subglacial ridges and valleys from ice surface datasets.

Spatial analysis tools such as slope, curvature, and edge detection will be applied to a range of datasets, and the results compared with each other, and with manual mapping, in order to evaluate the ability of each dataset-method combination to accurately identify subglacial ridges and valleys (c.f. Ross et al, 2014; Chang et al., 2016).

2. To map the subglacial valley and ridge network of the GSM region.

Mapping will be conducted in a GIS using satellite-derived datasets including Radarsat Antarctic Mapping Project (RAMP) (Jezek et al., 2013), Moderate-Resolution Imaging Spectroradiometer (MODIS) Mosaic of Antarctica (MOA) (Scambos et al., 2007) and Reference Elevation Model of Antarctica (REMA) (Howat et al., 2019). Valleys and ridges may be digitised by hand, or, where possible, mapping will be automated using spatial analysis tools (c.f. Ross et al., 2014; Chang et al., 2016; Jamieson et al., 2016).

3. To evaluate the mapping of the GSM region against existing bed elevation models and selected radio echo sounding (RES) data.

The results of mapping will be compared to pre-existing products, such as Bedmap2 (Fretwell et al., 2013) and BedMachine (Morlighem et al., 2020). Both of these contain RES survey data from the AGAP project in the central Gamburtsev region and will therefore allow us to assess how reliably our mapping conforms to actual measurements of the Antarctic ice Sheet bed (c.f. Ross et al., 2014, Jamieson et al., 2016).

Objectives 4 and 5 will address questions in Themes 2 and 3.

4. To analyse the morphometry of the valley network in the GSM region.

Morphometric analyses such as valley spacing, orientation, and layout will be applied to the mapped valley network (c.f. Bo et al., 2009; Rose et al., 2013).

5. To interpret the geological and geomorphological evolution of the GSM region with respect to glacial, fluvial and tectonic processes.

Based on morphometric analyses, we will assess the role of current and former glacial and pre-glacial (fluvial, tectonic) processes in the production of the PGV landscape. Inferences may be drawn about the timing and sequence of different processes based on existing knowledge of Antarctic geology, palaeoclimate and ice sheet history (c.f. Rose et al., 2013; Jamieson et al., 2014).

6. Consider whether these techniques help identify promising locations for further study for Oldest Ice drill sites.

We will explore the use of mapping analysis to potentially identify areas that meet the Oldest Ice criteria of key thickness ranges, long-term cold-based ice, and less chance of modification by flow over complex topography.

4. Methods

4.1. Overview

Several authors previously have found qualitative relationships between the shape of the Antarctic Ice Sheet surface and the large-scale structure of the underlying topography (Remy and Minster, 1997; Le Brocq et al., 2008; Ross et al., 2014; Jamieson et al., 2016; Chang et al., 2016). This includes using discrete features on the surface to infer the shapes, positions and/or connections between subglacial valleys, basins, and mountain ridges, usually as a complement to more conventional means of imaging the bed, such as Radio Echo Sounding (RES; Ross et al., 2014). In this thesis, we use satellite-derived datasets relating to ice surface morphology in isolation, to map the planform geometry of the central part of the Gamburtsev Subglacial Mountains (Fig. 4.1). We tested both automated and manual approaches to digitising changes in ice surface slope, inferred to represent subglacial valleys and ridges, and validated these against existing radar observations (Bell et al. 2011; Ferraccioli et al., 2011), and bed elevation model (Morlighem et al., 2020). We subsequently analysed the morphometric characteristics of the revealed valley and ridge networks, in order to investigate the nature of the subglacial landscape, and address the research questions and objectives detailed in Section 3.

4.2. Datasets

The data used for mapping were all derived from satellite observations of the Antarctic Ice Sheet surface. The two principal data products used were: (1) the Reference Elevation Model of Antarctica (REMA)[2], a high-resolution, continental-scale digital elevation model (DEM) constructed using stereophotogrammetry from commercial optical satellite imagery (Howat et al., 2019); and (2) the RADARSAT-1 Antarctic Mapping Project (RAMP) AMM-1 Synthetic Aperture Radar (SAR) image Mosaic of Antarctica, Version 2[3], representing the radar backscatter intensities recorded by the SAR sensor (Jezek et al., 2013). Both datasets were downloaded and operated on as GeoTIFF rasters in a polar stereographic projection.

4.2.1. Reference Elevation Model of Antarctica (REMA)

REMA is available at multiple horizontal spatial resolutions, with a minimum of 8 m in the study area (Howat et al., 2019), however, given the scale of the features being targeted for mapping (km-scale ridges and valleys), and the practical difficulties of working with large

[2] Available at: https://www.pgc.umn.edu/data/rema/ [accessed 26/10/2021]
[3] Available at: http://nsidc.org/data/NSIDC-0103/versions/2 [accessed 26/10/2021]

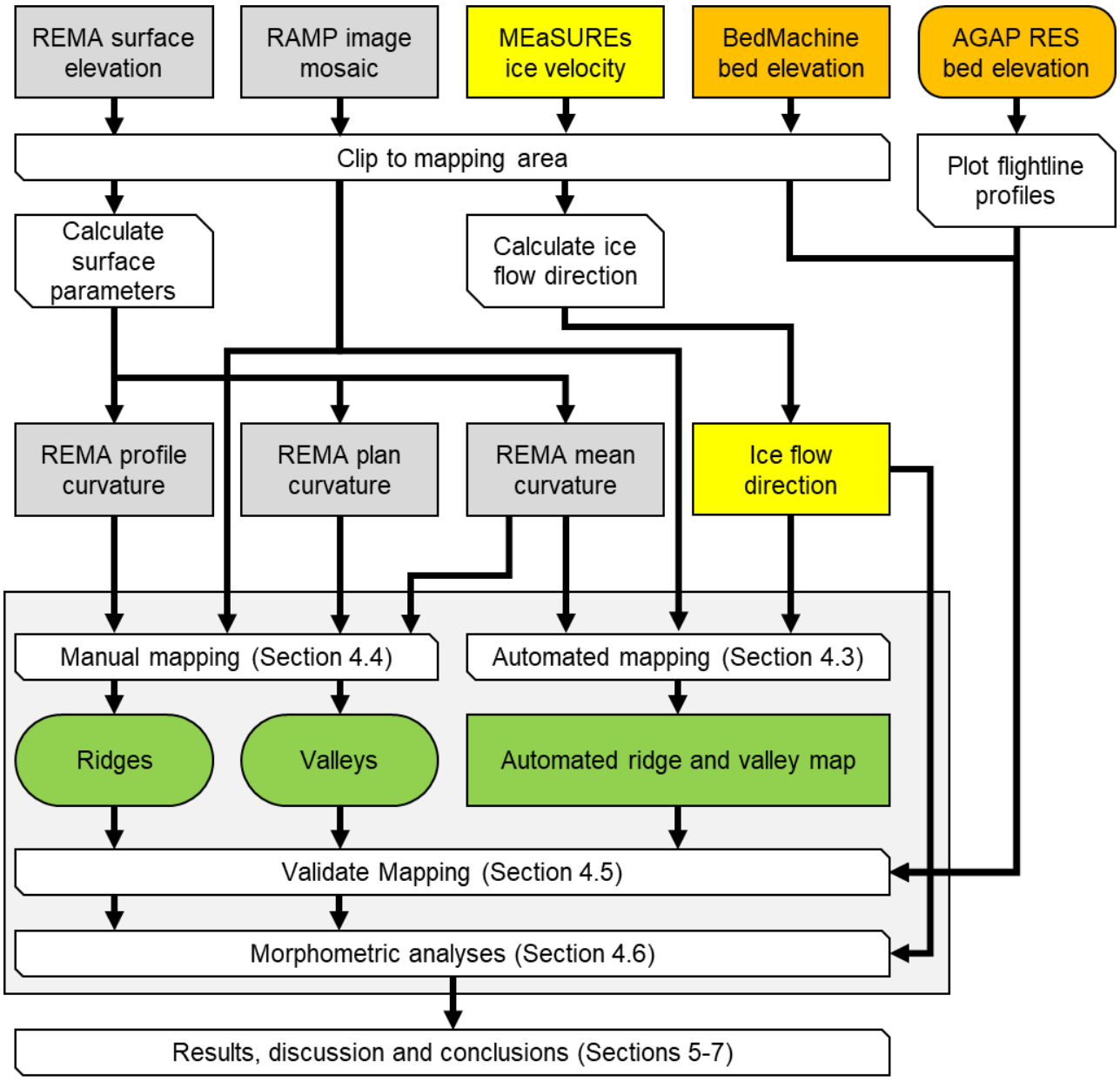

Figure 4.1 – Summary of methods, indicating which datasets were used, and at what stage, as well as how they were processed. Grey boxes = mapping inputs; yellow = auxiliary inputs; orange = validation data; green = mapping outputs. Square-ended boxes = raster datasets; round-ended boxes = vector datasets; cut-cornered boxes = operating steps. Processes within the pale grey box are outlined in greater detail in following sections. REMA = Reference Elevation Model of Antarctica; RAMP = RADARSAT-1 Antarctic Mapping Project; MEaSUREs = Making Earth System Data Records for Use in Research Environments; AGAP = Antarctica's Gamburtsev Province; RES = Radio Echo Sounding.

quantities of data, the 200-m horizontal resolution version was judged sufficient for this work. Vertical errors were calculated by Howat et al. (2019) to be predominantly less than 1 m, compared to airborne laser altimetry. Data coverage over the study area is very good, with data in 99.92% of 200-by-200 m cells. The imagery used to construct REMA spans a date

range of approximately 10 years, with a mean date of 9th May 2015 (Howat et al., 2019). Given the context of the study area, where rates of landscape modification, ice flow, and accumulation are small, it is to be expected that any change in either the subglacial landscape or the ice surface morphology during this time is negligible.

In order to more easily identify subtle changes in surface morphology during mapping, derivatives of elevation were calculated from the DEM using the "Surface Parameters" tool in ArcGIS Pro 2.8.2 (c.f. Ross et al., 2014). The outputs included (i) surface slope, that is the first derivative of elevation, and (ii) surface curvature, the second derivative, or the rate of change of slope (Rémy and Minster, 1997; Le Brocq et al., 2008; Ross et al., 2014). Three distinct versions of surface curvature can be calculated using this tool (Fig. 4.2): (a) profile curvature records the rate of change of slope in the direction of the greatest slope at each location (the along-slope direction); (b) plan curvature is the same quantity in the perpendicular direction (across-slope); (c) standard (or mean) curvature is a mixture of the

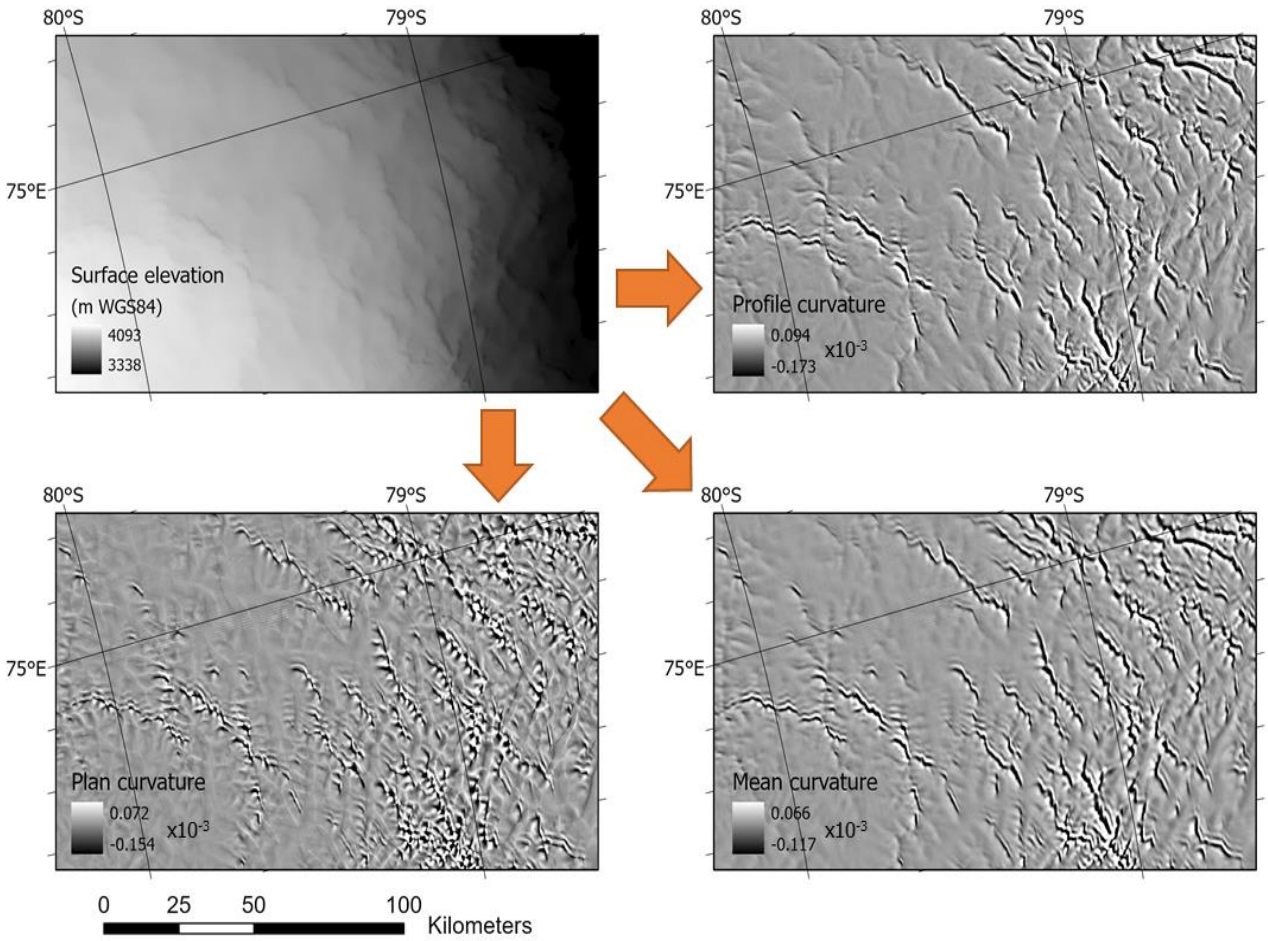

Figure 4.2 – Extracts showing REMA elevation (Howat et al., 2019) and three different types of curvature derived from it for a portion of the area mapped, at 200-m spatial resolution. Ridge and valley patterns are clearly apparent in the curvature data.

two. In each case, the tool calculates curvature from a neighbourhood surrounding each pixel, with the size of the neighbourhood defined by a distance which can be varied to suit the wavelength of variability in the surface. Increasing the neighbourhood distance can reduce the impact of short-wavelength noise, though it may also result in smoothing of sharp contrasts in the data. Several different neighbourhood distances were trialled, resulting in curvature rasters with varying degrees of definition and noise (Fig. 4.3). Based on a visual comparison, it was judged that a neighbourhood distance of 1000 m provided a curvature dataset with an appropriate balance between minimising noise and avoiding blurring of surface features.

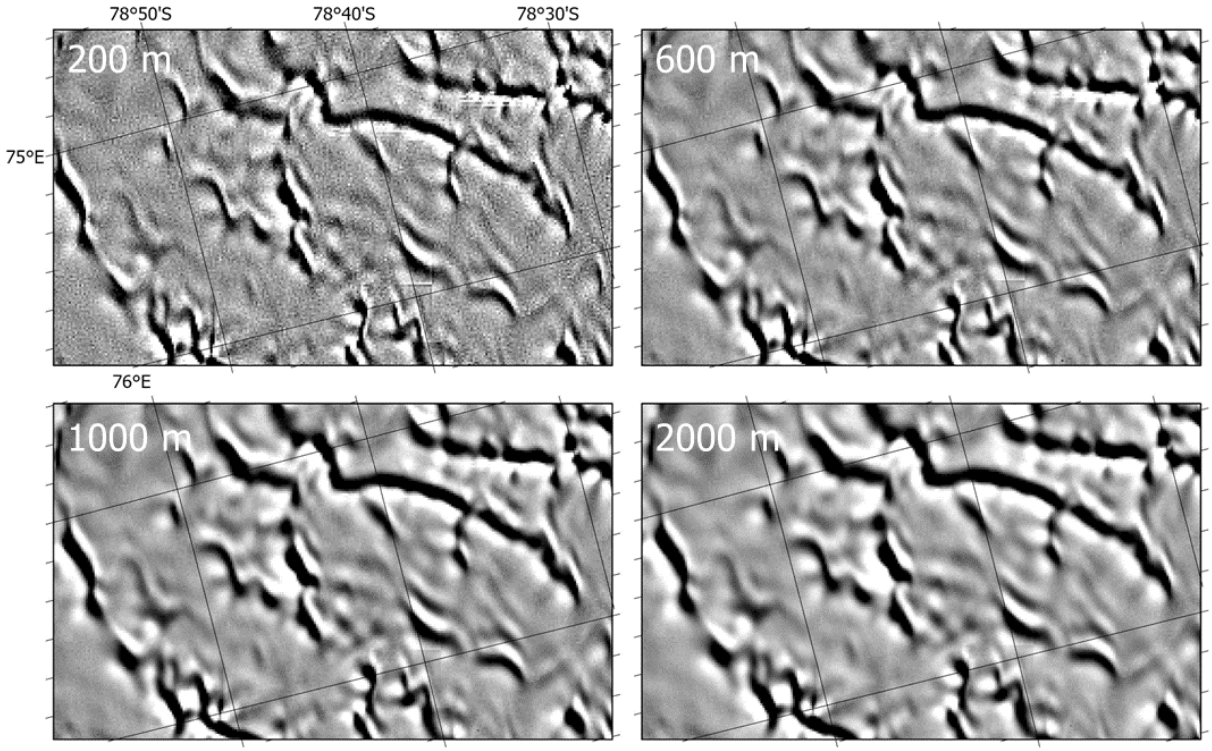

Figure 4.3 – Extracts showing mean curvature of REMA surface elevation calculated using different neighbourhood distances (indicated top-left of each frame). Note that the gradient scale for each image is different, due to the differences in range produced using different distances. The 1000 m version (bottom left) was used in all further mapping and analyses.

When compared to raw elevation and slope, the three curvature products were found to be more suitable for both manual and automated approaches to surface mapping, as they make it easier to identify the position of greatest slope in a step-change surface feature (inferred to have the closest correspondence with the position of a linear subglacial feature), represented by the transition from a curvature minimum to a curvature maximum (Fig. 4.4). Two points of caution in using these products were necessary, however: firstly, as a second-order statistic, surface curvature has a significantly higher noise-to-signal ratio than the

original data. This proved to be a greater issue for automated approaches to mapping than for manual digitisation, as the variability, while significant on a local scale, does not detract as much from the larger-scale structure which is readily discerned by a human observer, apart from in particularly noisy regions. Secondly, the sign attributed to curvature can vary, depending on the precise method of calculation – for the curvature products used here, a positive value represents convexity (i.e. surface curved upwards), and a negative value represents concavity (i.e. surface curved downwards).

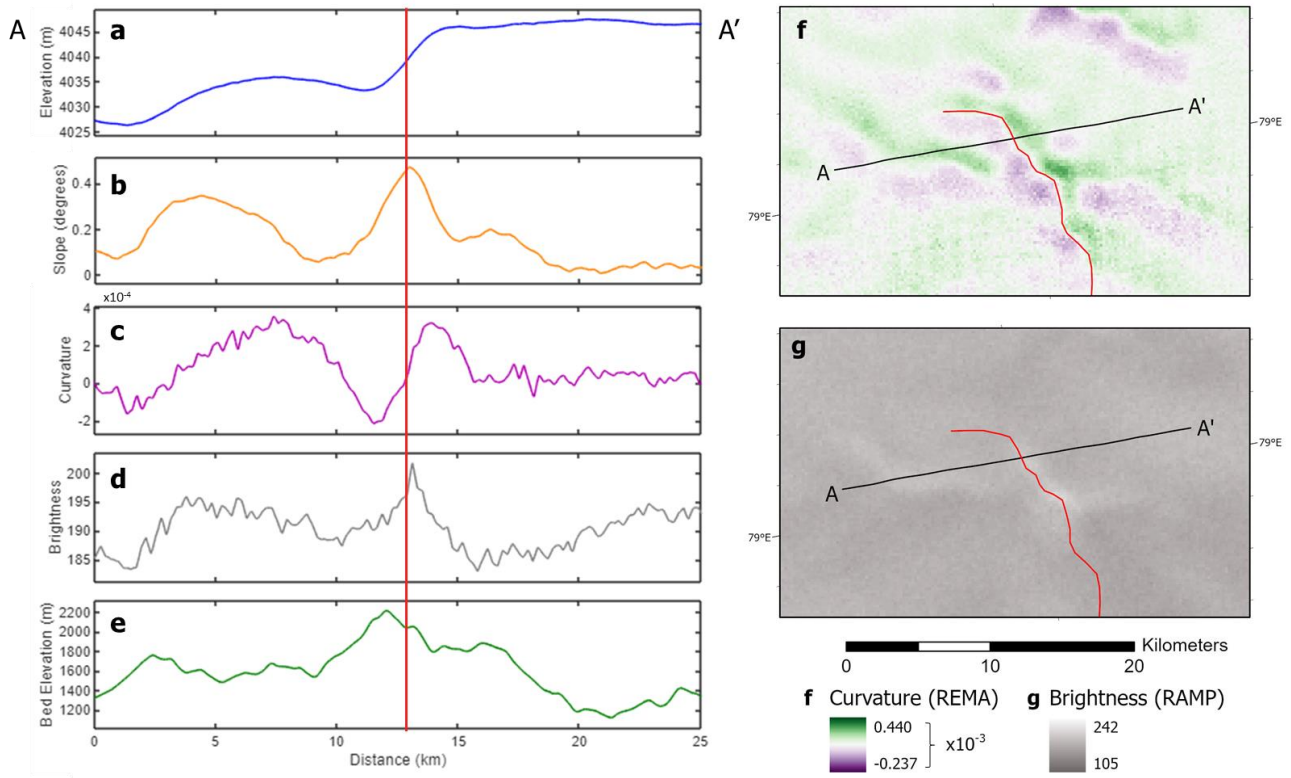

Figure 4.4 – Profile (A-A') across a typical ice surface feature (red line, digitised manually from datasets shown in (f) and (g)), demonstrating the correspondence between the location of a bed ridge and its surface expression in the two datasets used for mapping: a) Reference Elevation Model of Antarctica (REMA; Howat et al., 2019) surface elevation; b) REMA surface slope; c) and f) REMA surface mean curvature (second derivative); d) and g) RADARSAT-1 Antarctic Mapping Project version 2 (RAMP; Jezek et al., 2013) brightness (adjusted backscatter intensity); e) Radio Echo Sounding bed elevation, Antarctica's Gamburtsev Province (AGAP) survey (Bell et al., 2011; Ferraccioli et al., 2011; Corr et al., 2020.

4.2.2. RADARSAT Antarctic Mapping Project (RAMP)

The RAMP image mosaic is also available at multiple spatial resolutions (Jezek et al., 2013); for the reasons given above and for the sake of comparability with REMA, the version with 200 m spatial resolution was used (Fig. 4.5). The pixel values for this dataset represent a

qualitative rather than absolute measure of the intensity of radar backscatter, due to adjustments made to improve the mosaic quality, and are rescaled between 0 and 255 to display as a grayscale image (Jezek et al., 2013). The backscatter intensity is useful because it depends particularly on the slope angle of the ice surface – a flatter surface leads to more signal being reflected directly back to the sensor, and hence a brighter backscatter value (Fig. 4.4). The entire study area is covered without data gaps. The data were collected during September and October 1997 (Jezek et al., 2013).

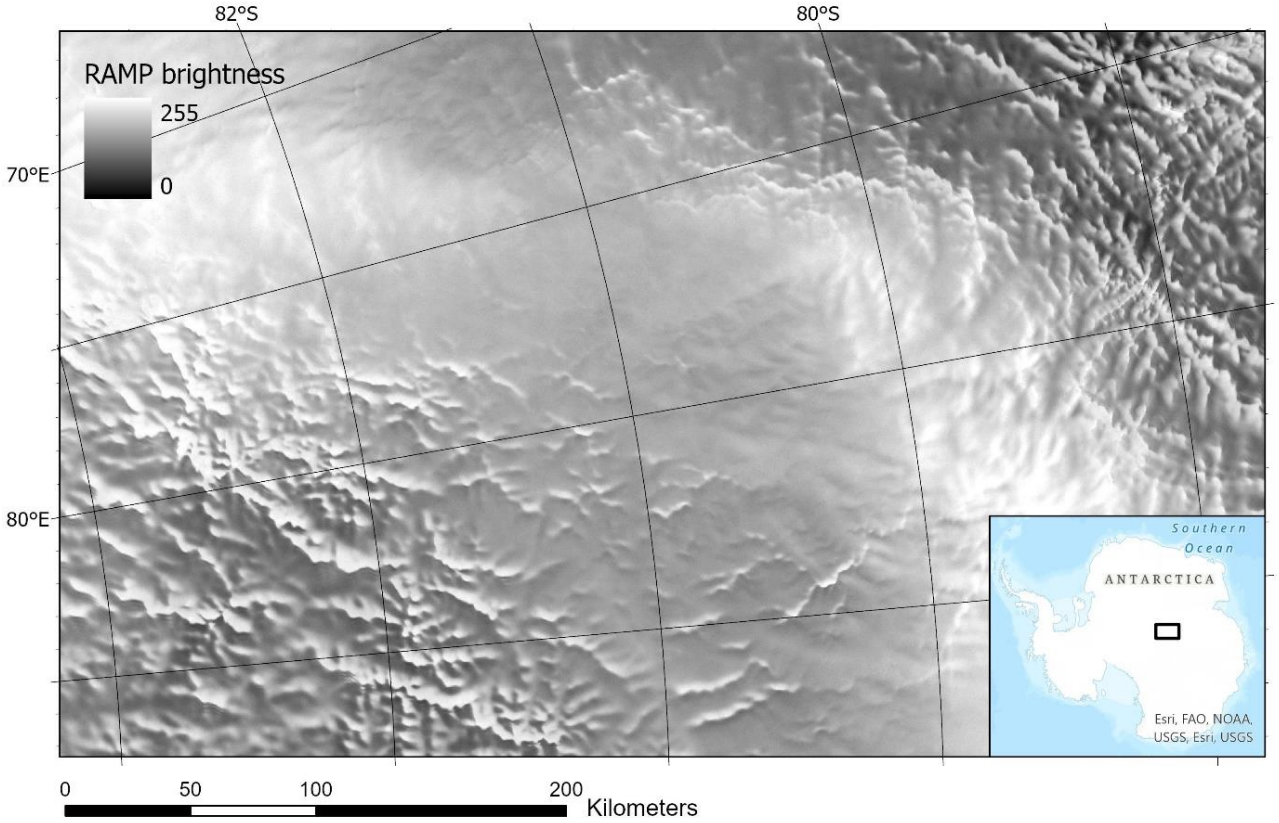

Figure 4.5 – Extract from RAMP image mosaic of Antarctica version 2 (Jezek et al., 2013) covering the area mapped, at 200-m spatial resolution.

4.3. Automated mapping

A variety of approaches to automating the mapping procedure were trialled, with the main aim of identifying edges or contrasts in the input data. The two main approaches tested were: (1) Thresholding – selectively viewing only portions of the data exceeding certain values, in order to isolate, for example, regions of particularly high curvature (c.f. Ross et al., 2014; Chang et al. 2016); and (2) Edge detection – using an automated method of identifying sharp contrasts in the data. Key difficulties in both cases included high noise-to-signal ratios in some of the data, and large spatial variability in contrast. As a result, a multi-step process was developed (Fig. 4.6) involving, first, an adaptive binary thresholding of the

clipped data, in order to account for differences in contrast across the study area, and second, an edge-detection algorithm with a directional input, to identify and categorise transitions in the binary image as linear features representing subglacial ridges and valleys. Additional pre- and post-processing procedures were used to smooth the data and reduce the impact of noise. Both the RAMP image mosaic and the REMA mean curvature product were used as inputs, though slightly different processing steps were required for each data type. InSAR[4] phase-based ice velocities[5] derived as part of the NASA MEaSUREs[6] program, resampled at 200m spatial resolution, provided the directional input for the edge-detection step (Mouginot et al., 2019). All input data were first clipped to the extent of the study area in a GIS, however the script itself (Appendix 1) was written in Matlab (version 2021a), to allow for additional flexibility in some operations (such as the adaptive method of binary thresholding). The full procedure is detailed in the following sections.

4.3.1. Pre-processing

The input data and their spatial referencing information are read into Matlab using the "readgeoraster" function, allowing the data to be operated on using image processing techniques. The following pre-processing steps were required:

1. (REMA only) Data gaps were filled with zero values, as a necessary condition for constructing an adaptive threshold.
2. The data were smoothed using a 5-by-5 pixel median filter, in order to remove noise at the pixel level while preserving the sharpness of edges or contrasts within the data (Fig. 4.7b).
3. thresholding process. Since the convex portion of a step-change in surface elevation occurs up-flow of the concave portion (Fig. 4.4), this allows for consistent identification of the maximal slope as the downflow edge of a positive region.

4.3.2. Adaptive thresholding

Before applying edge detection, a binary threshold was applied to each of the (pre-processed) input datasets. This produced a simplified representation of the data (mask) in which pixels were deemed either to have "high" (1) or "low" (0) curvature/brightness value, facilitating the identification of edges, particularly in regions of more gradual contrast. Rather than a global threshold value, an adaptive threshold matrix was constructed, in which a

[4] Interferometric Synthetic Aperture Radar
[5] Available at https://nsidc.org/data/nsidc-0754/versions/1 [accessed 29/07/2022]
[6] *M*aking *Ea*rth *S*ystem Data Records for *U*se in *R*esearch *E*nvironment*s*

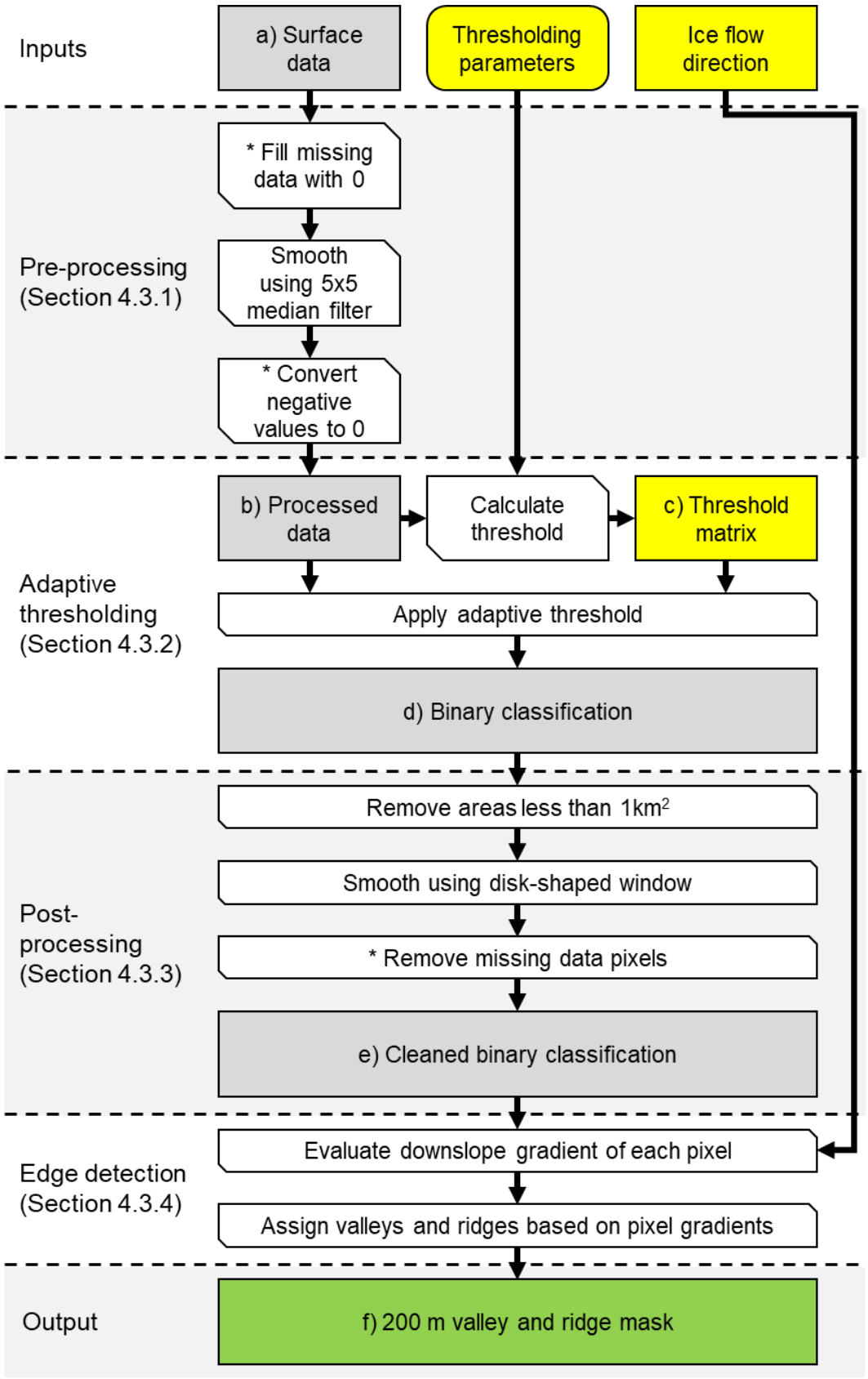

*Figure 4.6 – Summary of automated mapping procedure. Symbology as in Fig. 4.1 (round-cornered box representing user inputs). Steps marked with * were necessary only when using REMA curvature as the input surface dataset (due to data gaps).*

unique threshold was determined for each pixel based on the average intensity within a local neighbourhood (Fig. 4.7c). This method accounted for any spatial variability in contrast within the data, allowing for small but locally significant changes to be identified while reducing the impact of noise in high-variability regions.

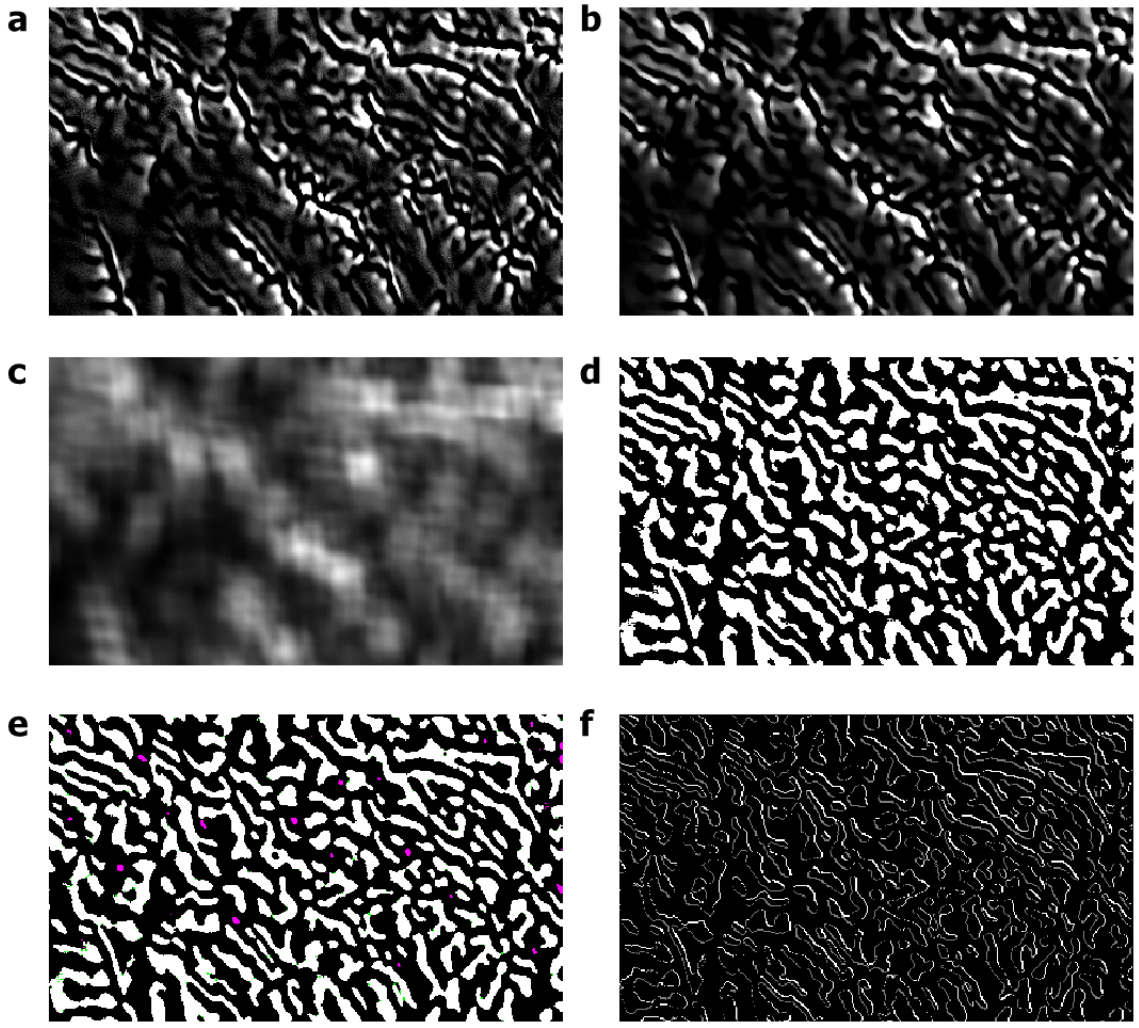

Figure 4.7 – Visualisations of different stages of the automated mapping procedure, using a 243-by-405 pixel (~ 4000 km^2) extract from REMA mean curvature as the input data (a). Subsequent panels show: b) the input after application of a 5-by-5 pixel median filter; c) the adaptive threshold matrix (brighter pixels indicating a higher threshold); d) the initial binary classification; e) the cleaned binary classification (magenta = pixels removed due to filtering of small regions, green = pixels added due to smoothing); and f) the final valley and ridge mask (black = background (0), grey = valley (1), white = ridge (2)). Note that values in images a-c have been arbitrarily adjusted and stretched over a black-to-white scale for ease of visualisation. Panel lettering corresponds to marked stages in flowchart in Fig. 4.6.

The adaptive thresholding algorithm used has several parameters that can be tuned, including the neighbourhood size, the statistic applied, and a sensitivity factor. In order to identify the most suitable values to use, each parameter was systematically varied (Table

4.1), such that several different maps were produced from each of the two input datasets (Fig. 4.8). Differences introduced by the variation of factors include particularly the identification of small and/or connecting features. When selecting which results to investigate further, extracts from the maps produced (after further processing and edge detection were applied) were inspected and compared, with those in which these smaller features were more often identified judged to be more useful. There was to an extent a trade-off made here between detail and the presence of potentially erroneous/artefact features; settings conducive to the identification of smaller features (low sensitivity, small neighbourhood size) were also more likely to misinterpret artefacts or noise in the data as genuine features. Based on this qualitative assessment, those maps selected as giving the optimal balance between representation of smaller features and oversensitivity to noise used the tuning parameters identified in bold in Table 4.1 (corresponding to extracts a and f in Fig. 4.8).

Table 4.1 – Tuning parameters for adaptive thresholding on the two datasets used.

Input Dataset	Parameter	Range / options	Increment	Optimal value
REMA mean curvature	Neighbourhood statistic	Mean, median, Gaussian weighted mean	N/A	**Mean**
	Sensitivity factor	0-1	0.1	**0.5**
	Neighbourhood size (N-by-N pixels / km)	25-275 / 5-35	50 / 10	**75 / 15**
RAMP image mosaic	Neighbourhood statistic	Mean, median, Gaussian weighted mean	N/A	**Mean**
	Sensitivity factor	0-1	0.1	**0.6**
	Neighbourhood size (N-by-N pixels / km)	25-275 / 5-35	50 / 10	**25 / 5**

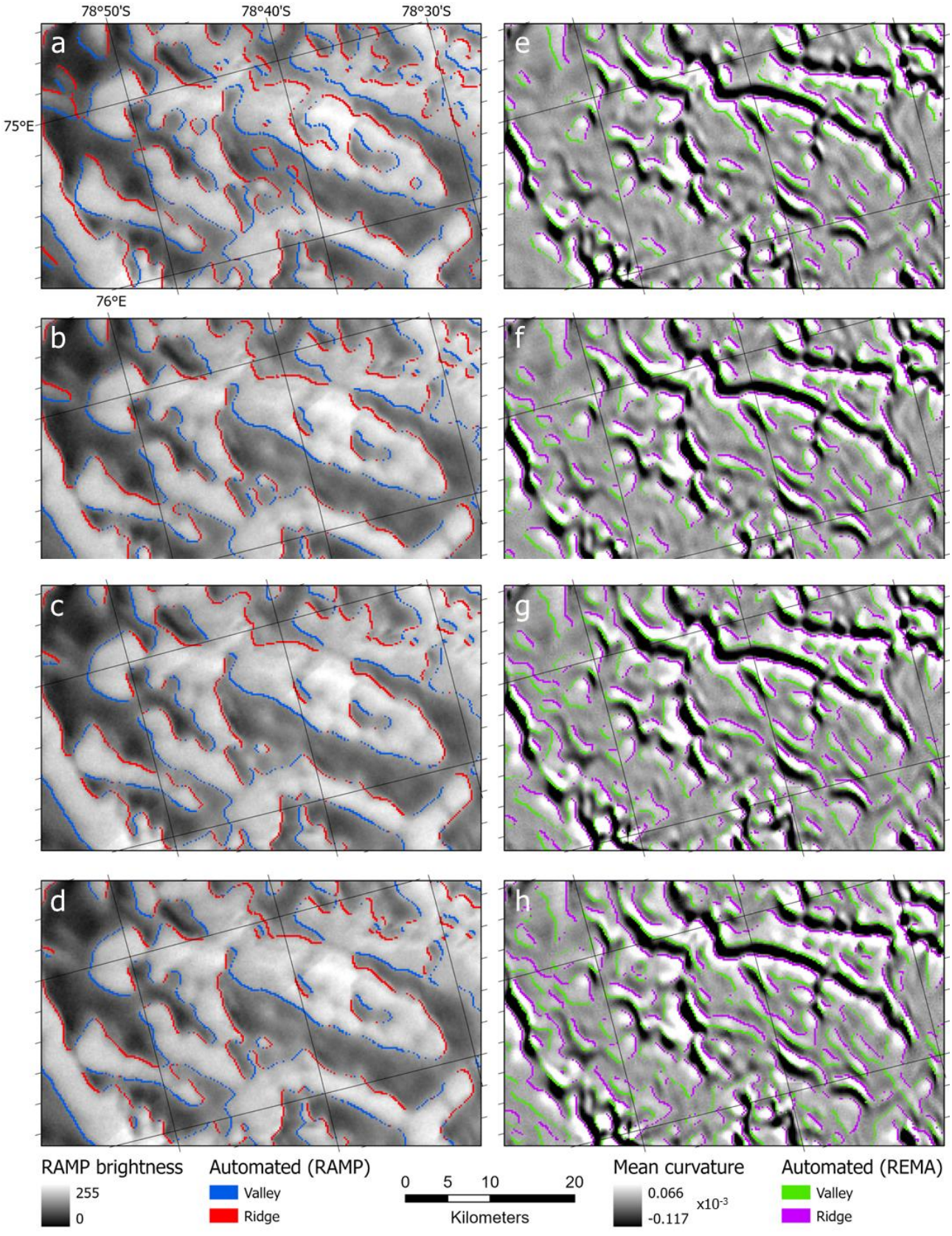

Figure 4.8 – Extracts from automated ridge and valley maps created using different input data, thresholding sensitivity and neighbourhood sizes, overlaid over the input data used (a-d: RAMP image mosaic; e-h: REMA mean curvature). For a-d: sensitivity = 0.5; neighbourhood size = a) 5; b) 15; c) 25; d) 35. For e-h: sensitivity = e) 0.1; f) 0.5 g) 0.7 h) 1; neighbourhood size = 15. Mean was used as the averaging statistic for all examples.

4.3.3. Post-processing

The following clean-up operations were applied to improve the mask quality before moving on to edge detection (Fig. 4.7e):

1. All positive regions of the mask with areas of less than 1 km^2 (25 pixels) were removed, as likely artefacts due to noise. This cut-off was selected because it had already been identified as the minimum appropriate window size for calculating curvature, due to noise dominating variability on smaller scales.
2. The mask was smoothed using a disk-shaped moving window of radius 1 pixel, to fill in small gaps likely caused by noise.
3. (REMA only) Every pixel for which original data were missing was removed from the mask.

4.3.4. Edge detection

An edge-detection algorithm was developed in which the gradient in the cleaned mask was evaluated for each pixel according to the mean flow direction – derived from MEaSUREs - within the corresponding 200-by-200-m area. For the purposes of this comparison, flow direction was rounded to the nearest 8-directional value (i.e. 45° 'sectors'), and each pixel in the mask was compared with its neighbour immediately downflow. If there was no change in value (i.e. both pixels had value 1 or both pixels had value 0), the pixel was marked as neither a ridge nor a valley (0). If there was a positive change downflow (from 0 to 1, representing increasing curvature/brightness), the pixel was marked as a valley (1). If there was a negative change downflow (from 1 to 0, representing decreasing curvature/brightness), the pixel was marked as a ridge (2). Every pixel for which original data were missing was then converted back to a missing data marker (-1). This procedure is summarised in Table 4.2. The resulting edge mask (Fig. 4.7f) was saved as a GeoTIFF file using the same spatial referencing information as the original data.

Table 4.2 – List of values and their meanings in the final feature masks.

Change downflow	Value assigned	Meaning
N/A	-1	Original data missing
None	0	Neither a ridge nor a valley
Positive (0 to 1)	1	Valley
Negative (1 to 0)	2	Ridge

4.4. Manual mapping

Manual mapping was conducted using a GIS, with changes in slope being manually traced as vector line features in a geodatabase, with reference to the RAMP image mosaic and all three versions of REMA curvature. An important difference between this approach and the automated procedure was that the manual mapping was conducted as a deliberately interpretive process. Ridges and valleys were digitised separately, distinguished from one another both by the local flow direction with regard to changes in curvature/brightness, and by the spatial relationships between features. Based on the existing knowledge from RES surveys (Bo et al., 2009; Rose et al., 2013), and initial impressions formed when examining the datasets used for mapping, it was assumed that the planform geometry being mapped would broadly resemble that of an alpine mountain landscape originally shaped by fluvial erosion. As a result of this assumption, inferences could be made which were not feasible to automate, particularly connections between features, such that isolated ridge or valley lines were joined – where small gaps existed - to depict the likely structures of mountain chains and drainage networks.

It was noted early on during mapping that ridgelines were often expressed more prominently, and with sharper transitions, than valley lines. This makes practical sense given that ice thickness over ridges must be significantly less than over valleys, leading to a greater flow disturbance and a rougher ice surface for the ridges than the valleys, which is reflected in the range of curvature values (Fig. 4.9). Because of this fact, a procedure for manual mapping was followed whereby ridges in an area were digitised first, followed by valleys. Following a similar principle, the most obvious features were traced first, then subtler lineations were picked out, especially where these connected with established ridges or valleys. All digitised features were subsequently treated equally, with some exceptions: in places, a connecting feature was inferred with no indication of its presence in any of the mapping data, or (in the case of valleys) two possible connections were marked where there was ambiguity. Such cases mostly arose due to the assumption that the landscape would constitute a physically plausible fluvial palaeo-drainage network, which, if true, occasionally required drainage routes or drainage divides that were not observed. These features were marked as “low confidence” and were later excluded from the dataset when performing some of the morphometric analyses.

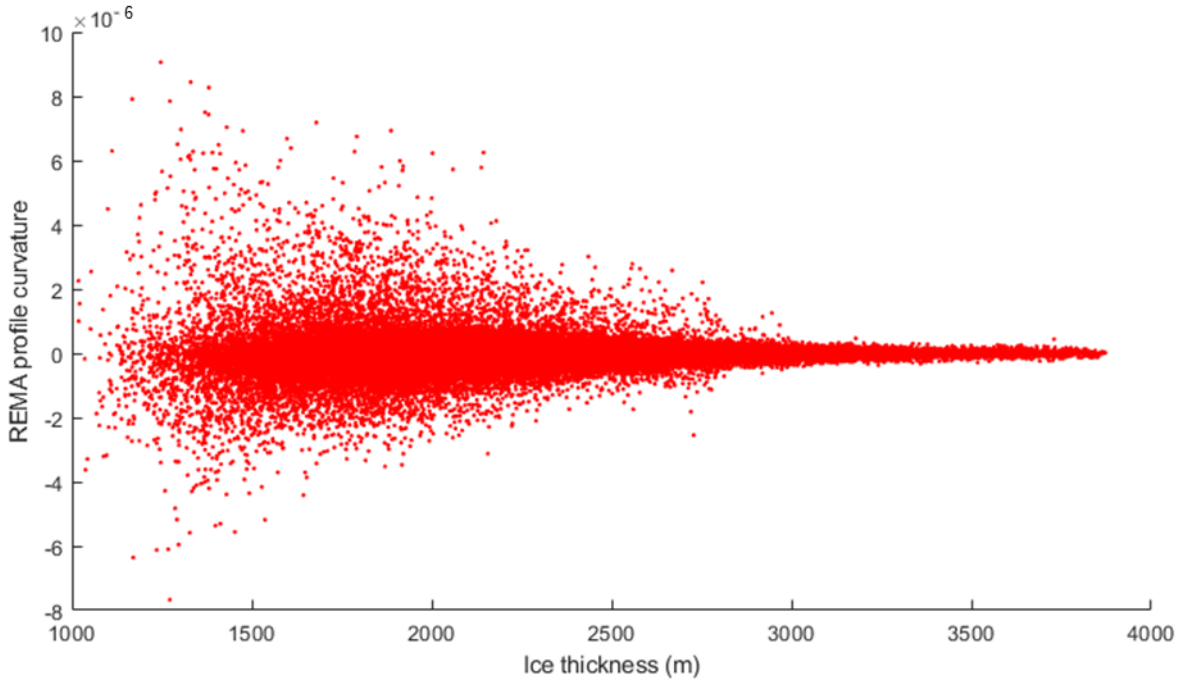

Figure 4.9 – Relationship between REMA profile curvature and Bedmap2 gridded ice thickness across the mapped area. Each point represents a 1-km^2 grid cell (the 1-km resolution version of REMA rather than the 200-m version was used to produce this plot, for comparability with Bedmap2 resolution and due to the high quantity of data).

4.4.1. Ridges

Ridge features proved to be easiest to observe and trace in the RAMP image and in the profile (along-slope) version of REMA surface curvature (Fig. 4.10, 1). The two datasets are broadly consistent in the shape and position of these features, though in places there is a small (generally less than 1 km) spatial offset between inferred ridge locations. In such cases, the location according to RAMP was preferred, due to the greater sharpness of the transitions representing the features in this image than in the curvature dataset making them easier to digitise consistently. In some areas, particularly near the ice divide, however, contrast in RAMP is greatly diminished; in these cases all positions were inferred from REMA. Additionally, while individual ridgelines were more clearly represented in RAMP, the connections between them were often much clearer in REMA profile curvature. Where possible, therefore, those ridges in an area able to be mapped from RAMP were digitised first, then those only clearly visible in REMA.

4.4.2. Valleys

Valley lines were easiest to trace from RAMP, and from the plan (across-slope) version of REMA curvature (Fig. 4.10, 2), though many were also inferred from the positions of the

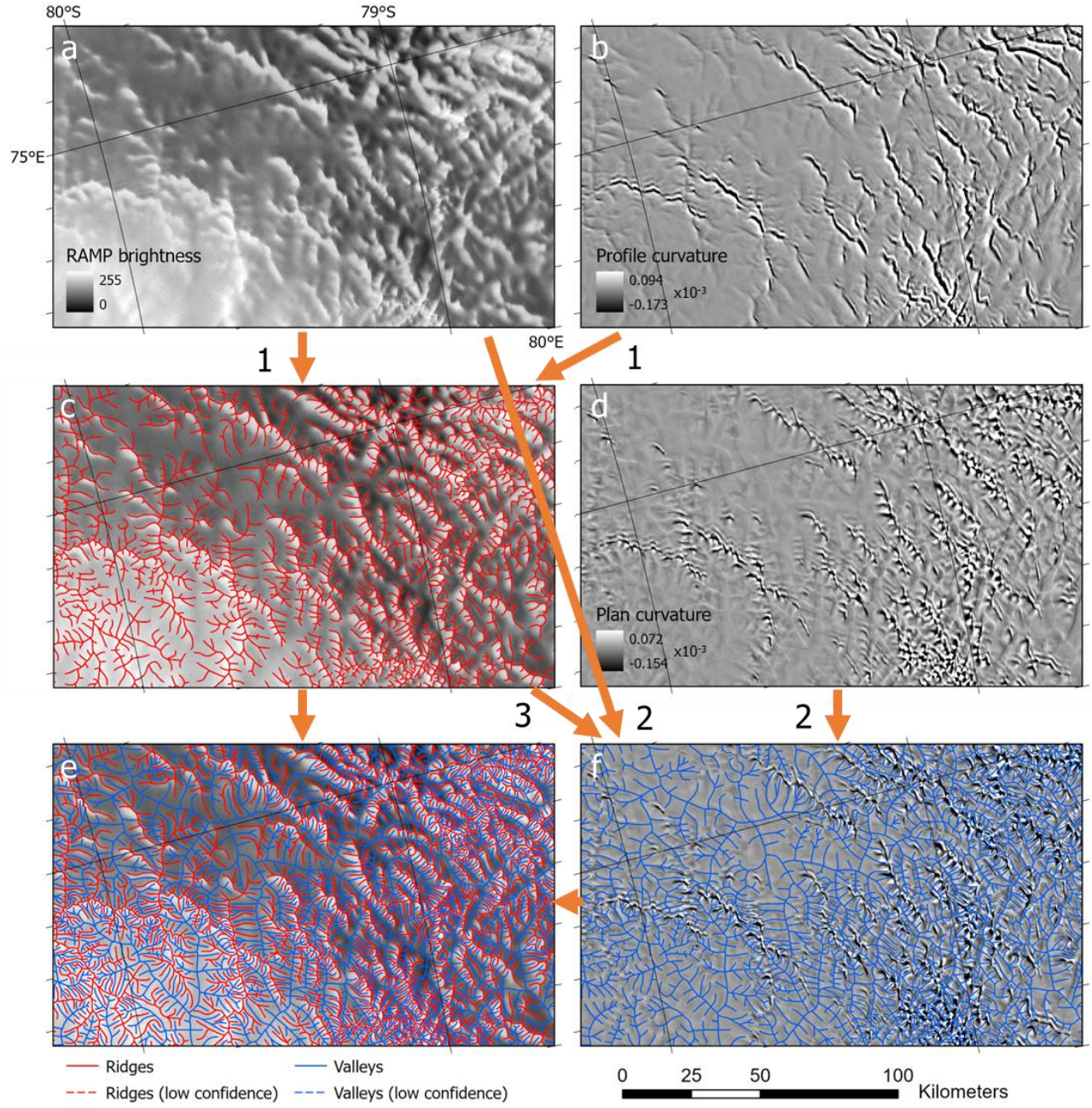

Figure 4.10 – Extracts from manual mapping demonstrating the datasets and procedure used to digitise ridges and valleys. Datasets: RAMP image mosaic (a, c, e); REMA profile curvature (b); REMA plan curvature (d, f). Orange arrows and numbers indicate steps referred to in text.

surrounding ridges (Fig. 4.10, 3). Where valleys appeared narrowest (~ 1-3 km), the transition from dark to bright in RAMP often coincided with a distinct maximum in plan curvature. Where valleys were slightly wider (~ 4-6 km), this transition would sometimes coincide with the centre of a broader plateau in plan curvature, bounded up-flow by a maximum and down-flow by a minimum. The widest valleys, which constitute the main trunk of the inferred palaeo-drainage system, were the least well defined, being represented for the most part by smoothness in both RAMP and REMA plan curvature. Each valley was

digitised from its upper end towards its terminus (usually where it joins another valley), such that the direction of each line would reflect the most likely direction of ice-free palaeo-drainage[7]. As much as was practicable, each valley line was extended as far as possible rather than segmenting what were likely to be continuous drainage routes, in order to preserve valley connectivity and the usefulness of valley length as an informative measure of the landscape.

4.5. Validation

Two kinds of data were used to validate the surface mapping: Radio Echo Sounding (RES) data from the Antarctica's Gamburtsev Province (AGAP) airborne survey[8] (Bell et al., 2011; Ferraccioli et al., 2011; Corr et al., 2020) were used to compare the locations of ridges and valleys with those mapped along discrete two-dimensional profiles, while the BedMachine Digital Elevation Model[9] (DEM; primarily constructed in this region using the AGAP data; Morlighem et al., 2020) allowed for comparison with the overall plan layout of the mapped data. Both methods were employed to qualitatively confirm the validity of using ice surface morphology to map bed features, by demonstrating the general correspondence of these maps with independent measurements of bed topography. No attempt was made to establish a quantitative relationship between locations mapped from the surface and those visible in the bed data, due to the observation made during initial trials that features mapped from the surface displayed minor but variable offsets from the bed features they were assumed to represent. An attempt was made to constrain the potential offset distances between bed features and their surface expression, however no systematic global analysis was carried out; as such, the accuracy in location of any *individual* mapped feature has an associated uncertainty (discussed below), despite any overall robustness established between the *patterns* of real and mapped planform geometry.

4.5.1. AGAP Radio Echo Sounding (RES) profiles

The processed AGAP RES data (Corr et al., 2020) were downloaded as point features, and twelve series of consecutive points that traversed significant ice surface features within the mapped area were selected, from both of the perpendicular horizontal directions sampled by the AGAP survey (Fig. 4.11). The bed elevation values from these points were extracted

[7] Determination of valley direction constituted the only instance in which existing bed models were referred to during mapping, as the theoretical flow direction was not always clear from the two-dimensional network alone. This affected only the direction of the mapped feature, not its position.
[8] Available at: https://data.bas.ac.uk/full-record.php?id=GB/NERC/BAS/PDC/01544 [accessed 25/07/2022]
[9] Available at: https://nsidc.org/data/nsidc-0756/versions/2 [accessed 23/01/2022]

and plotted as two-dimensional profiles. The locations of the mapped ridges and valleys from both automated and manual methods that intersected these profiles were identified in a GIS and added to the plots. These plots were inspected on a case-by-case basis to identify ridges and valleys from the bed elevation profiles and compare them to the locations predicted by each method of surface mapping. Metrics then calculated included the proportion of features that were successfully matched, the proportion of unsuccessful matches (either where a bed feature was not captured in the mapping, or where a mapped feature was not observed on the bed), and the mean offset distance between successfully matched bed features and their mapped locations.

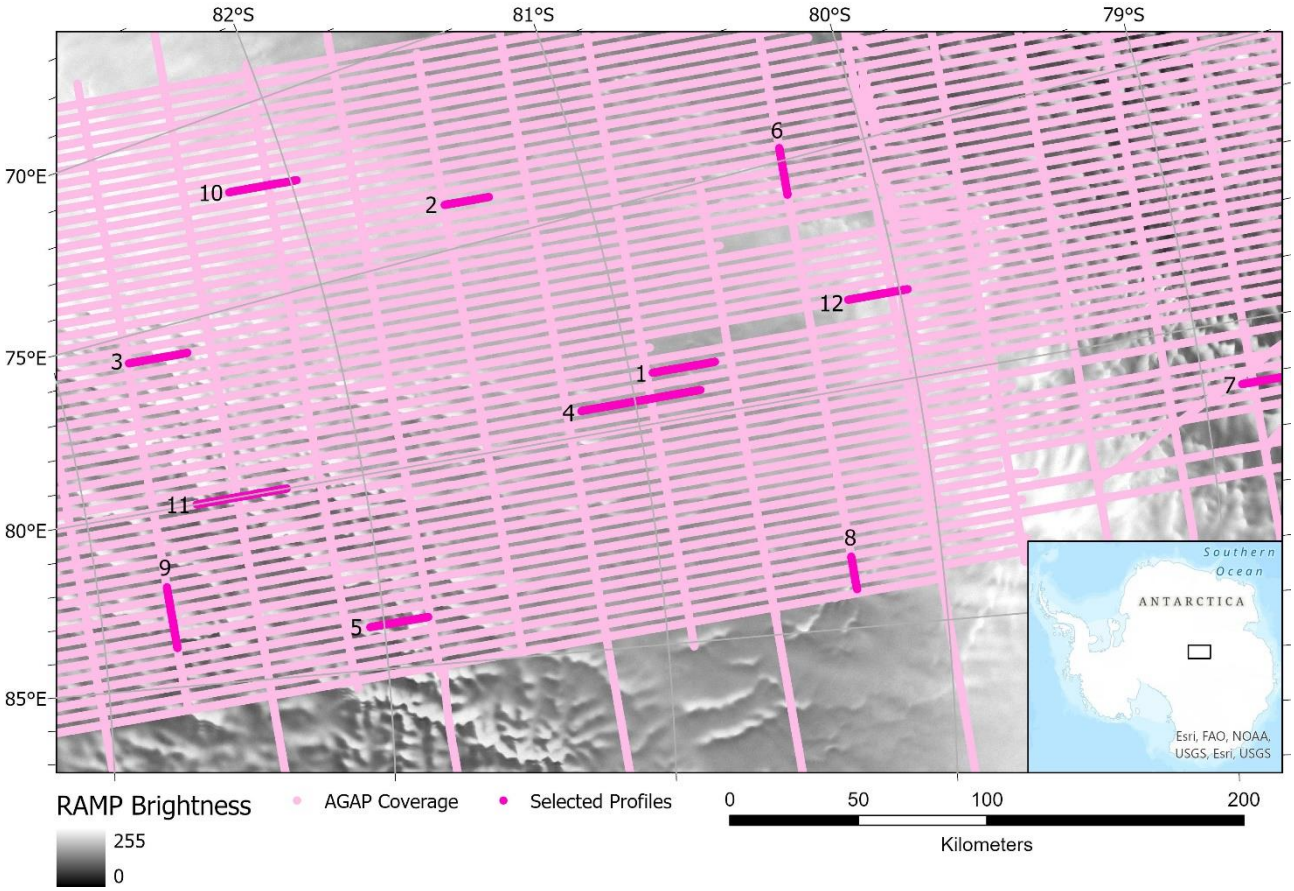

Figure 4.11 – Locations of bed profiles taken from AGAP RES data for comparison between observed and mapped subglacial features. Overlaid on RAMP v2 image mosaic (Jezek et al., 2013).

4.5.2. BedMachine Digital Elevation Model (DEM)

The BedMachine Antarctica version 2 bed DEM (Morlighem et al., 2020) was used to compare the planform ridge and valley networks derived via manual mapping to existing data across the whole area, and in three dimensions. Since no bed elevation data were used

during the mapping process[10], this was an independent test of mapping accuracy, as well as an opportunity to assess whether surface mapping offered any improvement to the level of detail in the observable planform geometry. Qualitative comparisons were made particularly of the locations of valleys and ridges that were large enough to be resolved in the DEM (typically no less than 5 km wide; Morlighem et al., 2020) and in areas where features mapped were not included in the gridded bed topography.

4.6. Morphometric analyses

4.6.1. Feature length and orientation

The lengths of both valley and ridge features were calculated, binned, and plotted as frequency distributions. The orientations (non-directional) of lines were calculated on a segment-by-segment basis, binned, and plotted as circular histograms (rose diagrams), with the bin totals scaled according to the total length of line rather than the number of line segments. “Low confidence” features were included in these calculations, however in the case of ridge features, a second set of histograms was also plotted, containing the lengths and orientations of the “low confidence” features only, to check whether there was any difference in directional trend to the overall network. Additionally, for each of these three groups of lines, the angle between each line segment and the local mean ice flow direction, was calculated and plotted between 0° (line direction parallel to ice flow) and 90° (line at right angles to ice flow), to assess whether there was a significant relationship between the direction of ice flow and the orientations of the features that could be observed on the ice surface.

4.6.2. Valley width

A map of valley spacing (equivalent to the ridge-to-ridge valley width, or the wavelength of valley-scale topography) was calculated based on the minimum distance of each cell from the nearest valley line. A 500-by-500 m grid concordant with BedMachine was used, for the sake of comparability. A local mean was taken using a circular moving window of radius 25 cells (12.5 km) to produce a more meaningful visualisation, from which variation in feature spacing across different regions could be assessed. Since the value calculated in the first step is equivalent to half the ridge-to-ridge valley width, the final statistic was multiplied by two to represent the full wavelength of the ridge-and-valley topography.

[10] Determination of valley direction constituted the only instance in which existing bed models were referred to during mapping, as the theoretical flow direction was not always clear from the two-dimensional network alone. This affected only the direction of the mapped feature, not its position.

4.6.3. Valley long-profiles

Valley long-profiles were derived from BedMachine Antarctica bed elevation (Morlighem et al., 2020) by interpolating along valley lines taken directly from the manually mapped valley network. Several lines were selected in order to provide a range of different valley types (e.g. varying length, width, mean elevation).

4.7. Palaeo-drainage modelling

Palaeo-drainage was investigated using a flow-direction raster interpolated from the directions of the individual valley lines, according to the method outlined in Figure 4.12. A set of point features was extracted at regular intervals along each line, containing the information about the direction of the line at that point, as derived from its geometry. These were used as input data for a tension spline interpolation to produce a continuous flow direction raster across the study area, gridded, like the other analytical results, at 500 m. Hydrological variables including flow accumulation and stream order were derived from this artificial flow direction raster using standard GIS tools. While line direction was originally calculated on a continuous scale from 0° to 360°, a simplified 8-point version (created by rounding to the nearest 45°) was required to assess stream ordering, due to the limitations of the GIS tools being used. As a result, two versions of flow accumulation were created – the more detailed version (V1) uses the continuous range of flow directions observed (a “D-INF” approach), while the simplified version that matches the derived stream network (V2) routes flow only in 8 directions (i.e. from each cell to one of its immediate neighbours; a “D8” approach). An additional flow direction raster was calculated by filling sinks in the BedMachine topography, and used to derive the same hydrological measures, to compare the level of detail achieved by the results derived from surface mapping. No correction was made in either case for isostatic elevation changes between the modern and pre-glacial landscapes, because (1) the ice thickness has no sharp gradients across the area, and will be smoothed by the relatively long-wavelength crustal uplift signal, and so there will be no *significant* differences likely in the regional pattern of uplift/subsidence across the area (testified by the preservation of a coherent fluvial valley network), and (2) the derivation of flow directions from the mapped network is largely independent of elevation in the first instance, simply relying on the context of the planform fluvial geometry (Section 4.2.2).

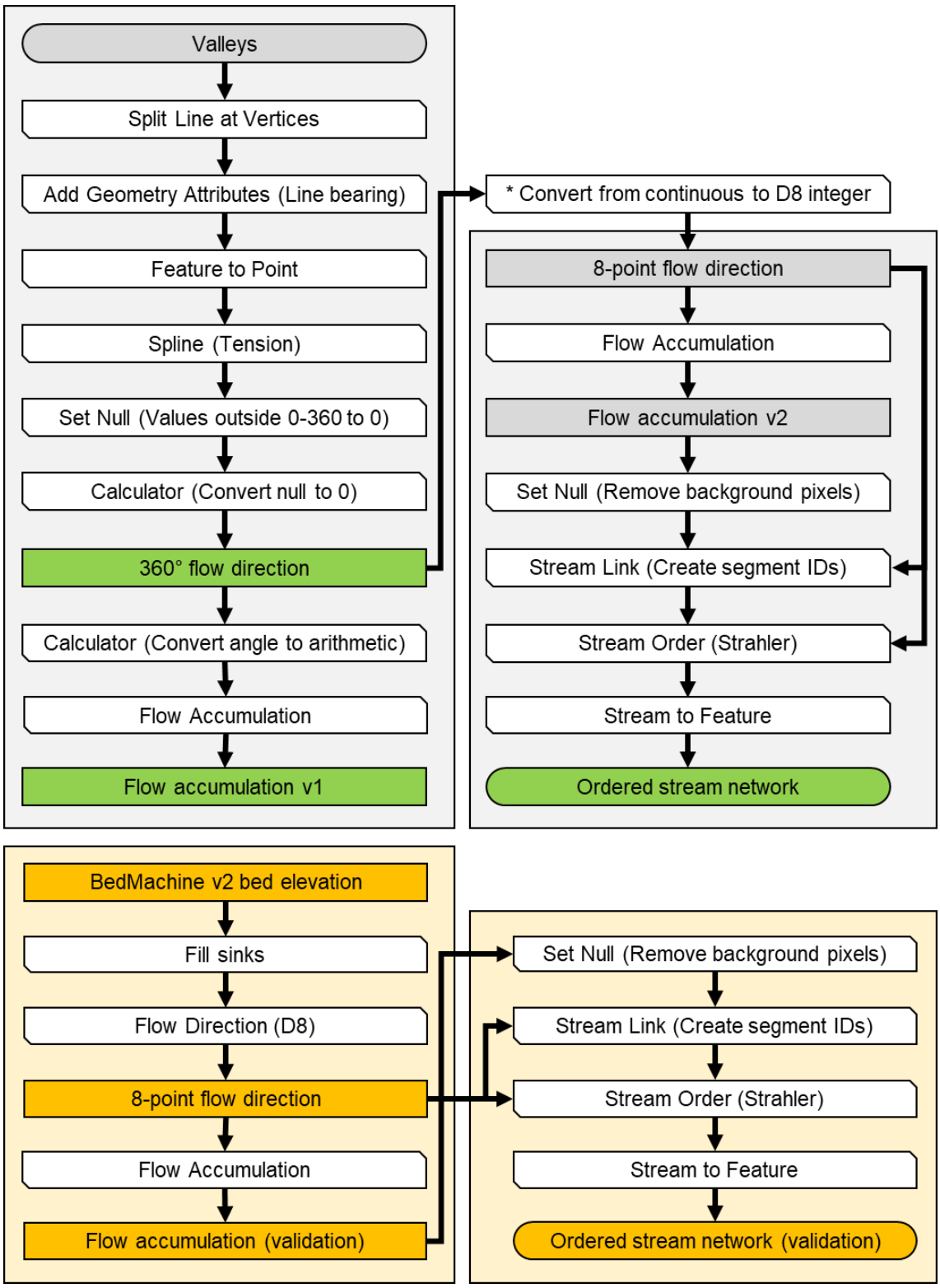

*Figure 4.12 – Summary of procedure used to derive palaeo-flow directions, drainage areas, and stream orders from manually-mapped valley lines, and for validation purposes from BedMachine v2 bed topography (Morlighem et al., 2020). Symbology as in Fig. 4.1. Procedures contained within pale grey/orange boxes were conducted as sequences of geoprocessing operations in ArcGIS Pro 2.8.2; steps marked with * were performed in Matlab (2021a) (Appendix 1). D8 refers to an 8-directional parameter (45-degree segments of a circular compass rose).*

5. Results

5.1. Automated mapping

The automated mapping results shown in Figure 5.1 indicate the inferred positions of bed valleys and ridges across the study area, based on application of the procedure outlined in Section 4.3 to the two input datasets, the RADARSAT-1 Antarctic Mapping Project (RAMP) version 2 image mosaic (Jezek et al., 2013) and the Reference Elevation Model of Antarctica (REMA; Howat et al., 2019) in the form of mean curvature. In the RAMP map (Fig. 5.1a), 4.22% of 200 m^2 grid cells were identified as valleys and 3.97% as ridges; in the REMA mask (Fig. 5.1b) 3.88% of cells were identified as valleys and 3.76% as ridges. Overall, the automated procedure appears to successfully identify the linear contrasts in both datasets, and is able to some extent to categorise them into those that represent valleys and those that represent ridges. There is, however, spatial variation across both datasets in how comprehensively these two tasks are achieved. In the case of the RAMP image, areas of high contrast are generally mapped effectively (see inset in Fig. 5.1a), whereas in areas of lower contrast (significantly in the west and southwest of the region i.e. grid north/northwest) it proves more difficult for the procedure to distinguish genuine contrasts from background noise, leading to a messier classification. Similar effects are also noticeable in the REMA curvature map, especially due to the abundance of linear artefacts produced during the dataset's composition (Howat et al., 2019; see inset in Fig. 5.1b). Nevertheless, the real contrasts in the data, taken to represent bed ridges or valleys, are still often clearly identified, even where they appear more subtle or are partially obscured by noise.

Despite these successes, there are difficulties in both masks which forestall their use in detailed analysis of the valley and ridge networks. Firstly, the lines of pixels which trace out the contrasts in the data are fragmented in many places (e.g. A, X), making it difficult to convert these patterns into linear features suitable for morphometric analyses. Secondly, in some places, cells appear to be wrongly identified (either as ridge when valley or vice versa) – this must be the case where one continuous linear feature is classified differently in different places (e.g. B, Y), and may be the case for entire strings of grid cells representing individual features (e.g. C, Z). These situations are difficult to eliminate and they increase uncertainty regarding the classification of the features identified. Finally, while at their best these maps provide accurate delineations of the individual features on the ice surface, they do not capture the interconnectivity necessary to assess the planform geometry on a larger scale – further processing, likely manual, would be necessary to infer from these masks the regional networks of subglacial valleys and ridges.

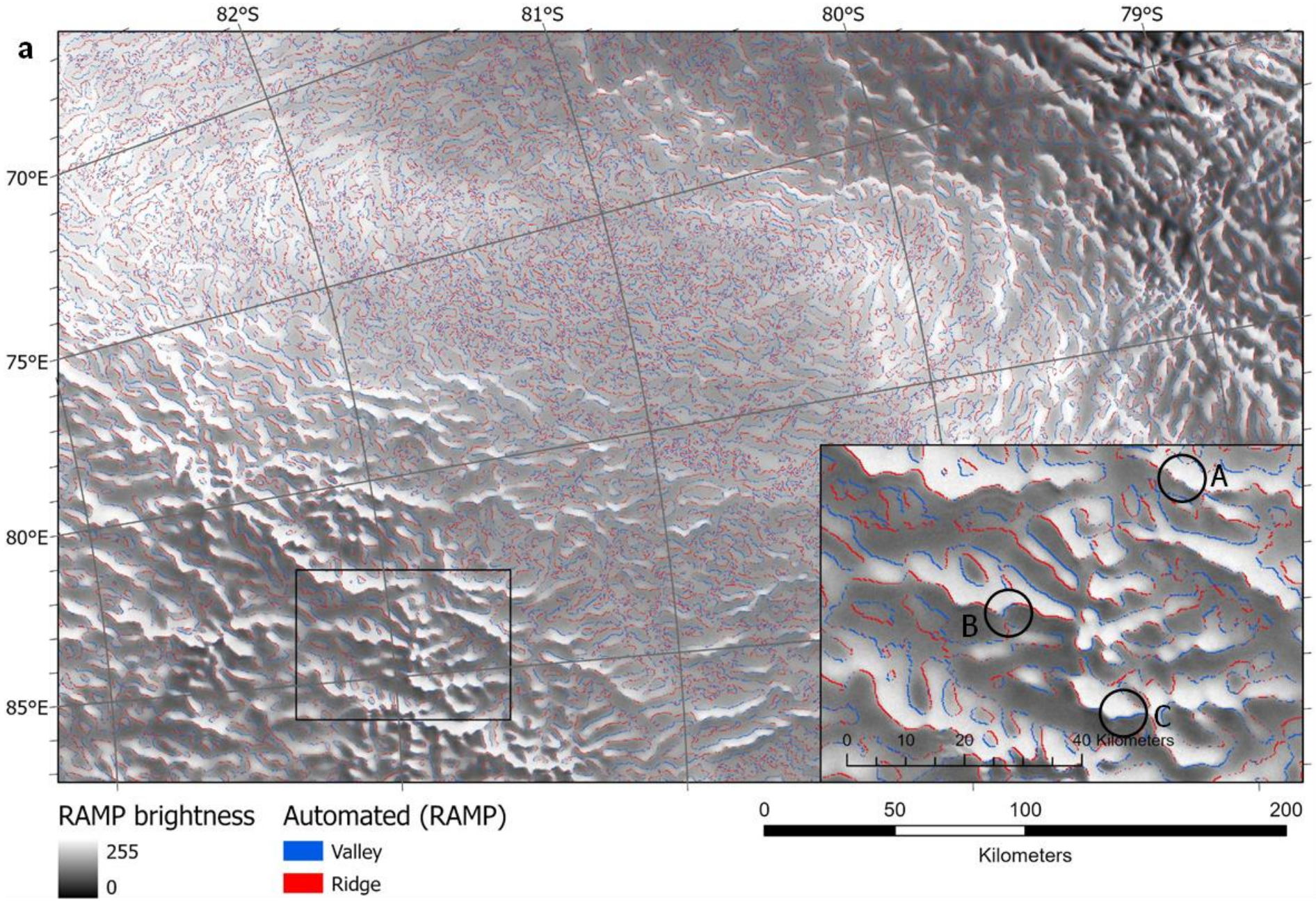
a
82°S
81°S
80°S
79°S
70°E
75°E
80°E
85°E
A
B
C
0 10 20 40 Kilometers
RAMP brightness
255
0
Automated (RAMP)
Valley
Ridge
0 50 100 200
Kilometers

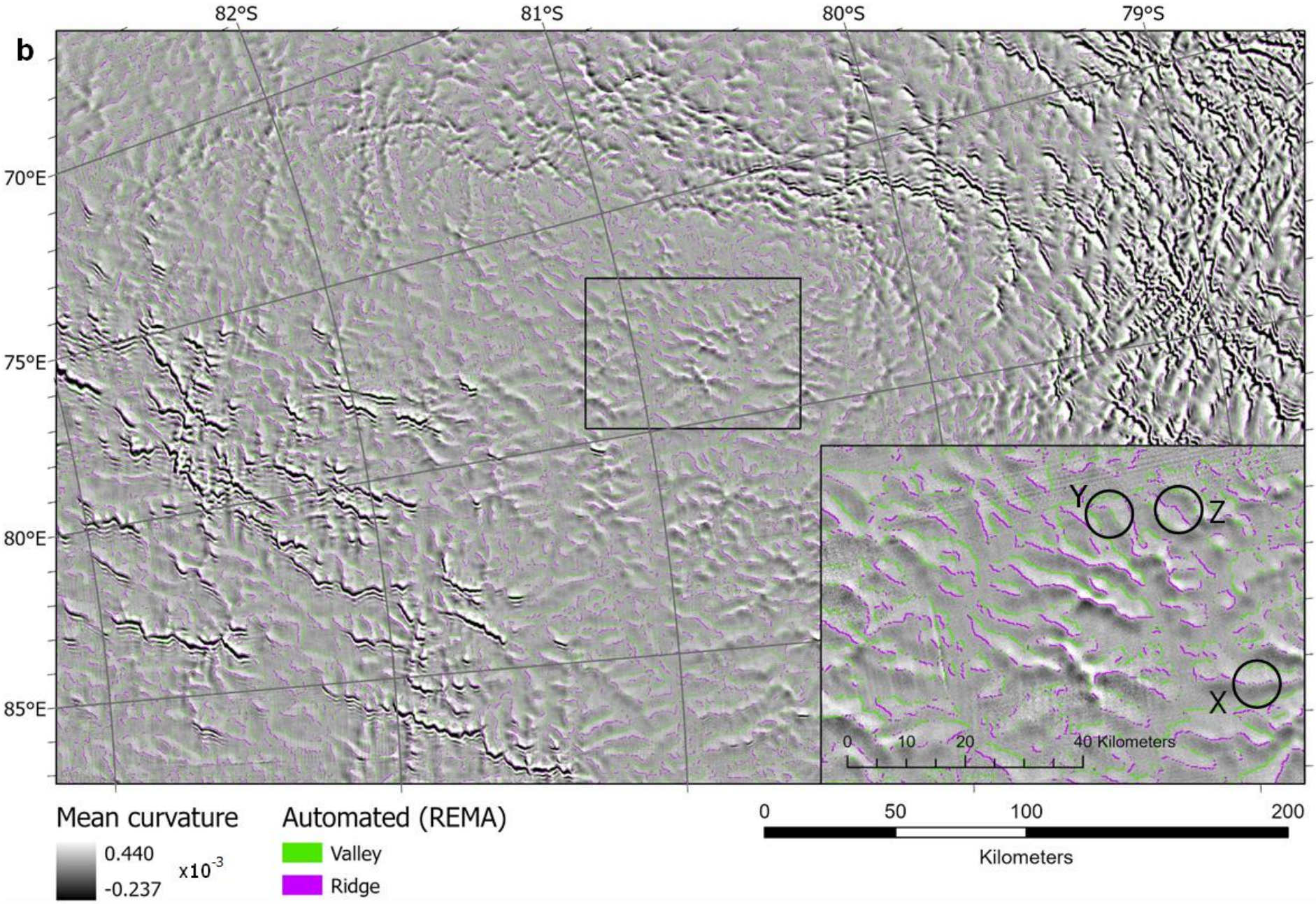
b
82°S
81°S
80°S
79°S
70°E
75°E
80°E
85°E
Y
Z
X
0
10
20
40 Kilometers
Mean curvature
0.440
-0.237
x10-3
Automated (REMA)
Valley
Ridge
0
50
100
200
Kilometers

Figure 5.1 – Automatically mapped ridge and valley locations in the study area using a) RADARSAT-1 Antarctic Mapping Project (RAMP) image mosaic of Antarctica (Jezek et al., 2013) and b) Reference Elevation Model of Antarctica (REMA; Howat et al., 2019) mean curvature. In each case the masks are overlaid on the input data, and a sample area is magnified in the inset. Identified features (A-C, X-Z) demonstrate issues mentioned in the text.

5.2. Manual mapping

The manually mapped ridge and valley networks shown in figure 5.2 cover an area of approximately 140,000 km^2 and comprise approximately 40,500 km (ridges) and 44,800 km (valleys) of total line length. The valley network appears dendritic, centred around two long sub-parallel central valleys, running roughly west-to-east. Under ice free conditions, these valleys would presumably form the principal drainage arteries of the mapped area (Rose et al., 2013), and where they join together at roughly 81°S, 85°E, they have a combined upstream area of approximately 68,700 km^2, more than the next largest drainage unit by an order of magnitude. Several other notably long, straight valleys within this region have orientations roughly southwest-to-northeast. Outside of the central basin, valleys appear to radiate outwards towards the lower elevation peripheries of the Gamburtsev Subglacial Mountains, including the area east of 85°E, which lies outside the densely sampled central grid of the AGAP RES survey (Bell et al., 2011; Ferraccioli et al., 2011).

The level of detail revealed by manual mapping is a significant improvement on the previous best knowledge of the planform geometry of this area (Fig. 5.2b), particularly in upland areas, where the spacing of ridges and valleys is less than the 5-km minimum line spacing of the AGAP survey grid. Since the areas of highest bed elevation closely correspond with where ice is thinnest, it is worth noting that the presence of smaller-scale features in these areas when compared with areas beneath thicker ice may be due to the damping effect of thicker ice on disturbances in flow caused by bed undulations, or by differences in flow caused by differences in basal conditions. However, given the assumption that the valley network does represent what was once a fluvial drainage system, it seems probable that there is to some extent a real change in the frequency of valleys and ridges with elevation, as would be expected from a fluvially-incised landscape.

In the following sections, the overall effectiveness of both manual and automated mapping approaches is validated against existing data following the procedures outlined in Section 4.5. Morphometric analyses are then carried out across the whole dataset of mapped valleys and ridges, and, finally, several extracts from the manual map are selected for closer examination of interesting areas and further comparison to existing datasets.

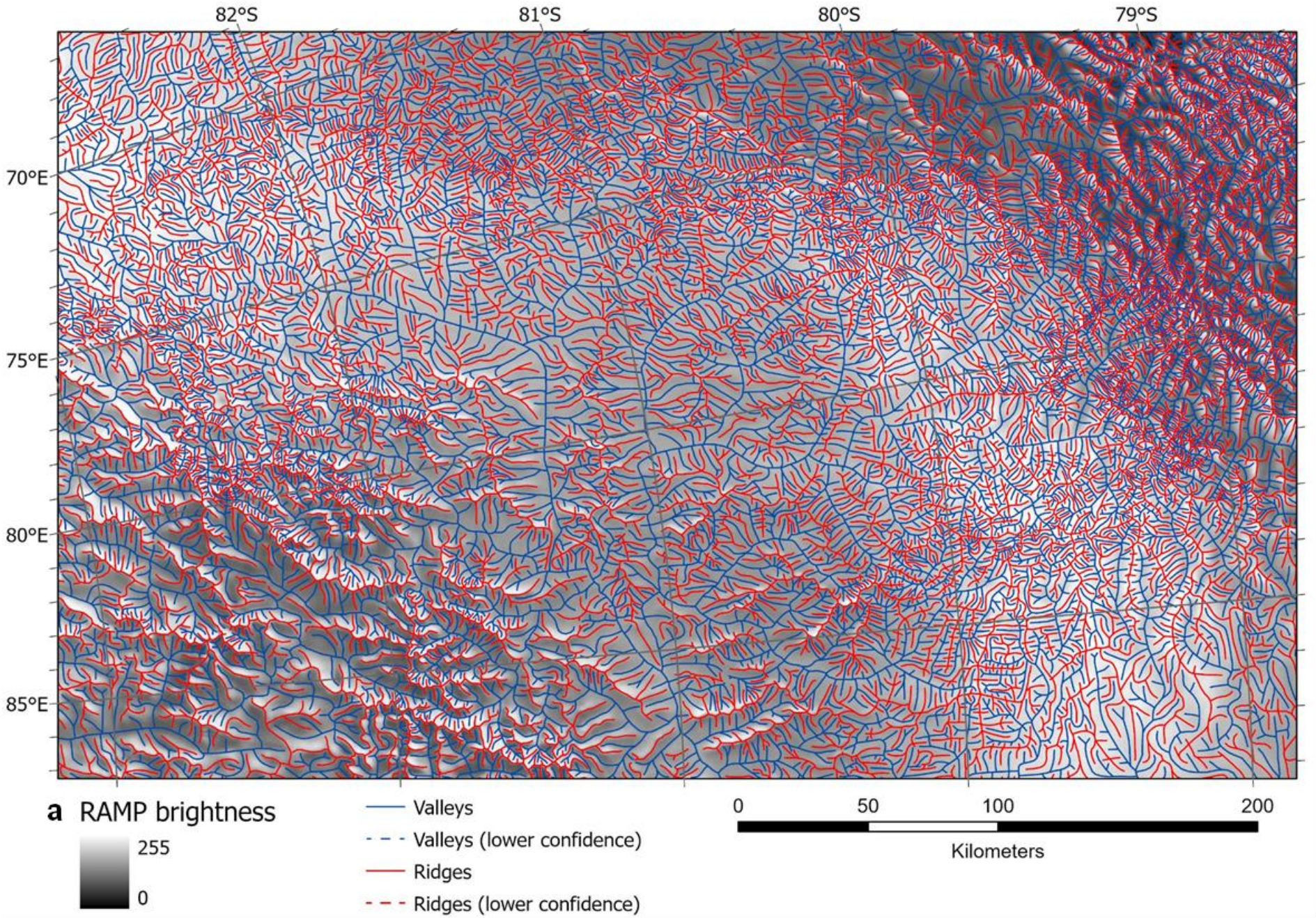
82°S
81°S
80°S
79°S
70°E
75°E
80°E
85°E
a RAMP brightness
255
0
Valleys
Valleys (lower confidence)
Ridges
Ridges (lower confidence)
0
50
100
200
Kilometers

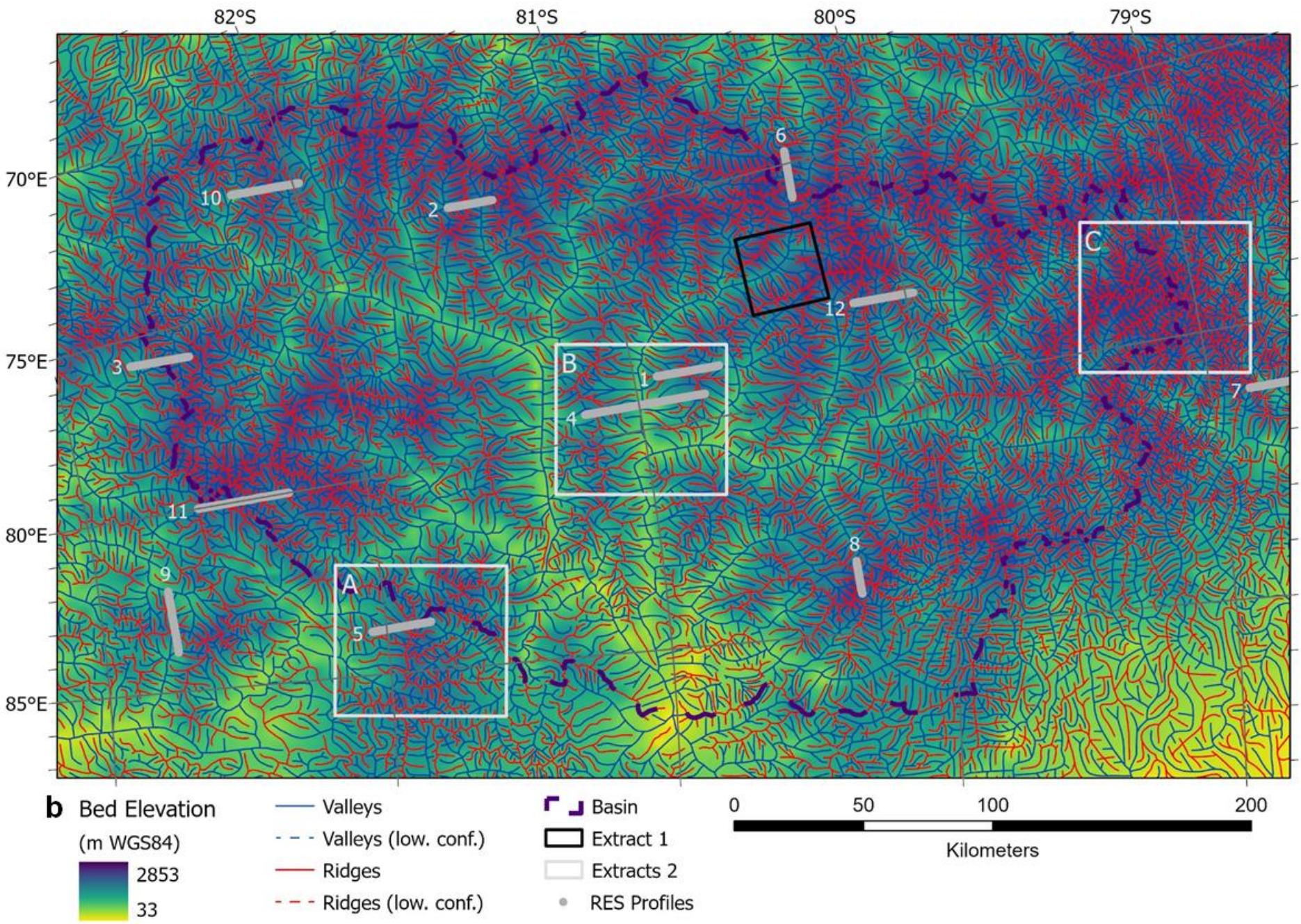
82°S
81°S
80°S
79°S
70°E
75°E
80°E
85°E
A
B
C
1
2
3
4
5
6
7
8
9
10
11
12
b Bed Elevation
(m WGS84)
2853
33
Valleys
Valleys (low. conf.)
Ridges
Ridges (low. conf.)
Basin
Extract 1
Extracts 2
RES Profiles
0
50
100
200
Kilometers

Figure 5.2 – Manually-mapped ridge and valley networks in the study area, overlaid on a) RADARSAT-1 Antarctic Mapping Project (RAMP) version 2 image mosaic (Jezek et al., 2013) and b) BedMachine Antarctica bed DEM (Morlighem et al., 2020). Profile locations correspond to Fig. 5.3, extracts to Fig. 5.9 (Extract 1) and 5.10 (Extracts 2).

5.3. Validation

The locations of mapped ridges and valleys were plotted against AGAP RES bed elevation profiles (Fig. 5.3), to assess the accuracy of the three different mapping methods (manual, automated using RAMP image as input, automated using REMA mean curvature as input). A total of 139 bed features were identified visually from twelve RES profiles, comprising 70 valleys and 69 ridges (Section 4.5); 79.9% of these features were successfully identified by at least one method, either manual or automated, with 64.8% matched to a manually mapped feature, and 51.1% being matched in one or both automated maps (Fig. 5.4). This demonstrates the advantages of using multiple datasets in the mapping process, and may suggest that in future, a hybrid mapping approach, involving both automated and manual interpretive steps offers the most comprehensive method of identifying bed features from ice surface data. Each individual method had a slightly greater chance of successfully identifying ridges than valleys, but a greater proportion of the valleys (85.7%) were matched in at least one of the three maps than was the case for ridges (73.9%).

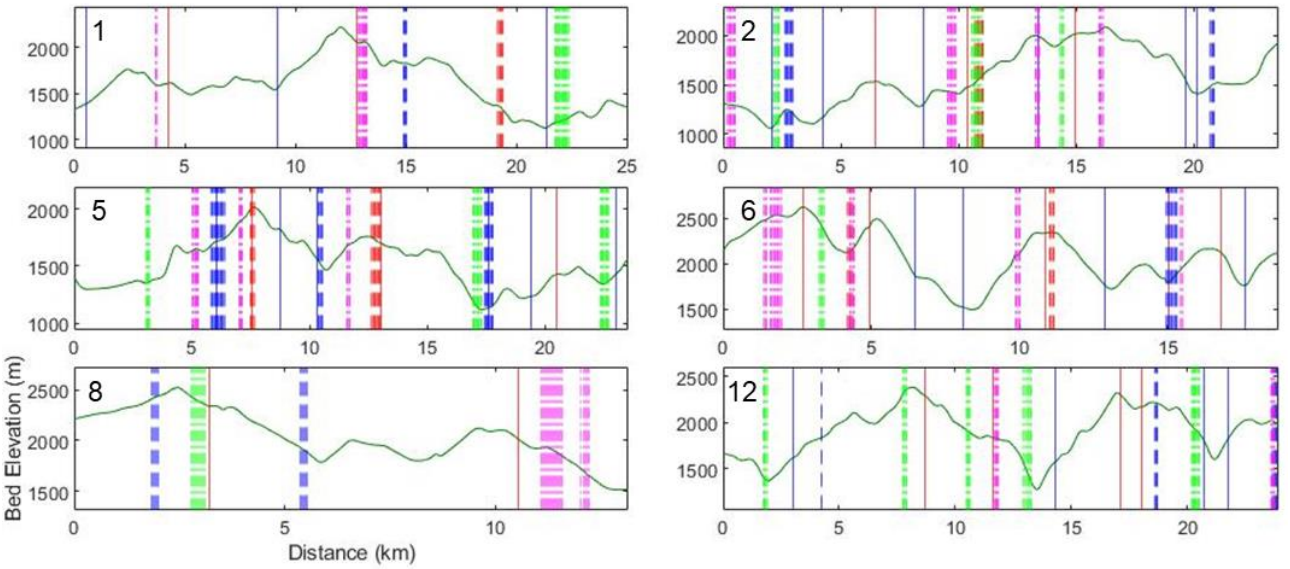

Figure 5.3 – Six of the twelve bed profiles sampled, with the locations of mapped ridges and valleys. Solid lines = manual map (Fig. 5.2) ridges (red) and valleys (blue); dashed lines = RAMP automated map (Fig. 5.1a) ridges (red) and valleys (blue); dot-dash line = REMA automated map (Fig. 5.1b) ridges (magenta) and valleys (green). Bed elevation profile data from AGAP RES survey (Bell et al., 2011; Ferraccioli et al., 2011; Corr et al., 2020). For profile locations see Fig. 5.2b.

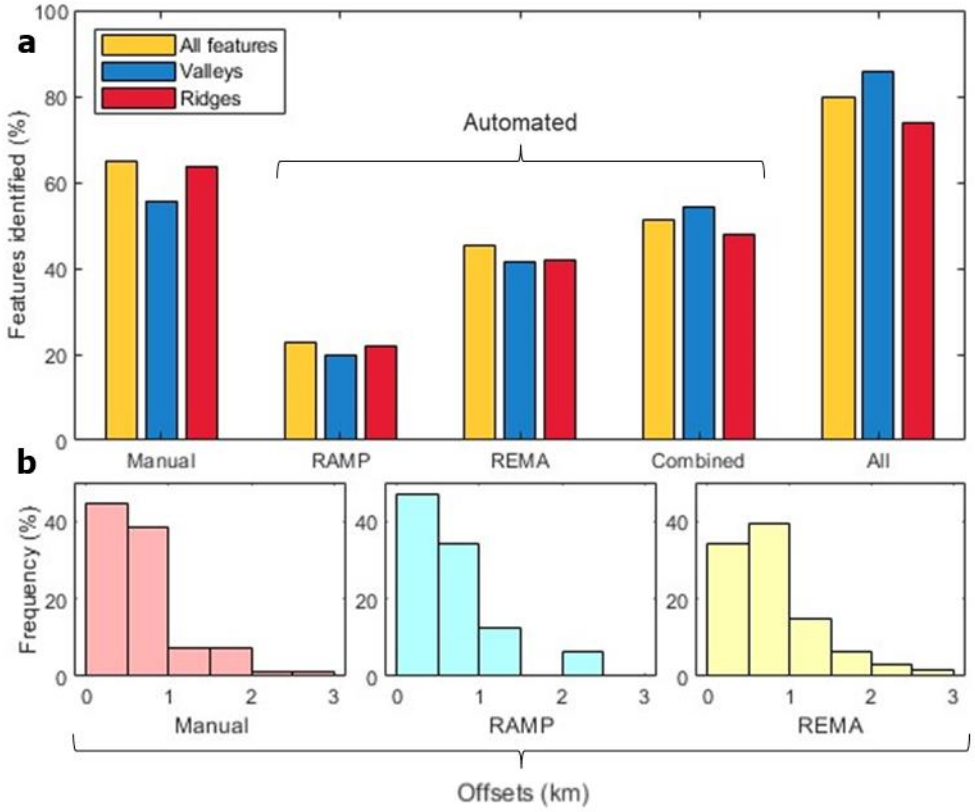

Figure 5.4 – Metrics of mapping accuracy, based on comparison of the three mapping results with twelve sample AGAP radio echo sounding bed profiles:
a) percentage of bed features successfully identified; and
b) Frequency distributions of horizontal offsets in mapped locations of bed features.

Among the manually mapped features along the sampled profiles, 17.8% were not matched with the indicated type of bed feature (Table 5.1), either because no feature was present, or because the incorrect type of feature was mapped (i.e. a valley was mapped where a ridge lay, or vice versa; e.g. profile 8 in Fig. 5.3). Compared with the figures for the automated maps, of 29.3% for RAMP and 23.7% for REMA, this demonstrates the advantage of manual mapping when it comes to avoiding erroneously mapping surface features that are not produced by topographic disruptions to flow, or are in fact artefacts in the mapping datasets. Manual mapping also resulted in the smallest mean horizontal offset for successfully matched features (570 m), with over 90% of offsets no more than 1 km (Fig. 5.4b).

Table 5.1 – Comparing the effectiveness of manual and automated methods in identifying bed features found in selected radar flightlines from the AGAP survey. The optimal value in each column is highlighted in bold.

Method	Features identified (%)	Features misidentified (%)	Mean offset distance (km)
Manual	64.8	**17.8**	**0.57**
Automated (RAMP)	22.7	29.3	0.63
Automated (REMA)	45.3	23.7	0.74
Automated combined	51.1	29.7	0.70
All combined	**79.9**	30.2	0.61

5.4. Morphometric Analyses

5.4.1. Feature length

The total set of manually mapped valleys and ridges range in length from less than 1 km to nearly 250 km, however the overall distribution in both cases is log-normal (Fig. 5.5a), with 61% of valleys and 55% of ridges between 1 and 5 km long, rising to 90% and 85% respectively between 1 and 15 km. This is largely due to the abundance of short features in higher elevation areas (Fig. 5.2b). The distribution of low confidence ridges shows a similar distribution but without so many of the higher ridge lengths (Fig 5.5c), indicating that the longer ridges are more likely to be picked up continuously by the mapping.

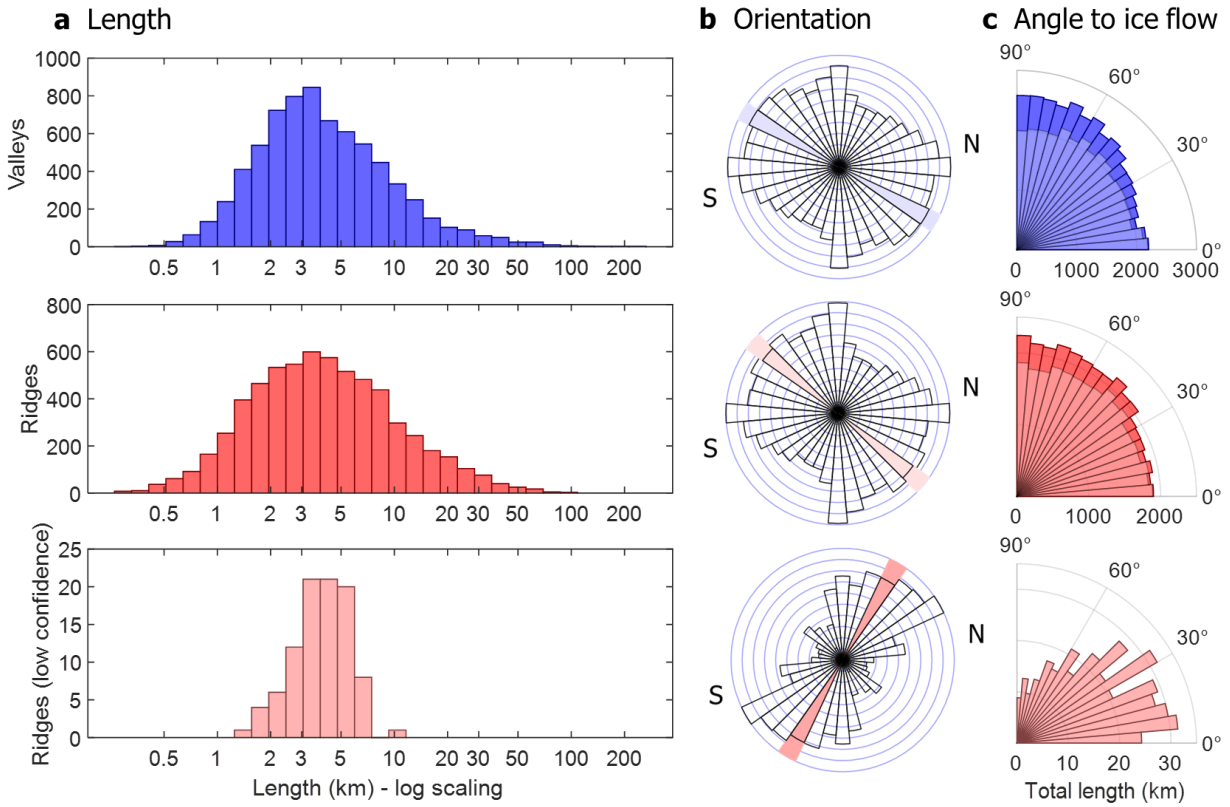

Figure 5.5 – a) Length and b) Orientation of manually mapped valleys (blue), ridges (red), and lower confidence ridges only (pink); c) Angle between mapped valleys/ridges and local mean ice flow direction (derived from Mouginot et al., 2019). Shaded bars in b) denote mean of binned orientations. Length axes in a) are scaled logarithmically; bars in b) and c) are scaled by total length of valley/ridge line rather than number of features. Inner bars on the top two plots in c) represent the baseline after removal of the increasing trend from 0° to 90°.The peaks at top, bottom, left and right of the top two plots in b) are artefacts introduced due to the pixelated nature of the mapping data.

5.4.2. Feature orientation

The orientations of ridges and valleys are similar, trending on average roughly southwest-to-northeast (Fig. 5.5b). This signal is contributed significantly to, but not dominated by, a few very long trunk valleys with this orientation (Fig. 5.2). This orientation is concordant with the Dome A ice divide that lies over the northern ridge of the GSM, and hence roughly perpendicular to the predominant ice flow directions (Fig. 5.6). Features oriented perpendicular to flow are more likely to be transmitted to the surface, because they present a greater obstacle to flow than those oriented parallel (Ockenden et al., 2021), and the trend observed here may therefore in part represent this bias. Comparison between feature orientations and local ice flow directions (Fig. 5.5c) indicates significant correlations between angle from flow and total length of valleys ($p = 0.93$) and ridges ($p = 0.92$), with 30% and 21% increases in the value of the linear least-squares fit between 0° and 90°, respectively. In both cases, however, the residual is evenly distributed ($|p| < 0.01$), and accounts for 87%

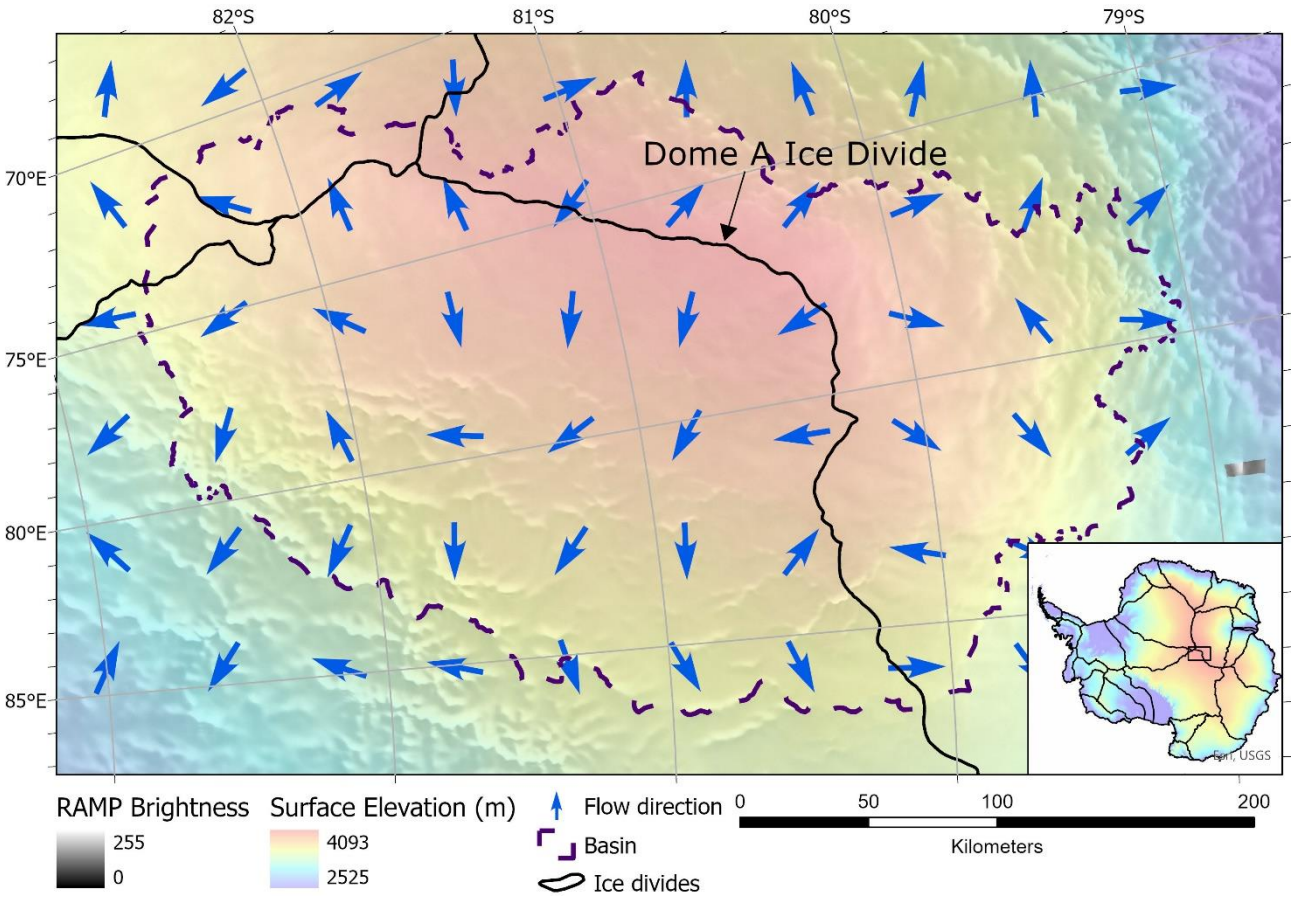

Figure 5.6 – Surface properties of the Antarctic Ice Sheet surrounding Dome A, with location of ice divides and the inferred palaeo-fluvial basin of the central Gamburtsev Subglacial Mountains (on the ice sheet bed). RAMP = Radarsat-1 Antarctic Mapping Project (Jezek et al., 2013). Surface elevation from Reference Elevation Model of Antarctica (REMA; Howat et al., 2019). Flow directions from Mouginot et al. (2019), ice divides from Zwally et al. (2012).

and 90% of the total length of valleys and ridges, indicating that selective bias caused by ice flow direction is relatively minor, and the vast majority of the variability observed in feature orientation (Fig. 5.5b) is genuinely representative of the subglacial landscape.

The “lower confidence” ridges display an opposite trend, with a clear preference for northwest-to-southeast orientations. The trend in angle to ice flow is also reversed, showing that these ridges are in general more closely aligned to ice flow. This supports the suggestion that these features are real, but that their absence of expression from the surface datasets is due to smoother ice flow associated with this alignment of orientation.

5.4.3. Valley width

Individual valley widths generally range between 1 and 15 km, however the local mean width (equivalent to local valley spacing) for 72% of the mapped area lies between 1.5 and 2.5 km, and is greater than 3 km for less than 2% (Fig. 5.7c). In general, valley width appears to be related both to valley length and to bed elevation: long, deep, trunk valleys are some of the widest, while narrower valleys tend to occur at higher elevations (Fig. 5.7a, b). Valley widths in these upland areas are consistently less than 5 km, which is the minimum spacing of RES survey lines throughout this region, suggesting that existing RES data are generally insufficient for mapping a significant part of the topographic variability present in the GSM. The northern block of the GSM in particular displays a high density of very narrow valleys, with local means dipping below 1 km in an area that coincides with the mapped region’s highest bed elevations. The extremes in elevation and valley width are complementary in suggesting that this northern block may have been particularly significant during early phases of Antarctic glaciation, due to the high altitude and abundance of potential sites for glacial ice formation it would have provided.

5.4.4. Valley long-profiles

The valley long-profiles displayed in Fig. 5.8 generally display concave forms, but are highly uneven, with frequent rises in elevation interposed on the overall downslope trends. These elevation changes of up to around 500 m generally seem to occur at the downslope ends of overdeepened hollows between 5 and 10 km long. In some cases, however, changes in elevation may occur as a result of deviation of the mapped valley lines from the true valley bottom, rather than being genuine along-profile features. It is difficult from these data to distinguish where this may be the case, but valleys for which the location of the centreline is less certain (e.g. beneath deeper ice where the surface is smoother) are likely more prone to producing this kind of error.

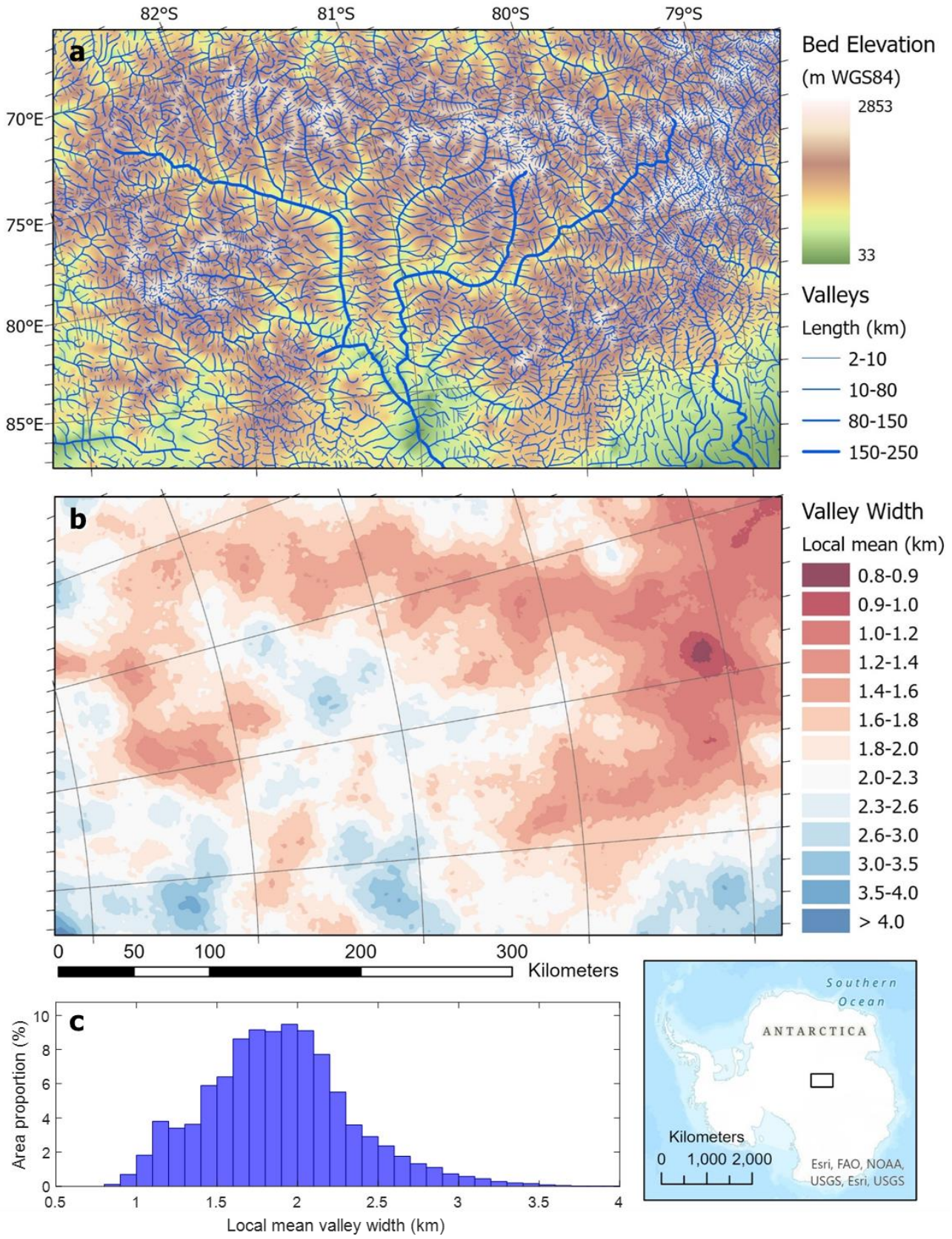

Figure 5.7 – Valley morphometry in the central Gamburtsev Subglacial Mountains: a) Planform valley network mapped manually from ice surface datasets, overlaid on BedMachine Antarctica version 2 bed elevation (Morlighem et al., 2020); b) Local mean valley width, calculated from network in a) as moving-window mean of twice the shortest distance to a mapped valley (see section 4.6.2); c) Frequency distribution of b).

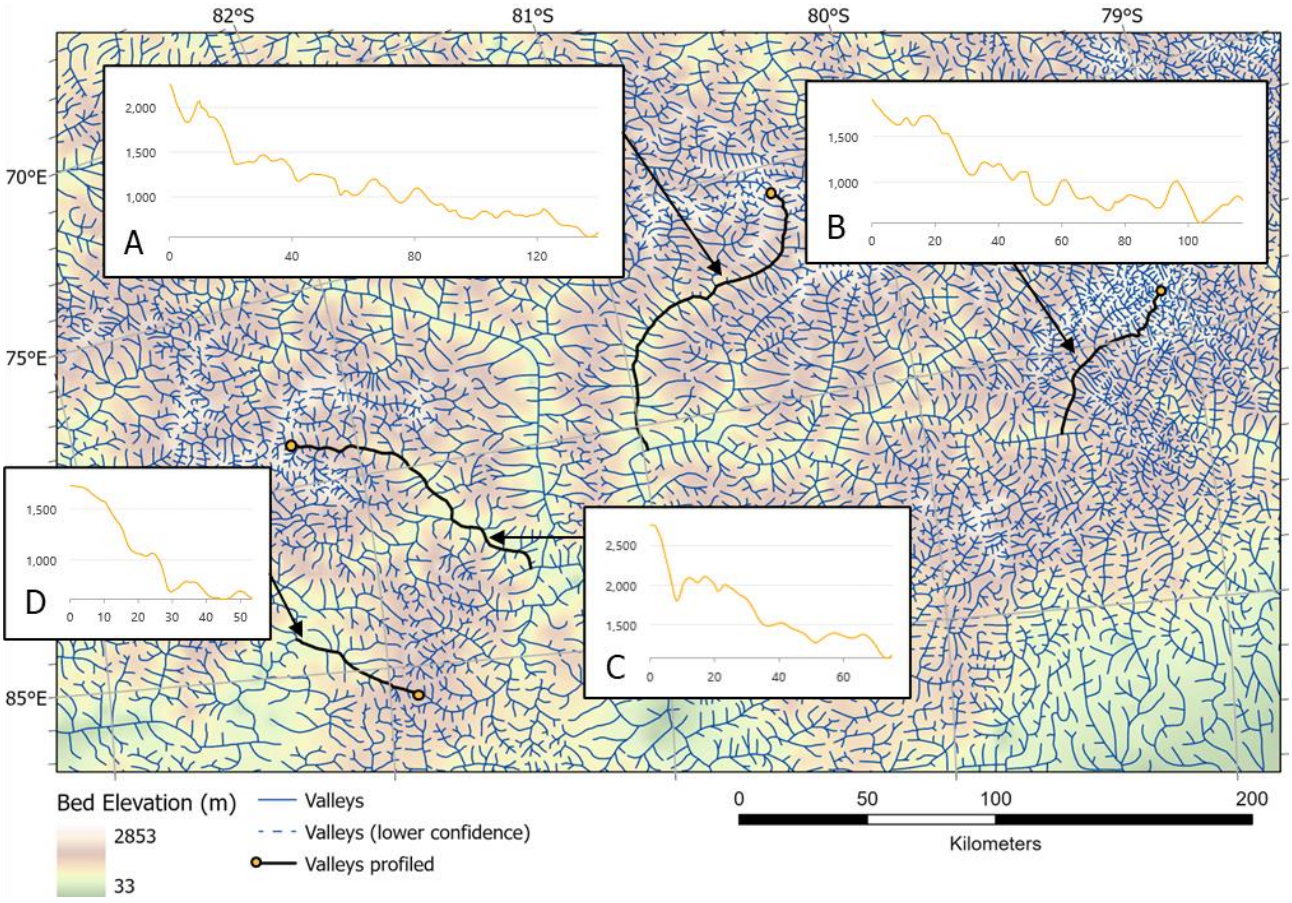

Figure 5.8 – Selected valley long-profiles, using bed elevation from BedMachine Antarctica (Morlighem et al., 2020) interpolated along mapped valley lines. Horizontal axes show distance in kilometres, vertical axes show elevation in metres. Circles on the map mark distance = 0 km.

5.5. Manual Mapping – Detailed Feature Comparisons

5.5.1. Extract 1 – comparison with Bo et al. (2009) DEM

The first detailed radar survey of the subglacial landscape within the study area was conducted by Bo et al. (2009) within a 30-by-30 km square near the high point of the Antarctic Ice Sheet at Dome A, and was used to produce a DEM of sufficiently high resolution to determine the planform geometry of the area in comparable detail to that mapped from the ice surface in this work (Fig. 5.9). Despite the fact that this is an area where both ice surface datasets offer a fairly poor picture of subglacial topography, due to the low amplitude of surficial features over the ice divide, and significant noise, manual mapping proves capable of identifying a network of valleys and ridges which is recognisably similar to that derived using the radar data.

The similarity extends to the pattern of tributary valleys in some of the higher elevation areas, although the position of the main valley centreline is more poorly matched – as previously

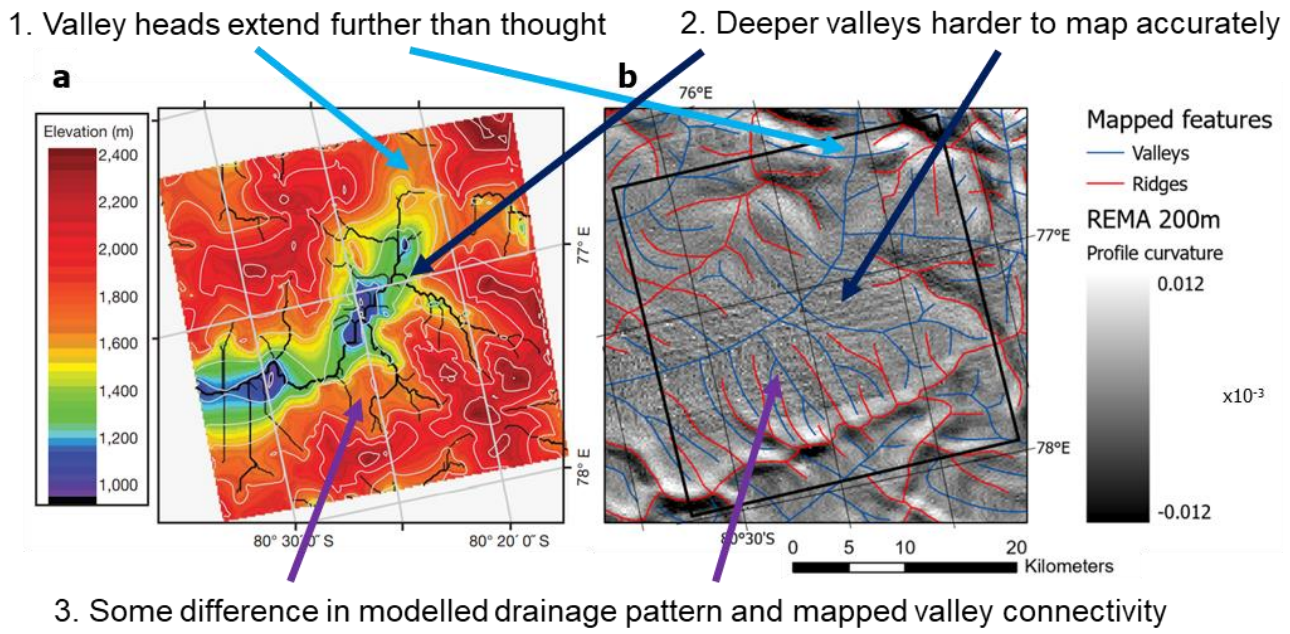

Figure 5.9 – Comparison between (a) bed elevation model produced by Bo et al. (2009), with modelled flow paths shown as black lines, and (b) manually mapped ridges and valleys overlaid on REMA profile curvature for the same 30-by-30 km area, with comments on notable similarities and differences. Location shown in Fig. 5.2b.

noted, this is to be expected due to the increased damping effect of thicker ice over deeper valleys resulting in a decreasing level of detail transmitted to the ice surface. Additionally, there appear to be a greater number of more closely spaced ridges and valleys in the manual map than in the DEM, particularly on the eastern side of the main valley (grid south). Other differences include the extension of the channel network further up-valley than was inferred from the DEM of Bo et al. (2009). This is largely due to the ability to put this small area into a wider context, and relates to the presence of apparently significant overdeepened basins in the northwestern corner of the DEM (grid northeast) – without knowledge of the wider ridge structure, the flow routing algorithm used by Bo et al. interpreted these basins as valley heads that, under ice-free conditions, would drain in the opposite direction to that inferred manually from the ice surface. Further discrepancies relate to the drainage pattern in some of the higher valleys along the lower edge of the main trunk – the radar-derived DEM suggests that the dendritic pattern of valley connectivity is likely to be more complex than the orderly trunk-and-branch structure, which, in the absence of more detailed information, has been inferred in the manual mapping. Despite these differences, it appears that the manually mapped planform geometry is relatively robust when compared to the highest-resolution DEM available in the study area, despite this coinciding with a region where the input data are of lower suitability for mapping than for most of the mapped area.

5.5.2. Extracts 2 – comparison with BedMachine DEM

Outside of the area intensively surveyed by Bo et al. (2009), the greatest resolution available for radar-based gridded bed topography in the Gamburtsev region is the 500-m BedMachine Antarctica DEM (Morlighem et al., 2020). Three extracts of approximately 60-by-60 km have been selected for closer examination, and comparison with the BedMachine DEM as an independent test of mapping effectiveness (Fig. 5.10).

Extract A shows a major ridge running E-W (grid N-S), which accords well with the central massif shown by BedMachine (D), as well as several peripheral ridges that also follow what can be seen in the DEM. Similarly, some of the lower elevation areas to the north and south match places where the manual mapping records widening valleys as narrower tributary valleys on either side of the main ridge converge.

Extract B shows a section of the northern of the two major E-W running valleys noted in Figure 5.2, where it is joined by a second deep valley running N-S. Both are captured well in the manual map, though the westernmost (up-valley) section of the main valley appears more sinuous in BedMachine (E) than has been mapped. The manual map also successfully records the locations of the surrounding ridges, despite these being at a lower elevation (i.e. beneath thicker ice) than those in extract A.

Extract C shows a very high density of small-scale ridges and valleys (mostly ~ 1 km wide, as shown in Fig. 5.7) surrounding the highest elevations recorded in the mapped region (~ 2.85 km above sea level). This level of detail significantly outstrips anything inferable from BedMachine alone, though the positions of larger valleys at the peripheries of this extract generally match topographic depressions in the DEM, and mapped ridgelines are similarly concordant with the intervening areas of higher elevation.

Across all three extracts, it is apparent that the level of detail in the planform geometry offered by manual mapping is a significant improvement over what can inferred from the Bedmachine DEM alone, especially when it comes to the smaller-scale branching structures that seem to characterise higher elevation ridges and valleys (extracts A and C). From these extracts, and from the full map shown in Figure 5.2, this increased degree of detail seems to be consistent across the region at different scales and different bed elevations. Notably, the positions of ridges marked as “lower confidence” (i.e. not directly represented in the datasets used for mapping, but inferred from spatial context of other mapped ridges and valleys; extracts A and B) also match well with the BedMachine DEM, demonstrating that the assumptions used to map these ridges (that the landscape would represent a coherent

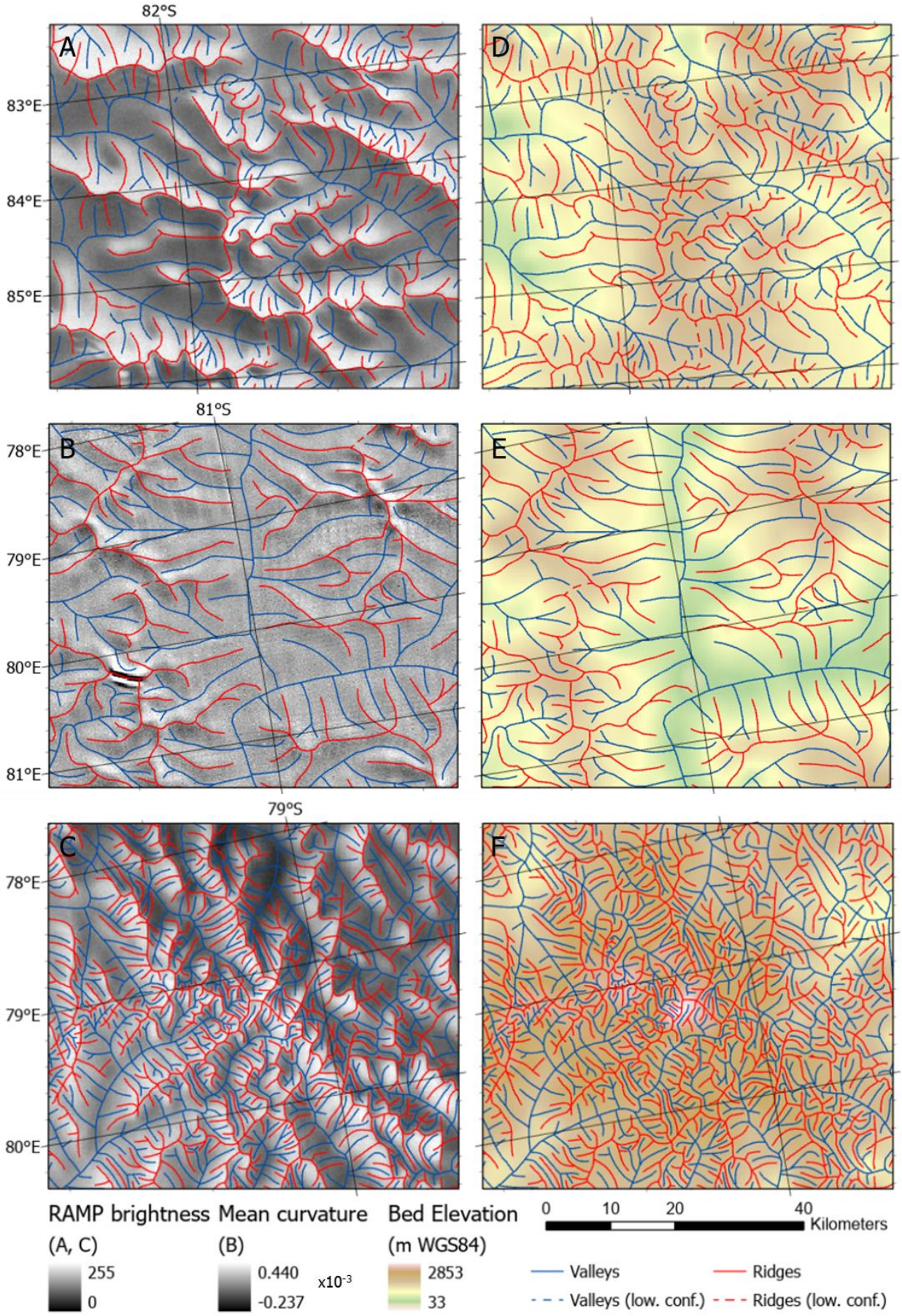

Figure 5.10 – Extracts from manually mapped ridge and valley networks overlaid on (A, C) RAMP image mosaic (Jezek et al., 2013), (B) REMA (Howat et al., 2019) mean curvature and (D-F) BedMachine Antarctica version 2 bed DEM (Morlighem et al., 2020). Locations shown in Fig. 5.2b.

fluvial drainage network, and that some ridges may have no ice surface expression), appear to hold reasonably well. The comparison with BedMachine also suggests that existing bed models such as this could be used to further refine valley and ridge networks mapped from ice surface data – for instance, where “lower confidence” valleys have been mapped (extract A), due to ambiguity over the direction of valley connectivity, the elevation model can be used to identify which path is the more likely (i.e., because it drains downslope).

5.6. Palaeo-Drainage Modelling

The results of hydrological modelling (Fig. 5.11) confirm the significance of the eastwards-facing central valleys as the primary outlets of a large catchment encompassing the central portion of the mapped area. The overall drainage pattern and stream ordering do not deviate significantly from those modelled by Rose et al. (2013). The highest-order stream segment here (of order 6) lies outside the region modelled in that study, and represents the combined flow of the two largest catchments in their model (basins 4 and 5 in Fig. 2.4). The model estimate of the upstream area of this segment (~ 50,000-80,000 km^2) is in agreement with that mapped by hand (68,700 km^2; Fig. 5.2b), despite erroneous features present in the model, including artificial disconnect in the upper reaches of the southern (grid western) branch, and several locations where flow appears to circulate infinitely. These are physical impossibilities which can occur in the model because the inferred flow direction is not derived from a physically plausible topography. An alternative approach, not attempted here, in which the flow direction is constrained by additional input of some elevation data, might prevent these errors.

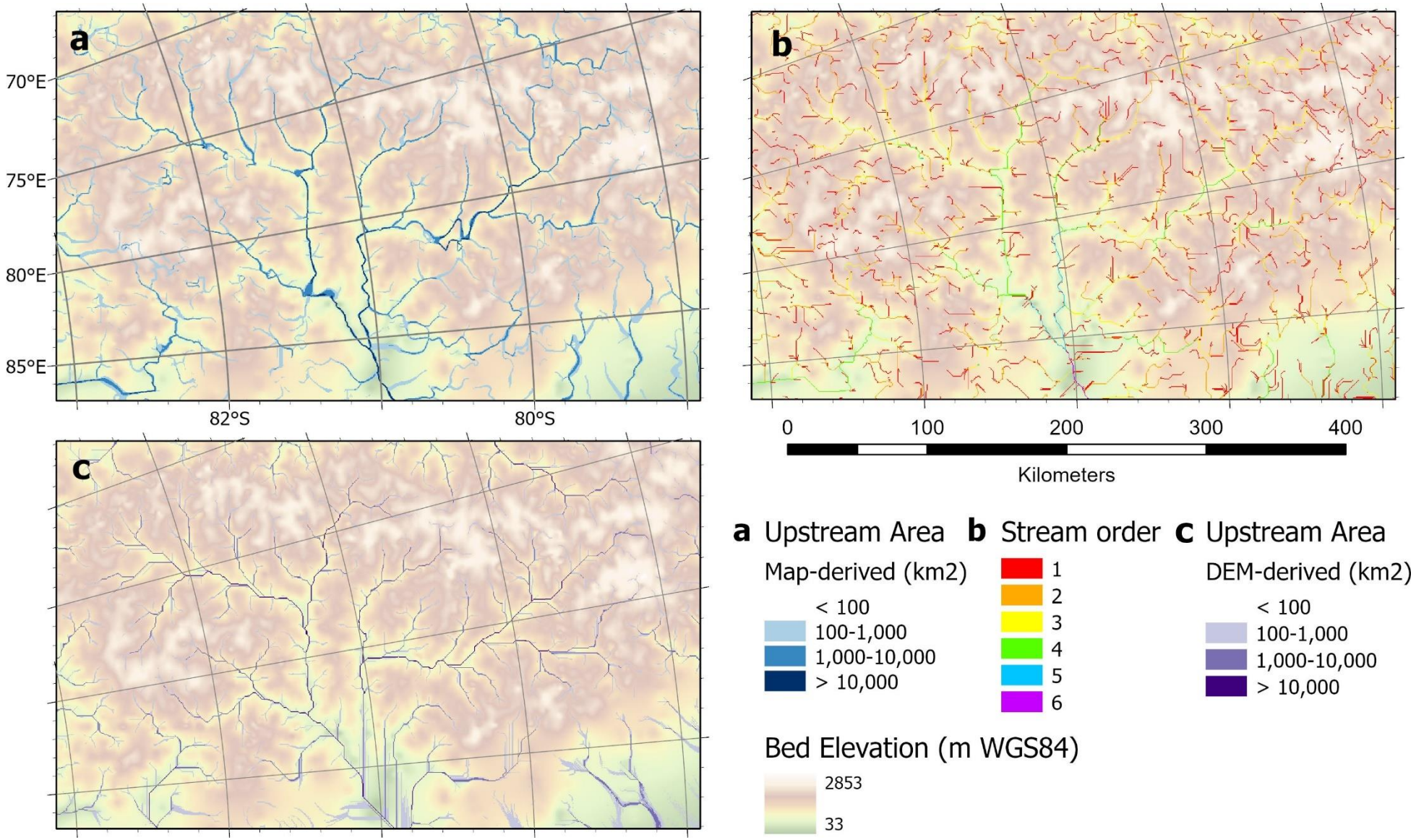

Figure 5.11 – Hydrological model of the preserved fluvial valley network mapped from the ice surface using continuous direction input (a) and 8-directional input (b); c) model using filled version of BedMachine Antarctica digital elevation model (Morlighem et al., 2020).

6. Discussion

The results show that the mapping of the surface ice sheet can be used to infer the planform detail of subglacial landscapes in the Gamburtsev Subglacial Mountains (GSM) region. Discussion follows the three key themes set out in Section 3.1, addressing the research questions identified by fulfilling the objectives detailed in Section 3.2.

6.1. Theme 1: Mapping subglacial landscapes from the ice sheet surface

The mapping results derived in this study (**Objectives 1 and 2**) via automated (Fig. 5.1) and manual mapping (Fig. 5.2) from remote sensing datasets of the surface of the Antarctic Ice Sheet demonstrate the capability of these approaches to derive the planform geometry of the subglacial landscape to a reasonable degree of accuracy (Fig. 5.4), and at greater levels of detail than possible using existing methods based on radio echo sounding (RES), in the context of a high-relief alpine landscape situated beneath slow-moving ice (c.f. Ross et al., 2014) (**Objective 3**). Mapping of ice surface characteristics may therefore provide a useful alternative, or complement, to these more traditional approaches. It is worth noting particularly, that while RES can provide high levels of detail in the along-track and vertical dimensions, the representation of topographic features in two horizontal dimensions is hampered by the lack of data in the intervals between flightlines (Fretwell et al., 2013), which, even at best, are usually not less than 5 km, and are in many places much greater. This study maps upland valleys in the Gamburtsev Subglacial Mountains (GSM) with ridge-to-ridge widths consistently below these limits (Fig. 5.7), confirming roughness observations from RES profiles that bed features of this size are commonplace in the GSM (Bell et al., 2011), despite not being well represented in existing bed elevation models (e.g. Fretwell et al., 2013; Morlighem et al., 2020). Although the GSM are an extreme case, there are several other subglacial highlands across Antarctica which may also possess greater small-scale topographic variability than is depicted in the gridded topographic models, and thus for which ice surface mapping might improve current knowledge of their topographic structure. Fig. 5.2 also indicates that the sparsely surveyed, lower-elevation foothills surrounding the central GSM may possess a similarly complex planform geometry to the higher-elevation massifs, suggesting significant potential for further application of surface mapping in these regions as well. Accurate representation of subglacial topography in bed elevation models is important as a boundary condition for ice sheet modelling, due to the influence that bed topography can have on ice sheet flow, and hence is a key goal for Antarctic science, as highlighted by continued efforts to update existing datasets such as BedMachine (Morlighem et al., 2020) and Bedmap (Frémand et al., 2022). While no new elevation data have been

created in this study, it may be possible to integrate the mapped planform geometry of the GSM with existing bed models or RES data to create more accurate, or at least, more representative models of the three-dimensional structure of the bed topography. This presents an opportunity for future work using ice surface mapping.

The discussion of the methodology (Section 4) and validation of results (Section 5.3) highlight several issues surrounding the choice of mapping procedure. Manual mapping (**Objectives 1 and 2**) is a time-consuming process, prone to human error, and also incorporating a significant element of subjectivity. It also requires some pre-existing knowledge or assumptions to be made about the landscape being mapped, for example, that the valley network represents a fluvial drainage system, as in this study. The automated mapping procedures (**Objectives 1 and 2**) are less accurate than manual mapping (Fig 5.4), and do not currently produce results of sufficient quality for detailed analysis, but they are significantly more rapid, and easier to upscale to larger areas. In addition, automated mapping appears to pick out some features missed by manual mapping, increasing the overall percentage of features successfully identified from 64.8% to 79.9% (Fig. 5.4a). This suggests that, in future, the optimal method for mapping bed features from surface datasets over large areas would likely involve both automated and manual components. It would be relatively straightforward, for example, to follow a hybrid procedure in which the results of an automated classification like the one used in this study were subsequently edited by hand.

Some unavoidable uncertainty results from the limitations of mapping bed features indirectly from the ice surface. Major difficulties arise from the damping effect of a thick ice column, making some features, especially valleys, much more difficult to discern than others. There appears, additionally, to be a key control exerted by the direction and magnitude of ice flow across a bed feature. The analysis of ridge and valley orientations in Section 5.4.2 suggests that features with closer alignments to ice flow may be less likely to cause sufficient perturbation to flow to be seen on the surface (c.f. Ockenden et al., 2021). On the other hand, turbulent ice flow can sometimes lead to complex surface expressions resulting from a single bed feature, causing some confusion, particularly when using automated approaches. Ice flow speeds, and ice surface slope, are extremely small close to the ice divide, resulting in surface features with much lower amplitudes than would otherwise be expected. This particular issue was addressed in the automated procedure by using an adaptive threshold to account for different levels of variability, or contrast, in the surface datasets with varying proximity to the ice divide. Likewise, the manual procedure, by allowing

comparison of multiple datasets and use of human judgement, was able to reduce the impacts of some of these issues. Some however, such as the persistence of variable and unpredictable offset distances between bed features and their mapped surface expressions (Fig. 5.4b), remain difficult to account for.

6.2. Theme 2: Interpreting processes of landscape evolution (**Objectives 4 and 5**)

Previously, the Gamburtsev Subglacial Mountains (GSM) have been interpreted as a pre-Oligocene fluvially incised landscape, subsequently modified by local, alpine-style glaciation (Bo et al., 2009; Rose et al., 2013). This gave way to topographically unconfined ice cap and ice sheet conditions (Pollard and DeConto, 2003), under which the GSM have been relatively well preserved for at least the last 34 Myr, due to the overlying ice remaining continually cold-based (Jamieson et al., 2010). It is possible that the tectonic forces that caused the uplift of the mountains have also left an imprint on the preserved landscape, though the apparent complexity (e.g. Ferraccioli et al., 2011) and continuing uncertainty surrounding these events (Heeszel et al., 2013; An et al., 2015; Paxman et al., 2016) makes this difficult to assess. The following sections will therefore consider, first, the properties of the pre-glacial fluvial landscape (**Objective 4**), using the information provided by the manually mapped valley network (all further references to the mapped ridge and/or valley networks refer to the manually mapped networks shown in Fig. 5.2) presented and analysed in Section 5 (primarily Figs. 5.2, 5.5, and 5.7), and secondly, the evidence within the mapped network for temperate glaciation of the GSM prior to ice sheet formation (**Objective 5**).

6.2.1. The pre-glacial fluvial landscape

The mapped valley network bears a predominantly fluvial signature, in the form of a dendritic structure, with identifiable drainage units (Fig. 5.2) and consistent stream ordering (Fig. 5.11). The valley network extends further than previously known, maintaining the fluvial signature beyond the central high-elevation region of the GSM into the foothills on the eastern side. This is significant for evincing wider-scale drainage patterns in pre-glacial Antarctica, and has implications for the development of the East Antarctic Ice Sheet over time, as will be discussed further in Section 6.3. There is also a greater frequency of small tributary valleys in upland areas than previously mapped, improving the detail of the fluvial network in its source regions. High elevation valley spacing in the central GSM is generally between 1 and 3 km (Fig. 5.7), which is comparable to other alpine mountain ranges such as the Rocky Mountains of North America (Pelletier et al., 2010). Previous reconstructions of the topography of the GSM did not generally resolve valleys this small (Figs. 5.9 and 5.10;

Bo et al., 2009; Rose et al., 2013; Morlighem et al., 2020), despite features of this size being apparent in radio echo sounding (RES) profiles (Bell et al., 2011). It is worth noting that in RES profiles, valley widths may be prone to overestimation, because radar flightlines often intersect valleys obliquely; knowledge of the planform geometry of the valley network is therefore useful in identifying true cross-sections of valley morphology (c.f. Rose et al., 2013).

It is possible to model the palaeo-fluvial system in more detail using the flow directions implied by the mapped valley network as inputs, to generate a map of flow direction across the mapped region independently of any direct elevation input (Section 4.7). The result (Fig. 5.11) allows characterisation of the network according to hydrological variables including upstream drainage area and stream ordering. While the absence of a real elevation surface as input causes notable issues such as the occurrence of impossible “infinitely-descending slopes”, the level of detail is greater than can be derived using the BedMachine DEM alone (Fig. 5.11c). This method of flow modelling, therefore, could have significant advantages if developed further.

6.2.2. Age of the fluvial network

Unlike other high elevation mountain ranges, the GSM have been inferred to be geologically ancient (van de Flierdt et al., 2008; Veevers and Saeed, 2008) and tectonically inactive (Boger, 2011), pre-dating the onset of widespread glaciation in Antarctica at the Eocene-Oligocene transition at 33.7 Ma (Miller et al., 2005; Scher et al., 2011). Given that the GSM are very unlikely to have been deglaciated since this time (Jamieson et al., 2010), it is reasonable to assume that the mapped fluvial network also predates 33.7 Ma (Rose et al., 2013; Paxman et al., 2016), having subsequently been preserved beneath continually cold-based, non-erosive ice (Van Liefferinge and Pattyn, 2013). If erosion rates since the Permian (ca. 250 Ma) were as low as 0.01-0.02 km/Myr (Cox et al., 2010), Paxman et al. (2016) calculate an upper bound of 200 Myr for the duration of fluvial incision, and therefore a maximum age of ca. 230 Ma for the mapped fluvial network (assuming no erosion for the past 30 Myr). Such an age, however, implies uplift of the GSM much more recently than the youngest age (~ 500 Ma) suggested by detrital thermochronology of Prydz Bay marine sediments (van de Flierdt et al., 2008; Veevers and Saeed, 2008; Gupta et al., 2022). It is worth noting that these sediments are presumed to have been sourced from the northern GSM via the Lambert Graben; however, the valley network (Fig. 5.2) and drainage pattern (Fig. 5.10) indicates that this would not have been the predominant route for sediments eroded from the central and southern GSM, with the large central basin draining east

towards the Ross Sea through what is now the Wilkes Subglacial Basin and/or the Transantarctic Mountains. Moreover, there is evidence of heterogeneity in the landscape structure between the northern block and the rest of the GSM, with valleys more closely spaced in the north (Fig. 5.7). This potentially suggests a control exerted by variance in the underlying geology of the two regions, hence the Prydz Bay sediments may not accurately represent bedrock characteristics across the whole GSM.

An alternative possibility for the apparently young age of the fluvial network is that protective cold-based glaciation was established in the GSM much earlier than 34 Ma, a hypothesis that is consistent with low long-term erosion rates (Cox et al., 2010) as well as sea-level and oceanographic changes apparently necessitating the growth of ephemeral Antarctic ice caps from the Cretaceous onwards (Miller et al., 2008; Stoll and Schrag, 1996). It has previously been suggested that tropical conditions on Antarctica's coast, as evidenced by the occurrence of coal beds (Holdgate et al., 2005; Turner and Padley, 1991), must preclude glaciation of the continent at this time. There is, however, supporting evidence for seasonal sea ice during the Late Cretaceous (Bowman et al., 2013), suggesting conditions also favourable for terrestrial glaciation. It may be that, with sufficiently strong moisture transport inland, the combination of unusual continentality, high altitude and high latitude that exists in the GSM, allowed for glacial cover of the region even during Greenhouse climates (Miller et al., 2008; Cox et al., 2010). If this is the case, the fluvial network may have begun life much earlier, potentially stretching back to the last known period of mountain building in East Antarctica, ca. 550-500 Ma (An et al., 2015).

6.2.3. Modification of the landscape by local-scale glaciation

Previous studies of the landscape of the GSM have identified features such as U-shaped valley cross-profiles, overdeepened basins, cirques, hanging valleys, and drainage divide breaches (Bo et al., 2009; Rose et al., 2013), which indicate a period of alpine-style, locally erosive glaciation prior to the onset of the cold-based, non-erosive regime which has characterised the GSM ever since the establishment of a continental-scale ice sheet (Jamieson et al., 2010). While the planform geometry of the landscape mapped in this study is primarily indicative of the fluvial processes that, in tandem with tectonic forces, led to its formation (Rose et al., 2013; Paxman et al., 2016), it does provide some support for the existence of these features, and hence, for a phase of localised, erosive glaciation, prior to ice sheet initiation, that modified the existing fluvial landscape.

A number of ridges mapped in this study, marked as “lower confidence” (LC), were inferred solely based on the requirements of the fluvial geometry (e.g. the closure of drainage units), because their presence was not indicated in the ice surface datasets. One possible explanation for their apparent absence is that they represent locations where ridges have been locally removed by glacial erosion (i.e. glacial breaches; Dury, 1957). A few minor features of this type were identified by Rose et al. (2013) from their AGAP RES-derived digital elevation model of GSM topography, predominantly at high elevations along the major mountain ridgelines. Another possibility, suggested by the preferential alignment of the LC features towards the local direction of ice surface flow (Fig 5.5), is that they persist beneath the ice, but because of their orientation do not present sufficient obstacle to ice flow to cause an expression visible on the ice surface (c.f. Ockenden et al., 2021). Not all of the LC ridges conform to this trend in orientation, however, so it seems probable that some number of them may in fact represent features removed by glacial erosion. It is not possible from the ice surface alone to distinguish them, but it may be reasonably supposed that those that lie at greater angles to the direction of ice surface flow are more likely to actually have been removed.

Another line of evidence that may be drawn relates to valley form. Rose et al. (2013) constructed valley long profiles for the GSM based on their digital elevation model, and found significant overdeepenings, indicating repeated erosion beneath alpine-style valley glaciers (Fig. 2.4). The planform geometry mapped here does not provide new information on the shape of valleys per se, but does provide alternative valley centrelines to use in constructing long profiles from a DEM (Fig. 5.8). At higher elevations, where the ice surface expression is generally clearer, the mapped flowlines may be more accurate than those derived using interpolated DEMs; beneath thicker ice, with a smoother surface expression, however, the positions of mapped lines are less certain (see mapping comparisons in Section 5.5), and hence the valley long-profiles may reflect lateral change with respect to the true thalweg rather than changes in elevation along-profile.

It remains uncertain whether any clear evidence of local-scale glaciation exists in the networks mapped in this study. In both cases, however, this is likely due to the intrinsic limitations of ice surface mapping rather than because glacial features are necessarily absent. Linear forms expressing ridges and valleys appear readily on the ice surface in the region of the GSM, but smaller features such as glacial cirques may be of insufficient size to cause the necessary flow perturbation. Since there is no independent way to infer relative elevations of features, except by inferring directions of flow from the fluvial geometry,

features such as hanging valleys and overdeepenings are also difficult to observe. Likewise, the shape of valley cross-profiles cannot be assessed, however, the knowledge of the location and planform shape of bed valleys may be of use in more accurately interpreting topography revealed by RES – for example, valley width profiles may be more accurately assessed when it is known at what angle the radar line intersects the valley long profile.

6.3. Theme 3: Ice sheet-landscape interactions (**Objectives 4, 5 and 6**)

6.3.1. Subglacial topography and basal thermal regime

As has been noted previously, a major implication of the widespread preservation of the pre-glacial landscape of the GSM is that there has been minimal erosion of the landscape by glaciation over the past ~ 34 Myr (or longer), implying continual coverage by cold-based ice (Jamieson et al., 2010; Rose et al., 2013). The mapping conducted here provides further support for this conclusion, suggesting only very minor alterations to the planform geometry of the pre-glacial ridge and valley networks (though noting the significant uncertainty associated with inferring such changes from the ice surface alone – see Section 6.2.3). This consistent absence of basal melting, along with the location of the GSM in a region of slow flow, close to an ice divide, has led several authors to suggest that they may host some of the oldest undisturbed basal ice in Antarctica (Fischer et al., 2013; Van Liefferinge and Pattyn, 2013; Wolovick et al., 2021), making them a promising target for drilling ice cores containing climate records stretching back up to 1.5 Myr. Such endeavours include the NSF-funded Center for Oldest Ice Exploration (COLDEX), which aims to begin exploratory surveying in the southern GSM during the 2022-23 Antarctic field season.

However, analysis of bright bed reflectors in AGAP RES data suggests that the GSM are not entirely cold-based, with subglacial water present in deep valleys due to melting at the base of thick overlying ice (Wolovick et al., 2013; Creyts et al., 2014). Melting can apparently occur on very small scales (Wolovick et al., 2013) thanks to the effects of local topography concentrating geothermal heat flows into topographic lows (Wolovick et al., 2021). Critically, modelling suggests that ridge-valley relief on wavelengths smaller than the spacing of existing RES flightlines (~ 5 km in the GSM) may be enough to induce melting in small-scale upland valleys otherwise assumed to lie within areas of permanently cold-based ice (Wolovick et al., 2021). This presents a difficult problem when searching for ice drilling sites, as currently available data are not sufficient to accurately identify (and avoid) these localised patches of warm-based ice.

Maps such as those presented here may therefore be useful tools to assist in searching for Oldest Ice drilling sites (**Objective 6**). The mapping techniques used in this study are not limited by the spacing or coverage of RES data, and as such they record ridge-and-valley-scale topographic variability in finer detail (wavelengths consistently below 5 km – Figs. 5.7, 5.10) than even the most comprehensive regional RES surveys (such as AGAP), without the associated costs of these surveys. They effectively identify areas of complex topography and may allow fine-scale RES surveys to be focused in locations that are more likely to yield suitable sites for drilling. Surface mapping also provides information about the orientation of bed ridges and valleys (e.g. Fig. 5.5) much more readily than RES (which may cross ridges/valleys obliquely). This information is of importance when considering the three-dimensional pattern of ice flow over complex obstacles, and whether this would affect the stratigraphic integrity of the ice column at a potential drilling site.

6.3.2. Subglacial topography and ice sheet hydrology

The mapped valley network may also be useful for investigating modern subglacial hydrology. Jamieson et al. (2016) mapped an extensive network of subglacial canyons in Princess Elizabeth Land from their ice surface expressions, and proposed that these were active subglacial conduits due to their association with a large subglacial lake, while Wright et al. (2012) also showed that low-lying bed topography in the Wilkes Subglacial Basin provides a route for subglacial drainage from the interior of the ice sheet to the coast. In the GSM, Wolovick et al. (2013) find evidence for restricted movement of subglacial water along corridors of low hydraulic potential, defined primarily by the high-relief bed topography; they find that, while the subglacial hydrological gradient, dictated by ice surface slope, drives the direction of these flows, the routes they take are determined by the existing subglacial valley network. This means that the mapped valley network may be an indicator of the pathways available to subglacial water beneath the modern ice sheet.

Where the grain of the subglacial topography is aligned with ice surface slope, water may flow freely either uphill or downhill; on the other hand, where bed topography is oriented transverse to ice surface slope, transport of subglacial water is inhibited (Wolovick et al., 2013). Unlike the long-distance hydrological connections inferred by Jamieson et al. (2016) and Wright et al. (2012), the subglacial hydrological networks of the GSM are therefore predominantly short (Wolovick et al., 2013), and often end in zones of basal refreezing where water is forced up reverse bed slopes under pressure and cools (Bell et al., 2011; Creyts et al., 2014). This occurs on valley sides (where bed topography is transverse to ice surface slope) and in valley heads (where bed topography is aligned with, but opposite to

surface slope, such that subglacial water flows up-valley). In the third case (where bed topography is aligned with, and sub-parallel to ice surface slope), longer-distance transport of subglacial water may be possible, uninterrupted by basal refreezing.

Comparing the mapped valley network with regional ice surface slope, indicates that, since the high point of the ice sheet (Dome A) lies broadly over the central, elongate basin of the GSM (Fig. 5.6), there is little scope for significant escape of subglacial water from the GSM either to the north or to the south, as it would generally be moving uphill in both directions. The same is true of the western flank of this basin, but the major valleys that would have drained it to the east are in closer accordance with the direction of ice surface slope, and may potentially offer a subglacial hydrological connection from the GSM to the wider EAIS. Note that this does not take into account transport of water up reverse bed slopes created by overdeepenings along valley long-profiles, which are reasonably common in the deep valleys of the GSM (Bo et al., 2009; Rose et al., 2013). Thus, any potential subglacial flow path identified from ice surface mapping should also be investigated with respect to actual changes in bed elevation along the route (c.f. Jamieson et al., 2016, Wolovick et al., 2013).

6.3.3. Subglacial topography and ice sheet evolution

As previously discussed, the mapped valley network extends beyond the central region of the GSM focused on by the AGAP RES survey, into the lower-elevation foothills to the east (Fig. 5.2). This is significant, as it demonstrates that, as inferred in the central GSM (Bo et al., 2009; Rose et al., 2013), glaciation of the surrounding landscape has been minimally erosive, or at least, that the pattern of ice flow, and hence the pattern of erosion, has been predominantly guided by the pre-existing fluvial geometry. This is consistent with the idea that the GSM were a key source of ice during the early Oligocene expansion of glaciation in Antarctica (DeConto and Pollard, 2003), because the marginal regions of an expanding ice cap centred on the GSM would likely have been initially thin and topographically confined, like many modern-day Arctic ice-caps which have topographically confined outlets (e.g. Baffin Island ice cap, Svalbard, Severnaya Zemlya and margins of SE Greenland). As these ice margins grew, erosion would have been concentrated along these topographic lows (Sugden and John, 1976), leading to a feedback whereby continued erosion promoted increased flow of ice along the same topographic corridors, further focusing erosive power along these routes (Jamieson et al., 2008). Even where ice has not remained exclusively cold-based, therefore, the broad strokes of the fluvial valley network of pre-glacial East Antarctica may be more widely preserved than previously understood.

If there was a period of erosive alpine-style glaciation in the GSM prior to the onset of cold-based conditions, the minimal modification of the topographic structure from its characteristically fluvial geometry, and apparent lack of significant eroded material (Cox et al., 2010; Thomson et al., 2013) suggest that this episode must have been short-lived, succeeded by a rapid transition to cold-based ice cover at the centre of an expanding East Antarctic ice mass (Jamieson et al., 2010). As other authors have noted, the preservation of this largely pre-glacial landscape is convincing evidence of exclusively cold-based conditions in the GSM ever since (Rose et al., 2013; Jamieson et al., 2014), indicating remarkable stability at the core of the East Antarctic Ice Sheet (EAIS), in contrast to dynamic oscillation of its margins (Young et al., 2011; Paxman et al., 2019a), which occurred during the period between ca. 33.7 and ca. 14 Ma (Naish et al., 2001), and during the Pliocene, ca. 5.3-3.3 Ma (Cook et al., 2013). It is suggested that the high topography of the GSM may not only have been an important seeding ground, but have remained a kind of keystone in the subglacial topography, preventing the deglaciation of the central EAIS during these climate-induced oscillations. This theory is supported by the accordance between the positions and orientations of the central ridge of the GSM and the overlying Dome A ice divide (Fig. 5.6), which thermomechanical modelling suggests has not moved significantly during at least the last glacial cycle (Wolovick et al., 2021). The smaller-scale topographic variability mapped in this study may have local impacts on ice flow (Mouginot et al., 2019) and basal thermal conditions (Wolovick et al., 2021), but does not seem to exert any major influence over ice sheet behaviour at the present day. Whether or not the role of this topography in influencing EAIS behaviour was elevated during periods of lesser ice extent remains an open question.

7. Conclusions

In this study, a new map of the planform ridge and valley geometry of the central Gamburtsev Subglacial Mountains (GSM), East Antarctica, was derived by using satellite remote sensing data to identify and interpret changes in ice surface slope. Manual and automated approaches to processing these data were tested, and existing bed elevation models and ice penetrating radar measurements were used to validate the correspondence between the resulting maps and the known bed topography. Furthermore, the morphometry of the manually mapped networks was analysed, revealing details about the structure of the pre-glacial fluvial landscape and its subsequent evolution under early phases of Antarctic glaciation. Implications of this increased knowledge of the basal topography for the evolution of the East Antarctic Ice Sheet and its subglacial hydrological systems were also discussed.

This thesis started with six objectives (Section 3.2) to address Research Questions (RQs) across three key themes (Section 3.1). All of the objectives have successfully been achieved and the Research Questions have been addressed, with key findings of the work as follows:

1. Mapping of subglacial topography from ice surface curvature is validated for the GSM by existing measurements of ice thickness from radio echo sounding (RES), and existing models of bed topography produced using the RES data. The maps presented here expand both the coverage and the level of detail available for the planform geometry of the GSM, particularly in high bed elevation/thinner ice areas. (**RQ 1A**)
2. Care must be taken when interpreting the data presented here to account for the limitations inherent in mapping bed features from the surface. Orientations of features represented may be biased by the direction of ice flow, with features aligned to flow less likely to produce a surface expression. The detail available also varies with the thickness of the ice column, with thicker ice dampening the effects of subglacial topography on flow. This can lead to ambiguity over the presence or interpretation of mapped features, suggesting the importance of using this approach in conjunction with other methods of mapping ice sheet beds, such as radio echo sounding. (**RQ 1A**)
3. Manual mapping identified a greater proportion of bed features (64.8%) than automated mapping (51.1%), produced fewer erroneous identifications, and had smaller offsets between mapped and actual features. The proportion of features successfully identified was increased further (79.9%) when all methods were considered together, suggesting that future mapping would maximise accuracy and comprehensiveness by combining automated and manual approaches. (**RQ 1B**)

4. The mapped valley network preserves information about the pre-glacial fluvial regime, suggesting the former existence of a large central catchment (68,700 km^2) draining east towards the Ross Sea. Behaviour of the fluvial network can potentially be modelled by taking the directions of the mapped valley network as indicators of palaeo-flow, and using them to produce a map of flow direction which is independent of any elevation data (Section 4.7). (**RQ 2A**)
5. There is some evidence for modification of the fluvial valley network by local- to regional-scale erosive ice through the breaching of fluvial drainage divides and the overdeepening of valley long-profiles, however, uncertainty in the mapping of these features produces ambiguity in their interpretation. (**RQ 2A**)
6. The minimum wavelength of detectable topographic variability (< 5 km) is smaller than can be reproduced in bed models using existing RES or other data. Ridge and valley structures on this scale may play an important role in governing local fluctuations in bed conditions, including occurrences of basal melting and routing of subglacial water flows. Maps of planform landscape geometry such as those presented here may therefore be useful in geophysical survey planning and evaluating sites for the preservation of Oldest Ice (> 1 Myr) cores in regions of highly variable subglacial topography. (**RQ 3A**)
7. The preservation of the pre-glacial fluvial valley network more widely than previously known indicates, for the area surrounding the GSM, long-term ice sheet behaviour which is either consistently non-erosive, or sufficiently influenced by the bed topography to concentrate erosion in pre-existing topographic lows. This is suggested to document the importance of the GSM as a centre of growth for the early East Antarctic Ice Sheet, and as a stabilising influence during its subsequent evolution. (**RQ 3B**)
8. In addition to the applications mentioned, the production of synthesised bed elevation models using the mapped network, or through combining the mapped network with existing data, has not been attempted, but may be an avenue to explore in future. Such products could be of use for ice sheet models that seek to simulate more accurately the effects of high-relief basal topography on ice flow or basal hydrology.

Appendices

Appendix 1 – Processing Scripts (MATLAB 2021a)

Automated feature mapping procedure (Section 4.3)

```
% SETUP
% Display results?
show = true;
save = false;
% Choose data
data_filename = "REMA_200m_clip_curv.tif";
data_name = "REMA";
% Load geotiff files and set no data values to zero
[input,res,ref,ndref] = readgeosetnd(data_filename,0);
if show
    imshow(imadjust(input(1:243,2001:end)),[])
    title("Input")
end
% Load flow direction raster (must be snapped to image)
flowdir = readgeosetnd("Ice_velo_dir_200m.tif",NaN);
flowdir = round(flowdir./45); % Convert to 8 directions

% PREPROCESSING
% Smooth input data and operate only on positive values
pos = medfilt2(input,[5 5],"symmetric");   % Median filter preserves edges while
removing noise
pos(pos < 0) = 0;                       % Set negative values to zero
if show
    imshow(imadjust(pos(1:243,2001:end)),[])
    title("Smoothed input")
end

% THRESHOLDING
% Choose parameters for adaptive threshold
statistic = "mean";              % Recommended mean
sensitivity =0.5;      % Range between 0 and 1, recommended 0.5
nhood_size = 5;       % In thousand meters; must be odd, recommended 35
% Define adaptive threshold
thresh =
adaptthresh(pos,sensitivity,"Statistic",statistic,"NeighborhoodSize",round(nhood_si
ze*1000./res));
if show
    imshow(thresh(1:243,2001:end),[])
    title("Threshold matrix")
end
% Apply adaptive threshold to produce classification
binary = imbinarize(pos,thresh);
if show
    imshow(binary(1:243,2001:end))
    title("Binary classification")
end

% POSTPROCESSING
% Clean mask by removing areas of less than 1 km squared
binaryClean = bwareaopen(binary,round(1000000/prod(res)));
% Smooth mask using a morphological operation
```

```
binaryClean = imclose(binaryClean,strel("disk",1));
% Revert all original missing values to false
binaryClean(ndref) = 0;
if show
    imshowpair(binaryClean(1:243,2001:end),binary(1:243,2001:end))
    title("Cleaned binary classification")
end

% EDGE DETECTION
% Caclulate downslope change across mask
[x,y] = size(input);
image = binaryClean;
map = zeros(x,y);
for i = 2:x-1
    for j = 2:y-1
        switch flowdir(i,j)
            case 0
                r = -1;
                c = 0;
            case 1
                r = -1;
                c = 1;
            case 2
                r = 0;
                c = 1;
            case 3
                r = 1;
                c = 1;
            case 4 | -4
                r = 1;
                c = 0;
            case -3
                r = 1;
                c = -1;
            case -2
                r = 0;
                c = -1;
            case -1
                r = -1;
                c = -1;
            otherwise
                r = 0;
                c = 0;
        end
        grad = image(i+r,j+c) - image(i,j);
        map(i,j) = map(i,j) + grad;
    end
end
if show
    imshow(map(1:243,2001:end),[])
    title("Detected edges")
end
% Assign valleys and ridges
valleys = map > 0;
ridges = map < 0;

% EXPORT RESULTS
% Compile final masks
```

```
mask = 2.*ridges + valleys;
mask(ndref) = NaN;
if show
    imshow(mask(1:243,2001:end),[])
end
% Save results
if save
      geotiffwrite("Mask_"+data_name+"_"+res(1)+"m_"+sensitivity+"_"+nhood_size+".t
if",mask,ref,"CoordRefSysCode",3031)
end
```

7.1.1. Automated feature mapping auxiliary – "readgeosetnd.mlx"

```
% Inputs:
% "filename" = name of raster to import (e.g. .tif)
% "setnd" = value to convert no data values to
% Ouputs:
% "raster" = image matrix with no data values set to the 'setnd' value
% "res" = spatial resolution of the raster in the x and y directions
% "ref" = a spatial referencing object for the raster (used to save a result using
the same spatial information)
% "ndref" = logical matrix indicating which pixels were originally 'no data'
function [raster,res,ref,ndref] = readgeosetnd(filename,setnd)
    [raster,ref] = readgeoraster(filename);
    info = georasterinfo(filename);
    nd = info.MissingDataIndicator;
    ndref = raster == nd;
    if any(ndref,"all")
        raster(ndref) = setnd;
    end
    res =
[info.RasterReference.CellExtentInWorldX,info.RasterReference.CellExtentInWorldY];
end
```

7.1.2. Flow modelling auxiliary – Flow direction conversion

```
% Converts continuous direction raster to integer values representing 8
% directions
[fd,ref] = readgeoraster("Fd_math.tif");
fd8 = round(fd./45);
[x,y] = size(fd8);
d8 = zeros(x,y,"uint8");
for i = 1:x
    for j =1:y
        cell = fd8(i,j);
        switch cell
            case 1
                d8(i,j) = 128;
            case 2
                d8(i,j) = 64;
            case 3
                d8(i,j) = 32;
            case 4
                d8(i,j) = 16;
            case 5
                d8(i,j) = 8;
            case 6
                d8(i,j) = 4;
```

```
            case 7
                d8(i,j) = 2;
            otherwise
                d8(i,j) = 1;
        end
    end
end
geotiffwrite("Fd8.tif",d8,ref,"CoordRefSysCode",3031)
```

References

An, M., Wiens., D.A., Zhao, Y., Feng, M., Nyblade, A.A., Kanao, M., Li, Y., Maggi, A. and Lévêque, J-J. (2015) 'S-velocity model and inferred Moho topography beneath the Antarctic Plate from Rayleigh waves', *Journal of Geophysical Research: Solid Earth*, 120(1), pp. 359–383. Available at: https://doi.org/10.1002/2014JB011332.

Bamber, J.L., Gomez-Dans, J.L. and Griggs, J.A. (2009) 'A new 1 km digital elevation model of the Antarctic derived from combined satellite radar and laser data – Part 1: Data and methods', *The Cryosphere*, 3(1), pp. 101–111. Available at: https://doi.org/10.5194/tc-3-101-2009.

Bell, R.E., Studinger, M., Fahnestock, M.A. and Shuman, C.A. (2006) 'Tectonically controlled subglacial lakes on the flanks of the Gamburtsev Subglacial Mountains, East Antarctica', *Geophysical Research Letters*, 33(2). Available at: https://doi.org/10.1029/2005GL025207.

Bell, R.E., Ferraccioli, F., Creyts, T.T., Braaten, D., Corr, H., Das, I., Damaske, D., Frearson, N., Jordan, T., Rose, K., Studinger, M. and Wolovick, M. (2011) 'Widespread Persistent Thickening of the East Antarctic Ice Sheet by Freezing from the Base', *Science*, 331(6024), pp. 1592–1595. Available at: https://doi.org/10.1126/science.1200109.

Block, A.E., Bell, R.E. and Studinger, M. (2009) 'Antarctic crustal thickness from satellite gravity: Implications for the Transantarctic and Gamburtsev Subglacial Mountains', *Earth and Planetary Science Letters*, 288(1), pp. 194–203. Available at: https://doi.org/10.1016/j.epsl.2009.09.022.

Bo, S., Siegert, M.J., Mudd, S.M., Sugden, D., Fujita, S., Xiangbin, C., Yunyun, J., Xueyang, T. and Yuansheng, L. (2009) 'The Gamburtsev mountains and the origin and early evolution of the Antarctic Ice Sheet', *Nature*, 459(7247), pp. 690–693. Available at: https://doi.org/10.1038/nature08024.

Boger, S.D. (2011) 'Antarctica — Before and after Gondwana', *Gondwana Research*, 19(2), pp. 335–371. Available at: https://doi.org/10.1016/j.gr.2010.09.003.

Bowman, V.C., Francis, J.E. and Riding, J.B. (2013) 'Late Cretaceous winter sea ice in Antarctica?', *Geology*, 41(12), pp. 1227–1230. Available at: https://doi.org/10.1130/G34891.1.

Brook, E. (2020) 'Center for OLDest Ice EXploration (COLDEX): Proposal to NSF Science and Technology Center (STC) Competition' [online] Available at: https://icedrill.org/sites/default/files/08.Brook_COLDEX_ICWG_2020.pdf [Accessed 02/12/2022].

Chang, M., Jamieson, S.S.R., Bentley, M.J. and Stokes, C.R. (2016) 'The surficial and subglacial geomorphology of western Dronning Maud Land, Antarctica', *Journal of Maps*, 12(5), pp. 892–903. Available at: https://doi.org/10.1080/17445647.2015.1097289.

Cook, C.P., van de Flierdt, T., Williams, T., Hemming, S.R., Iwai, M., Kobayashi, M., Jimenez-Espejo, F.J., Escutia, C., González, J.J., Khim, B.-K., McKay, R.M., Passchier, S., Bohaty, S.M.,

Riesselman, C.R., Tauxe, L., Sugisaki, S., Galindo, A.L., Patterson, M.O., Sangiorgi, F., Pierce, E.L., Brinkhuis, H., Klaus, A., Fehr, A., Bendle, J.A.P., Bijl, P.K., Carr, S.A., Dunbar, R.B., Flores, J.A., Hayden, T.G., Katsuki, K., Kong, G.S., Nakai, M., Olney, M.P., Pekar, S.F., Pross, J., Röhl, U., Sakai, T., Shrivastava, P.K., Stickley, C.E., Tuo, S., Welsh, K. and Yamane, M. (2013) 'Dynamic behaviour of the East Antarctic ice sheet during Pliocene warmth', *Nature Geoscience*, 6(9), pp. 765–769. Available at: https://doi.org/10.1038/ngeo1889.

Corr, H., Ferraccioli, F., Jordan, T., & Robinson, C. (2020) 'Antarctica's Gamburtsev Province (AGAP) Project - Radio-echo sounding data (2007-2009)' [Data set]. UK Polar Data Centre, Natural Environment Research Council, UK Research & Innovation. https://doi.org/10.5285/0F6F5A45-D8AF-4511-A264-B0B35EE34AF6

Cox, S.E., Thomson, S.N., Reiners, P.W., Hemming, S.R. and van de Flierdt, T. (2010) 'Extremely low long-term erosion rates around the Gamburtsev Mountains in interior East Antarctica', *Geophysical Research Letters*, 37(22). Available at: https://doi.org/10.1029/2010GL045106.

Coxall, H.K., Wilson, P.A., Pälike, H., Lear, C.H. and Backman, J. (2005) 'Rapid stepwise onset of Antarctic glaciation and deeper calcite compensation in the Pacific Ocean', *Nature*, 433(7021), pp. 53–57. Available at: https://doi.org/10.1038/nature03135.

Creyts, T.T., Ferraccioli, F., Bell, R.E., Wolovick, M., Corr, H., Rose, K.C., Frearson, N., Damaske, D., Jordan, T., Braaten, D. and Finn, C. (2014) 'Freezing of ridges and water networks preserves the Gamburtsev Subglacial Mountains for millions of years', *Geophysical Research Letters*, 41(22), pp. 8114–8122. Available at: https://doi.org/10.1002/2014GL061491.

De Rydt, J., Gudmundsson, G.H., Corr, H.F.J. and Christoffersen, P. (2013) 'Surface undulations of Antarctic ice streams tightly controlled by bedrock topography', *The Cryosphere*, 7(2), pp. 407–417. Available at: https://doi.org/10.5194/tc-7-407-2013.

DeConto, R.M. and Pollard, D. (2003) 'Rapid Cenozoic glaciation of Antarctica induced by declining atmospheric CO2', *Nature*, 421(6920), pp. 245–249. Available at: https://doi.org/10.1038/nature01290.

Dury, G.H. (1957) 'A glacially breached watershed in Donegal', *Irish Geography*, 3(4), pp. 171–180. Available at: https://doi.org/10.1080/00750775709555507.

Ferraccioli, F., Finn, C.A., Jordan, T.A., Bell, R.E., Anderson, L.M. and Damaske, D. (2011) 'East Antarctic rifting triggers uplift of the Gamburtsev Mountains', *Nature*, 479(7373), pp. 388–392. Available at: https://doi.org/10.1038/nature10566.

Ferraccioli, F., Mather, B., Armadillo, E., Forsberg, R., Ebbing, J., Ford, J., Gohl, K., Eagles, G., Green, C., Fullea, J., Verdoya, M. and de la Cruz, J.L.C. (2022) 4D Antarctica: recent aeromagnetic, aerogravity and satellite data compilations provide a new tool to estimate subglacial geothermal heat

flux; EGU22-13195. Copernicus Meetings. Available at: https://doi.org/10.5194/egusphere-egu22-13195.

Fischer, H., Severinghaus, J., Brook, E., Wolff, E., Albert, M., Alemany, O., Arthern, R., Bentley, C., Blankenship, D., Chappellaz, J., Creyts, T., Dahl-Jensen, D., Dinn, M., Frezzotti, M., Fujita, S., Gallee, H., Hindmarsh, R., Hudspeth, D., Jugie, G., Kawamura, K., Lipenkov, V., Miller, H., Mulvaney, R., Parrenin, F., Pattyn, F., Ritz, C., Schwander, J., Steinhage, D., van Ommen, T. and Wilhelms, F. (2013) 'Where to find 1.5 million yr old ice for the IPICS "Oldest-Ice" ice core', *Climate of the Past*, 9(6), pp. 2489–2505. Available at: https://doi.org/10.5194/cp-9-2489-2013.

Fitzsimons, I.C.W. (2000) 'Grenville-age basement provinces in East Antarctica: Evidence for three separate collisional orogens', *Geology*, 28(10), pp. 879–882. Available at: https://doi.org/10.1130/0091-7613(2000)28<879:GBPIEA>2.0.CO;2.

Fitzsimons, I.C.W. (2003) 'Proterozoic basement provinces of southern and southwestern Australia, and their correlation with Antarctica', *Geological Society, London, Special Publications*, 206(1), pp. 93–130. Available at: https://doi.org/10.1144/GSL.SP.2003.206.01.07.

Franke, S., Eiserman, H., Jokat, W., Eagles, G., Asseng, J., Miller, H., Steinhage, D., Helm, V., Eisen, O. and Jansen, D. (2021) 'Preserved landscapes underneath the Antarctic Ice Sheet reveal the geomorphological history of Jutulstraumen Basin', *Earth Surface Processes and Landforms*, 46(13), pp. 2728-2745. Available at: https://doi.org/10.1002/esp.5203.

Fretwell, P., Pritchard, H.D., Vaughan, D.J., Bamber, J.L., Barrand, N.E., Bell, R., Bianchi, C., Bingham, R.G., Blankenship, D.D., Casassa, G., Catania, G., Callens, D., Conway, H., Cook, A.J., Corr, H.F.J., Damaske, D., Damm, V., Ferraccioli, F., Forsberg, R., Fujita, S., Gim, Y., Gogineni, P., Griggs, J.A., Hindmarsh, R.C.A., Holmlund, P., Holt, J.W., Jacobel, R.W., Jenkins, A., Jokat, W., Jordan, T., King, E.C., Kohler, J., Krabill, W., Riger-Kusk, M., Langley, K.A., Leitchenkov, G., Leuschen, C., Luyendyk, B.P., Matsuoka, K., Mouginot, J., Nitsche, F.O., Nogi, Y., Nost, O.A., Popov, S.V., Rignot, E., Pippin, D.M., Rivera, A., Roberts, J., Ross, N., Siegert, M.J., Smith, A.M., Steinhage, D., Studinger, M., Sun, B., Tinto, B.K., Welch, B.C., Wilson, D., Young, D.A., Xianbing, C. and Zirizzotti, A. (2013) 'Bedmap2: improved ice bed, surface and thickness datasets for Antarctica', *The Cryosphere*, 7(1), pp. 375–393. Available at: https://doi.org/10.5194/tc-7-375-2013.

Frémand, A.C., Fretwell, P., Bodart, J., Pritchard, H.D., Aitken, A., Bamber, J.L., Bell, R., Bianchi, C. Bingham, R.G., Blankenship, D.D., Casassa, G., Catania, G., Christianson, K., Conway, H., Corr, H.F.J., Cui, X., Damaske, D., Damm, V., Drews, R., Eagles, G., Eisen, O., Eisermann, H., Ferraccioli, F., Field, E., Forsberg, R., Franke, S., Fujita, S., Gim, Y., Goel, V., Gogineni, S.P., Greenbaum, J., Hills, B., Hindmarsh, R.C.A., Holmlund, P., Holschuh, N., Holt, J.W., Humbert, A., Jacobel, r.w., Jansen, D., Jenkins, A., Jokat, W., Jordan, T., King, E., Kohler, J., Krabill, W., Langley, K., Lee, J., Leitchenkov, G., Leuschen, C., Luyendyk, B., MacGregor, J., MacKie, E., Matsuoka, K., Morlighem,

M., Mouginot, J., Nitsche, F.O., Nogi, Y., Nost, O.A., Paden, J., Pattyn, F., Popov, S.V., Riger-Kusk, M., Rignot, E., Rippin, D.M., Rivera, A., Roberts, J., Ross, N., Ruppel, A., Schroeder, D.M., Siegert, M.J., Smith, A.M., Steinhage, D., Studinger, M., Sun, B., Tabacco, I., Tinto, K., Urbini, S., Vaughan, D., Welch, B.C., Wilson, D.S., Young, D.A. and Zirizotti, A. (2022) 'Antarctic Bedmap data: FAIR sharing of 60 years of ice bed, surface and thickness data', *Earth System Science Data Discussions*, pp. 1–25. Available at: https://doi.org/10.5194/essd-2022-355.

Fujita, S., Holmlund, P., Matsuoka, K., Enomoto, H., Fukui, K., Nakazawa, F., Sugiyama, S. and Surdyk, S. (2012) 'Radar diagnosis of the subglacial conditions in Dronning Maud Land, East Antarctica', *The Cryosphere*, 6(5), pp. 1203–1219. Available at: https://doi.org/10.5194/tc-6-1203-2012.

Gudmundsson, G.H. (2003) 'Transmission of basal variability to a glacier surface', *Journal of Geophysical Research: Solid Earth*, 108(B5). Available at: https://doi.org/10.1029/2002JB002107.

Gudmundsson, G.H. (2008) 'Analytical solutions for the surface response to small amplitude perturbations in boundary data in the shallow-ice-stream approximation', *The Cryosphere*, 2(2), pp. 77–93. Available at: https://doi.org/10.5194/tc-2-77-2008.

Gupta, R., Pandey, M., Arora, D., Pant, N.C. and Rao, N.V.C. (2022) 'Evincing the presence of a trans-Gondwanian mobile belt in the interior of the Princess Elizabeth Land, East Antarctica: insights from offshore detrital sediments, rock fragments, and monazite geochronology', *Geological Journal*, 57(7), pp. 2581–2607. Available at: https://doi.org/10.1002/gj.4430.

Heeszel, D.S., Wiens, D.A., Nyblade, A.A., Hansen, S.E., Kanao, M., An, M. and Zhao, Y. (2013) 'Rayleigh wave constraints on the structure and tectonic history of the Gamburtsev Subglacial Mountains, East Antarctica', *Journal of Geophysical Research: Solid Earth*, 118(5), pp. 2138–2153. Available at: https://doi.org/10.1002/jgrb.50171.

Holdgate, G.R., McLoughlin, S., Drinnan, A.N., Finkelman, R.B., Willett, J.C. and Chiehowsky, L.A. (2005) 'Inorganic chemistry, petrography and palaeobotany of Permian coals in the Prince Charles Mountains, East Antarctica', *International Journal of Coal Geology*, 63(1), pp. 156–177. Available at: https://doi.org/10.1016/j.coal.2005.02.011.

Holt, J.W., Blankenship, D.D., Morse, D.L., Young, D.A., Peters, M.E., Kempf, S.D., Richter, T.G., Vaughan, D.G. and Corr, H.F.J. (2006) 'New boundary conditions for the West Antarctic Ice Sheet: Subglacial topography of the Thwaites and Smith glacier catchments', *Geophysical Research Letters*, 33(9). Available at: https://doi.org/10.1029/2005GL025561.

Howat, I.M., Porter, C., Smith, B.E., Noh, M.-J. and Morin, P. (2019) 'The Reference Elevation Model of Antarctica', *The Cryosphere*, 13(2), pp. 665–674. Available at: https://doi.org/10.5194/tc-13-665-2019.

IPCC (2021) ‘Summary for Policymakers.’ In: V. Masson-Delmotte, P. Zhai, A. Pirani, S.L. Connors, C. Péan, S. Berger, N. Caud, Y. Chen, L. Goldfarb, M.I. Gomis, M. Huang, K. Leitzell, E. Lonnoy, J.B.R. Matthews, T.K. Maycock, T. Waterfield, O. Yelekçi, R. Yu, and B. Zhou (Eds.) *Climate Change 2021: The Physical Science Basis. Contribution of Working Group I to the Sixth Assessment Report of the Intergovernmental Panel on Climate Change*. In Press.

Jamieson, S.S.R., Stokes, C.R., Ross, N., Rippin, D.M., Bingham, R.G., Wilson, D.S., Margold, M. and Bentley, M.J. (2014) ‘The glacial geomorphology of the Antarctic ice sheet bed’, *Antarctic Science*, 26(6), pp. 724–741. Available at: https://doi.org/10.1017/S0954102014000212.

Jamieson, S.S.R., Ross, N., Greenbaum, J.S., Young, D.A., Aitken, A.R.A., Roberts, J.L., Blankenship, D.D., Bo, S. and Siegert, M.J. (2016) ‘An extensive subglacial lake and canyon system in Princess Elizabeth Land, East Antarctica’, *Geology*, 44(2), pp. 87–90. Available at: https://doi.org/10.1130/G37220.1.

Jamieson, S.S.R., Hulton, N.R.J. and Hagdorn, M. (2008) ‘Modelling landscape evolution under ice sheets’, *Geomorphology*, 97(1), pp. 91–108. Available at: https://doi.org/10.1016/j.geomorph.2007.02.047.

Jamieson, S.S.R. and Sugden, D.E. (2008) ‘Landscape evolution of Antarctica.’ In A.K. Cooper, P. J. Barrett, H. Stagg, B. Storey, E. Stump, and W. Wise (Eds.) *Antarctica: A Keystone in a Changing World: Proceedings of the 10th International Symposium on Antarctic Earth Sciences*. Washington D.C.: National Academies Press, pp. 39-54.

Jamieson, S.S.R., Sugden, D.E. and Hulton, N.R.J. (2010) ‘The evolution of the subglacial landscape of Antarctica’, *Earth and Planetary Science Letters*, 293(1), pp. 1–27. Available at: https://doi.org/10.1016/j.epsl.2010.02.012.

Jezek, K., Curlander, J., Carsey, F., Wales, C. and Barry, R. (2013) ‘RAMP AMM-1 SAR Image Mosaic of Antarctica, Version 2’ [Data Set]. NASA National Snow and Ice Data Center DAAC. Boulder, Colorado USA. NASA National Snow and Ice Data Center Distributed Active Archive Center. Available at: https://doi.org/10.5067/8AF4ZRPULS4H.

Joughin, I., Smith, B.E. and Medley, B. (2014) ‘Marine Ice Sheet Collapse Potentially Under Way for the Thwaites Glacier Basin, West Antarctica’, *Science*, 344(6185), pp. 735–738. Available at: https://doi.org/10.1126/science.1249055.

Kumar, A., Hansen, S.E. and Emry, E.L. (2021) ‘Tectonic Structure of East Antarctica from Full Waveform Ambient Noise Tomography’, Geological Society of America, Southeastern Section 2021 Meeting [Preprint]. Available at: https://par.nsf.gov/biblio/10226571-tectonic-structure-east-antarctica-from-full-waveform-ambient-noise-tomography (Accessed: 11 July 2022).

Le Brocq, A.M., Hubbard, A., Bentley, M.J. and Bamber, J.L. (2008) 'Subglacial topography inferred from ice surface terrain analysis reveals a large un-surveyed basin below sea level in East Antarctica', *Geophysical Research Letters*, 35(16). Available at: https://doi.org/10.1029/2008GL034728.

Livingstone, S.J., Clark, C.D., Woodward, J. and Kingslake, J. (2013) 'Potential subglacial lakes and meltwater drainage pathways beneath the Antarctic and Greenland ice sheets', *The Cryosphere*, 7, pp. 1721–1740.

Livingstone, S.J., Li, Y., Rutishauser, A., Sanderson, R.J., Winter, K., Micucki, J.A., Björnsson, H., Bowling, J.S., Chu, W., Dow, C.F., Fricker, H.A., McMillan, M., Ng, F.S.L., Ross, N. Siegert, M.J., Siegfried, M. and Sole, A.J. (2022) 'Subglacial lakes and their changing role in a warming climate', *Nature Reviews Earth & Environment*, 3(2), pp. 106–124. Available at: https://doi.org/10.1038/s43017-021-00246-9.

Lythe, M.B. and Vaughan, D.G. (2001) 'BEDMAP: A new ice thickness and subglacial topographic model of Antarctica', *Journal of Geophysical Research: Solid Earth*, 106(B6), pp. 11335–11351. Available at: https://doi.org/10.1029/2000JB900449.

Miller, K.G., Wright, J.D., Katz, M.E., Browning, J.V., Cramer, B.S., Wade, B.S. and Mizintseva, S.F. (2008) 'A view of Antarctic Ice-Sheet evolution from sea-level and deep-sea isotope changes during the Late Cretaceous-Cenozoic'. In: A.K. Cooper, P. Barrett, H. Stagg, B. Storey, E. Stump and W. Wise (Eds.) *Antarctica: A Keystone in a Changing World: Proceedings of the 10th International Symposium on Antarctic Earth Sciences*. Washington D.C.: National Academies Press, pp. 55-70.

Morlighem, M., Rignot, E., Seroussi, H., Larour, E., Ben Dhia, H. and Aubry, D. (2011) 'A mass conservation approach for mapping glacier ice thickness', *Geophysical Research Letters*, 38(19). Available at: https://doi.org/10.1029/2011GL048659.

Morlighem, M., Rignot, E., Binder, T., Blankenship, D., Drews, R., Eagles, G., Eisen, O., Ferraccioli, F., Forsberg, R., Fretwell, P., Goel, V., Greenbaum, J.S., Gudmundsson, H., Guo, Jingxue, Helm, V., Hofstede, C., Howat, I., Humbert, A., Jokat, W., Karlsson, N.B., Lee, W.S., Matsuoka, K., Millan, R., Mouginot, J., Paden, J., Pattyn, F., Roberts, J., Rosier, S., Ruppel, A., Seroussi, H., Smith, E.C., Steinhage, D., Sun, B., van den Broke, M.R., van Ommen, T.D., van Wessem, M. and Young, D.A. (2020) 'Deep glacial troughs and stabilizing ridges unveiled beneath the margins of the Antarctic ice sheet', *Nature Geoscience*, 13(2), pp. 132–137.

Mouginot, J., Rignot, E. and Scheuchl, B. (2019) MEaSUREs Phase-Based Antarctica Ice Velocity Map, Version 1 [Data Set]. Boulder, Colorado USA. NASA National Snow and Ice Data Center Distributed Active Archive Center. Available at: https://doi.org/10.5067/PZ3NJ5RXRH10.

Naish, T.R., Woolfe, K.J., Barrett, P.J., Wilson, G.S., Atkins, C., Bohaty, S.M., Bücker, C.J., Claps, M., Davey, F.J., Dunbar, G.B., Dunn, A.G., Fielding, C.R., Florindo, F., Hannah, M.J., Harwood,

D.M., Henrys, S.A., Krissek, L.A., Lavelle, M., van der Meer, J., McIntosh, W.C., Niessen, F., Passchier, S., Powell, R.D., Roberts, A.P., Sagnotti, L., Scherer, R.P., Strong, C.P., Talarico, F., Verosub, K.L., Villa, G., Watkins, D.K., Webb, P.-N. and Wonik, T. (2001) 'Orbitally induced oscillations in the East Antarctic ice sheet at the Oligocene/Miocene boundary', *Nature*, 413(6857), pp. 719–723. Available at: https://doi.org/10.1038/35099534.

Ockenden, H., Bingham, R.G., Curtis, A. and Goldberg, D. (2021) 'Inverting ice surface elevation and velocity for bed topography and slipperiness beneath Thwaites Glacier', *The Cryosphere Discussions*, pp. 1–34. Available at: https://doi.org/10.5194/tc-2021-287.

Paxman, G.J.G., Watts, A.B., Ferraccioli, F., Jordan, T.A., Bell, R.E., Jamieson, S.S.R. and Finn, C.A. (2016) 'Erosion-driven uplift in the Gamburtsev Subglacial Mountains of East Antarctica', *Earth and Planetary Science Letters*, 452, pp. 1–14. Available at: https://doi.org/10.1016/j.epsl.2016.07.040.

Paxman, G.J.G., Jamieson, S.S.R., Ferraccioli, F., Bentley, M.J., Ross, N., Armadillo, E., Gasson, E.G.W., Leitchenkov, G. and DeConto, R.M. (2018) 'Bedrock Erosion Surfaces Record Former East Antarctic Ice Sheet Extent', *Geophysical Research Letters*, 45(9), pp. 4114–4123. Available at: https://doi.org/10.1029/2018GL077268.

Paxman, G.J.G., Jamieson, S.S.R., Ferraccioli, F., Bentley, M.J., Ross, N., Watts, A.B., Leitchenkov, G., Armadillo, E. and Young, D.A. (2019a) 'The Role of Lithospheric Flexure in the Landscape Evolution of the Wilkes Subglacial Basin and Transantarctic Mountains, East Antarctica', *Journal of Geophysical Research: Earth Surface*, 124(3), pp. 812–829. Available at: https://doi.org/10.1029/2018JF004705.

Paxman, G.J.G., Jamieson, S.S.R., Ferraccioli, F., Jordan, T.A., Bentley, M.J., Ross, N., Forsberg, R., Matsuoka, K., Steinhage, D., Eagles, G. and Casal, T.G. (2019b) 'Subglacial Geology and Geomorphology of the Pensacola-Pole Basin, East Antarctica', *Geochemistry, Geophysics, Geosystems*, 20(6), pp. 2786–2807. Available at: https://doi.org/10.1029/2018GC008126.

Paxman, G.J.G., Gasson, E.G., Jamieson, S.S.R., Bentley, M.J. and Ferraccioli, F. (2020) 'Long-Term Increase in Antarctic Ice Sheet Vulnerability Driven by Bed Topography Evolution', Geophysical Research Letters, 47(20), p. e2020GL090003. Available at: https://doi.org/10.1029/2020GL090003.

Pelletier, J.D., Comeau, D. and Kargel, J. (2010) 'Controls of glacial valley spacing on earth and mars', Geomorphology, 116(1), pp. 189–201. Available at: https://doi.org/10.1016/j.geomorph.2009.10.018.

Popov, S. (2022) 'Ice Cover, Subglacial Landscape, and Estimation of Bottom Melting of Mac. Robertson, Princess Elizabeth, Wilhelm II, and Western Queen Mary Lands, East Antarctica', *Remote Sensing*, 14(1), p. 241. Available at: https://doi.org/10.3390/rs14010241.

Pritchard, H.D. (2014) ‘Bedgap: where next for Antarctic subglacial mapping?’, *Antarctic Science*, 26(6), pp. 742–757. Available at: https://doi.org/10.1017/S095410201400025X.

Raymond, M.J. and Gudmundsson, G.H. (2005) ‘On the relationship between surface and basal properties on glaciers, ice sheets, and ice streams’, *Journal of Geophysical Research: Solid Earth*, 110(B8). Available at: https://doi.org/10.1029/2005JB003681.

Raymond, M.J. and Gudmundsson, G.H. (2009) ‘Estimating basal properties of ice streams from surface measurements: a non-linear Bayesian inverse approach applied to synthetic data’, *The Cryosphere*, 3(2), pp. 265–278. Available at: https://doi.org/10.5194/tc-3-265-2009.

Rémy, F. and Minster, J.-F. (1997) ‘Antarctica Ice Sheet Curvature and its relation with ice flow and boundary conditions’, *Geophysical Research Letters*, 24(9), pp. 1039–1042. Available at: https://doi.org/10.1029/97GL00959.

Ridley, J.K., Cudlip, W. and Laxon, S.W. (1993) ‘Identification of subglacial lakes using ERS-1 radar altimeter’, *Journal of Glaciology*, 39(133), pp. 625-634.

Rose, K.C., Ferraccioli, F., Jamieson, S.S.R., Bell, R.E., Corr, H., Creyts, T.T., Braaten, D., Jordan T.A., Fretwell, P.T. and Damaske, D. (2013) ‘Early East Antarctic Ice Sheet growth recorded in the landscape of the Gamburtsev Subglacial Mountains’, Earth and Planetary Science Letters, 375, pp. 1–12. Available at: https://doi.org/10.1016/j.epsl.2013.03.053.

Rose, K.C., Ross, N., Bingham, R.G., Corr, H.F.J., Ferraccioli, F., Jordan, T.A., Le Brocq, A.M., Rippin, D.M. and Siegert, M.J. (2014) ‘A temperate former West Antarctic ice sheet suggested by an extensive zone of subglacial meltwater channels’, *Geology*, 42(11), pp. 971–974. Available at: https://doi.org/10.1130/G35980.1.

Rose, K.C., Ross, N., Jordan, T.A., Bingham, R.G., Corr, H.F.J., Ferraccioli, F., Le Brocq, A.M., Rippin, D.M. and Siegert, M.J. (2015) ‘Ancient pre-glacial erosion surfaces preserved beneath the West Antarctic Ice Sheet’, *Earth Surface Dynamics*, 3(1), pp. 139–152. Available at: https://doi.org/10.5194/esurf-3-139-2015.

Ross, N., Jordan, T.A., Bingham, R.G., Corr, H.F.J., Ferraccioli, F., Le Brocq, A.M., Rippin, D.M., Wright, A.P. and Siegert, M.J. (2014) ‘The Ellsworth Subglacial Highlands: Inception and retreat of the West Antarctic Ice Sheet’, *GSA Bulletin*, 126(1–2), pp. 3–15. Available at: https://doi.org/10.1130/B30794.1.

Scambos, T.A., Haran, T.M., Fahnestock, M.A., Painter, T.H. and Bohlander, J. (2007) ‘MODIS-based Mosaic of Antarctica (MOA) data sets: Continent-wide surface morphology and snow grain size’, *Remote Sensing of Environment*, 111(2), pp. 242–257. Available at: https://doi.org/10.1016/j.rse.2006.12.020.

Scher, H.D., Bohaty, S.M., Zachos, J.C. and Delaney, M.L. (2011) 'Two-stepping into the icehouse: East Antarctic weathering during progressive ice-sheet expansion at the Eocene-Oligocene transition', *Geology*, 39(4), pp. 383–386. Available at: https://doi.org/10.1130/G31726.1.

Shen, W., Wiens, D.A., Anandakrishnan, S., Aster, R.C., Gerstoft, P., Bromirski, P.D., Hansen, S.E., Dalziel, I.W.D., Heeszel, D.S., Huerta, A.D., Nyblade, A.A., Stephen, R., Wilson, T.J. and Winberry, J.P. (2018) 'The Crust and Upper Mantle Structure of Central and West Antarctica from Bayesian Inversion of Rayleigh Wave and Receiver Functions', *Journal of Geophysical Research: Solid Earth*, 123(9), pp. 7824–7849. Available at: https://doi.org/10.1029/2017JB015346.

Siegert, M.J. (1999) 'On the origin, nature and uses of Antarctic ice-sheet radio-echo layering', *Progress in Physical Geography: Earth and Environment*, 23(2), pp. 159–179. Available at: https://doi.org/10.1177/030913339902300201.

Siegert, M.J. (2008) 'Antarctic subglacial topography and ice-sheet evolution', *Earth Surface Processes and Landforms*, 33(4), pp. 646–660. Available at: https://doi.org/10.1002/esp.1670.

Siegert, M.J., Ross, N. and Le Brocq, A.M. (2016) 'Recent advances in understanding Antarctic subglacial lakes and hydrology', *Philosophical Transactions of the Royal Society A: Mathematical, Physical and Engineering Sciences*, 374(2059), p. 20140306. Available at: https://doi.org/10.1098/rsta.2014.0306.

Siegert, M.J., Taylor, J. and Payne, A.J. (2005) 'Spectral roughness of subglacial topography and implications for former ice-sheet dynamics in East Antarctica', *Global and Planetary Change*, 45(1), pp. 249–263. Available at: https://doi.org/10.1016/j.gloplacha.2004.09.008.

Sleep, N.H. (2006) 'Mantle plumes from top to bottom', *Earth-Science Reviews*, 77(4), pp. 231–271. Available at: https://doi.org/10.1016/j.earscirev.2006.03.007.

Smith, B.E., Fricker, H.A., Joughin, I.R. and Tulaczyk, S. (2009) 'An inventory of active subglacial lakes in Antarctica detected by ICESat (2003–2008)', *Journal of Glaciology*, 55(192), pp. 573–595. Available at: https://doi.org/10.3189/002214309789470879.

Stokes, C.R., Abram, N.J., Bentley, M.J., Edwards, T.L., England, M.H., Foppert, A., Jamieson, S.S.R., Jones, R.S., King, M.A., Lenaerts, J.T.M., Medley, B., Miles, B.W.J., Paxman, G.J.G., Ritz, C., van de Flierdt, T. and Whitehouse, P. (2022) 'Response of the East Antarctic Ice Sheet to past and future climate change', *Nature*, 608(7922), pp. 275–286. Available at: https://doi.org/10.1038/s41586-022-04946-0.

Stoll, H.M. and Schrag, D.P. (1996) 'Evidence for Glacial Control of Rapid Sea Level Changes in the Early Cretaceous', *Science*, 272(5269), pp. 1771–1774. Available at: https://doi.org/10.1126/science.272.5269.1771.

Studinger, M., Karner, G.D., Bell, R.E., Levin, V., Raymond, C.A. and Tikku, A.A. (2003) 'Geophysical models for the tectonic framework of the Lake Vostok region, East Antarctica', *Earth and Planetary Science Letters*, 216(4), pp. 663–677. Available at: https://doi.org/10.1016/S0012-821X(03)00548-X.

Sugden, D.E. and Jamieson, S.S.R. (2018) 'The pre-glacial landscape of Antarctica', *Scottish Geographical Journal*, 134(3–4), pp. 203–223. Available at: https://doi.org/10.1080/14702541.2018.1535090.

Sugden, D.E. and John, B.S. (1976) *Glaciers and Landscape*. ?

Swain, C.J. and Kirby, J.F. (2021) 'Effective Elastic Thickness Map Reveals Subglacial Structure of East Antarctica', *Geophysical Research Letters*, 48(4), p. e2020GL091576. Available at: https://doi.org/10.1029/2020GL091576.

Thomson, S.N., Reiners, P.W., Hemming, S.R. and Gehrels, G.E. (2013) 'The contribution of glacial erosion to shaping the hidden landscape of East Antarctica', *Nature Geoscience*, 6(3), pp. 203–207. Available at: https://doi.org/10.1038/ngeo1722.

Van Breedam, J., Huybrechts, P. and Crucifix, M. (2022) 'Modelling evidence for late Eocene Antarctic glaciations', *Earth and Planetary Science Letters*, 586, p. 117532. Available at: https://doi.org/10.1016/j.epsl.2022.117532.

van de Flierdt, T., Hemming, S.R., Goldstein, S.L., Gehrels, G.E. and Cox, S.E. (2008) 'Evidence against a young volcanic origin of the Gamburtsev Subglacial Mountains, Antarctica', *Geophysical Research Letters*, 35(21). Available at: https://doi.org/10.1029/2008GL035564.

Van Liefferinge, B. and Pattyn, F. (2013) 'Using ice-flow models to evaluate potential sites of million year-old ice in Antarctica', *Climate of the Past*, 9(5), pp. 2335–2345. Available at: https://doi.org/10.5194/cp-9-2335-2013.

Vaughan, D.G., Corr, H.F.J., Ferraccioli, F., Frearson, N., O'Hare, A., Mach, D., Holt, J.W., Blankenship, D.D., Morse, D.L. and Young, D.A. (2006) 'New boundary conditions for the West Antarctic ice sheet: Subglacial topography beneath Pine Island Glacier', *Geophysical Research Letters*, 33(9). Available at: https://doi.org/10.1029/2005GL025588.

Veevers, J.J. (1994) 'Case for the Gamburtsev Subglacial Mountains of East Antarctica originating by mid-Carboniferous shortening of an intracratonic basin', *Geology*, 22(7), pp. 593–596. Available at: https://doi.org/10.1130/0091-7613(1994)022<0593:CFTGSM>2.3.CO;2.

Veevers, J.J., Saeed, A., Pearson, N., Belousova, E. and Kinny, P.D. (2008) 'Zircons and clay from morainal Permian siltstone at Mt Rymill (73°S, 66°E), Prince Charles Mountains, Antarctica, reflect the ancestral Gamburtsev Subglacial Mountains–Vostok Subglacial Highlands complex', *Gondwana Research*, 14(3), pp. 343–354. Available at: https://doi.org/10.1016/j.gr.2007.12.006.

Veevers, J.J. and Saeed, A. (2008) 'Gamburtsev Subglacial Mountains provenance of Permian–Triassic sandstones in the Prince Charles Mountains and offshore Prydz Bay: Integrated U–Pb and TDM ages and host-rock affinity from detrital zircons', *Gondwana Research*, 14(3), pp. 316–342. Available at: https://doi.org/10.1016/j.gr.2007.12.007.

Wolovick, M.J., Bell, R.E., Creyts, T.T. and Frearson, N. (2013) 'Identification and control of subglacial water networks under Dome A, Antarctica', *Journal of Geophysical Research: Earth Surface*, 118(1), pp. 140–154. Available at: https://doi.org/10.1029/2012JF002555.

Wolovick, M.J., Moore, J.C. and Zhao, L. (2021) 'Joint Inversion for Surface Accumulation Rate and Geothermal Heat Flow From Ice-Penetrating Radar Observations at Dome A, East Antarctica. Part II: Ice Sheet State and Geophysical Analysis', *Journal of Geophysical Research: Earth Surface*, 126(5), p. e2020JF005936. Available at: https://doi.org/10.1029/2020JF005936.

Wright, A.P., Young, D.A., Roberts, J.L., Schroeder, D.M., Bamber, J.L., Dowdeswell, J.A., Young, N.W., Le Brocq, A.M., Warner, R.C., Payne, A.J., Blankenship, D.D., van Ommen, T.D. and Siegert, M.J. (2012) 'Evidence of a hydrological connection between the ice divide and ice sheet margin in the Aurora Subglacial Basin, East Antarctica', *Journal of Geophysical Research: Earth Surface*, 117(F1). Available at: https://doi.org/10.1029/2011JF002066.

Young, D.A., Wright, A.P., Roberts, J.L., Warner, R.C., Young, N.W., Greenbaum, J.S., Schroeder, D.M., Holt, J.W., Sugden, D.E., Blankenship, D.D., van Ommen, T.D. and Siegert, M.J. (2011) 'A dynamic early East Antarctic Ice Sheet suggested by ice-covered fjord landscapes', *Nature*, 474(7349), pp. 72–75. Available at: https://doi.org/10.1038/nature10114.

Zachos, J., Pagani, M., Sloan, L., Thomas, E. and Billups, K. (2001) 'Trends, Rhythms, and Aberrations in Global Climate 65 Ma to Present', *Science*, 292(5517), pp. 686–693. Available at: https://doi.org/10.1126/science.1059412.

Zwally, H.J., Giovinetto, M.B., Beckley, M.A. and Saba, J.L. (2012) 'Antarctic and Greenland Drainage Systems' [Data Set]. GSFC Cryospheric Sciences Laboratory. Available at http://icesat4.gsfc.nasa.gov/cryo_data/ant_grn_drainage_systems.php